Micro-Reactor Design for Fast Liquid-Liquid Reactions

By Patrick Plouffe

Thesis submitted to the Faculty of Graduate and Postdoctoral Studies as required for the degree of Doctor of Philosophy

In

Department of Chemical and Biological Engineering

Faculty of Engineering

uOttawa

University of Ottawa

Abstract

Continuous operation presents multiple advantages over batch chemistry, yet its usage in the fine chemical and pharmaceutical industry remains limited due to its complexity.

A holistic tool-box approach for process development is presented to facilitate technology transfer. Reaction kinetics and reacting phases were taken into consideration for the selection of the most appropriate reactor module and operating conditions.

A micro-reactor was then more specifically developed for fast liquid-liquid reactions. The effect of physical properties was investigated in a serpentine micro-reactor using a reactive liquid-liquid extraction and different organic solvents (n-butanol, n-hexanol, MTBE and toluene). The generated droplets yielded a specific interfacial area of 10^4-10^5 m^2/m^3, compared to $\sim 10^2$ m^2/m^3 with conventional equipment. Two models were developed to predict the mass transfer rates for other reactive systems.

Further, the effect of geometry was investigated with five different micro-reactors using either curvature-based or obstacle-based micro-mixers. Curvature-based micro-mixers promoted the undesired parallel flow pattern due to stabilizing centrifugal forces, while obstacle-based micro-mixers avoided it.

A scale-up approach was finally proposed on a micro-reactor using an optimized micro-mixer. The mass transfer coefficients in a small-scale (1.5-15 mL/min) and a large-scale (12.5-125 mL/min) systems were compared and demonstrated its validity.

The obtained results allowed the prediction, the optimization, and the scaling of performance for liquid-liquid systems in the context of process development from molecular discovery to clinical trials and pilot scale production.

Résumé

Les procédés chimiques opérants de façon continue plutôt que discontinue présentent plusieurs avantages pour les industries chimiques fines et pharmaceutiques. Malgré tout, leur utilisation reste limitée due à la complexité de leur implémentation.

Une approche modulaire holistique aux fins de développement de procédés est présentée afin de faciliter le transfert technologique. La cinétique des réactions ainsi que les phases des réactifs furent prises en considération afin de déterminer le réacteur et les conditions d'opérations les plus appropriées.

Un micro-réacteur a ensuite été développé plus spécifiquement pour les réactions rapides liquide-liquide. L'effet des propriétés physiques des phases fut étudié dans un réacteur utilisant un mélangeur serpentin à l'aide d'une extraction réactive liquide-liquide et en variant la phase organique utilisée (n-butanol, n-hexanol, MTBE et toluène). Les gouttes générées avaient une aire spécifique interfaciale de 10^4-10^5 m^2/m^3 comparativement à $\sim 10^2$ m^2/m^3 à l'aide d'équipements conventionnels. Deux modèles furent développés afin de prédire les taux de transfert de matières pour d'autres systèmes réactionnels.

L'effet de la géométrie fut étudié à l'aide de cinq micro-réacteurs différents utilisant une technique de mélange fondée sur des courbes ou sur des obstacles. Il fut possible de démontrer que les courbes, à l'opposé des obstacles, favorisaient la formation d'un écoulement indésirable de type parallèle.

Une approche pour la mise à l'échèle fut finalement proposée sur un micro-réacteur utilisant un mélangeur optimisé. Les coefficients de transfert de matières d'un petit mélangeur (pour des débits de 1.5-15 mL/min) et d'un grand mélangeur (pour des débits de 12.5-125 mL/min) ont été comparés et en ont démontré la validité.

Les résultats obtenus permettent la prédiction, l'optimisation et la mise à l'échèle de la performance des systèmes liquide-liquide pour le développement de procédés de la découverte de nouvelles molécules jusqu'à la production à l'échèle pilote.

Declaration of Contributors

I hereby declare that I am the sole author of this thesis. My supervisors, Arturo Macchi and Dominique Roberge, provided comments and corrections throughout my work.

Except for the “Spade” reactor, I designed all the micro-reactors used in Sections 3, 4 and 5 using AutoCAD. The micro-mixers “Venturi”, the “Sickle” and the one used in Section 5 were also designed by me. The reactors were machined by Ehrfeld Mikrotechnik BTS in Germany.

Section 2.5 is presented as a review of different scenarios. Consequently, the results were not obtained by me, but by my supervisor Dominique Roberge prior to my studies.

All the experiments of Sections 3, 4 and 5 were designed by myself while at the R&D laboratories of Lonza AG. Two laboratory technicians, Michel Bittel and Jonas Sieber, helped me perform some experiments and are named as co-authors of Sections 3 and 5. Also, due to time constrains, the experiments of Section 5 were performed remotely after my return to Ottawa with the help of laboratory technicians at Lonza AG.

All the results of Section 7.2 were obtained by myself at the University of Ottawa. I installed the experimental systems, and I programmed the data acquisition using LabView. A summer student, Ross Anthony, helped me and is acknowledged as a co-author.

All the presented data analysis and modeling were performed by myself only.

Acknowledgements

I would first like to thank both of my supervisors Dominique Roberge and Arturo Macchi for their mentorship throughout my degree. I have no doubt that most of my success came from their guidance and help.

Then I would like to thank my family and my friends with whom I shared my life these past years. They are the reasons I have been able to climb over mountains (sometime literally). I would like also to thank all my colleagues with whom I discussed about research, science or simply generally; fresh eyes on a data set always helped interpreting it. More specifically, I thank Sébastien Mongeon and Eric Mielke for their help and wish them good luck pursuing the project.

I would like to also acknowledge the financial support of Lonza AG, of the Natural Sciences and Engineering Research Council of Canada, of the Ontario Graduate Scholarship Program, and of the University of Ottawa. They have made possible getting these extra data points.

Finally, I would like to express my gratitude toward past science teachers (Julien Roy, Philippe Lemieux) and numerous shows and Youtube channels (Découverte, Cosmos, Crash Course, SciShow, Vsauce, Veritasium, Smarter Every Day, Numberphile, and many more) for having always made me curious and wanting to know more about science and how the world works.

Table of Content

List of Figures

List of Tables

1 Introduction

The development of new medicinal molecules requires many years where the pharmacokinetics, mechanisms of excretion, and toxicity, or side effects are studied [1]. During this period, an increasing amount of the compound is needed to go through the different evaluations and clinical trials. The manufacturing of the molecules is initially done inside the R&D laboratories of the pharmaceutical companies, but is also outsourced to a specialized manufacturing company for larger campaigns. One such company is Lonza AG participating to this research.

1.1 Production of active pharmaceutical ingredients and fine chemicals

Campaigns for the production of active pharmaceutical ingredients are traditionally performed batch or semi-batch wise. Their duration vary depending on the amount of material required, but an analysis by Roberge et al. [2,3] found an average campaign length of 4-8 weeks during which as much as 1.5 ton of material can be produced in a day for the larger scale productions. An average yield of 77% was reported and most of their operating cost came from materials. The processes can therefore be made more economical by an optimization of the yields.

The molecules could be produced in one batch using a sufficiently large reactor. However, this can create temperature control problems since the area to volume ratio for heat transfer varies proportionally to the inverse of the reactor's dimension. To ensure proper temperature control, the reactants are diluted to dampen and absorb the heat released. This reduces the reaction rate and can result in non-optimal operating conditions, and is contrary to the philosophy of process intensification. This can be solved by making multiple smaller batches, but there is a risk of batch to batch variability due to human error and workup.

An alternative solution is to use a continuous process for the manufacture of molecules. The reactor volume is minimized compared to a batch process (for example see **Figure 1.1**), which ensures better area to volume ratios for heat transfer and safer reactors. This also enables intensified operating conditions for a better yield [4]. The automated nature of the process reduces variability and frees time for the laboratory technicians to focus

on more complex and valuable tasks. Potentially, the use of continuous processes can lead to reduced costs and a higher product quality for the manufacturer.

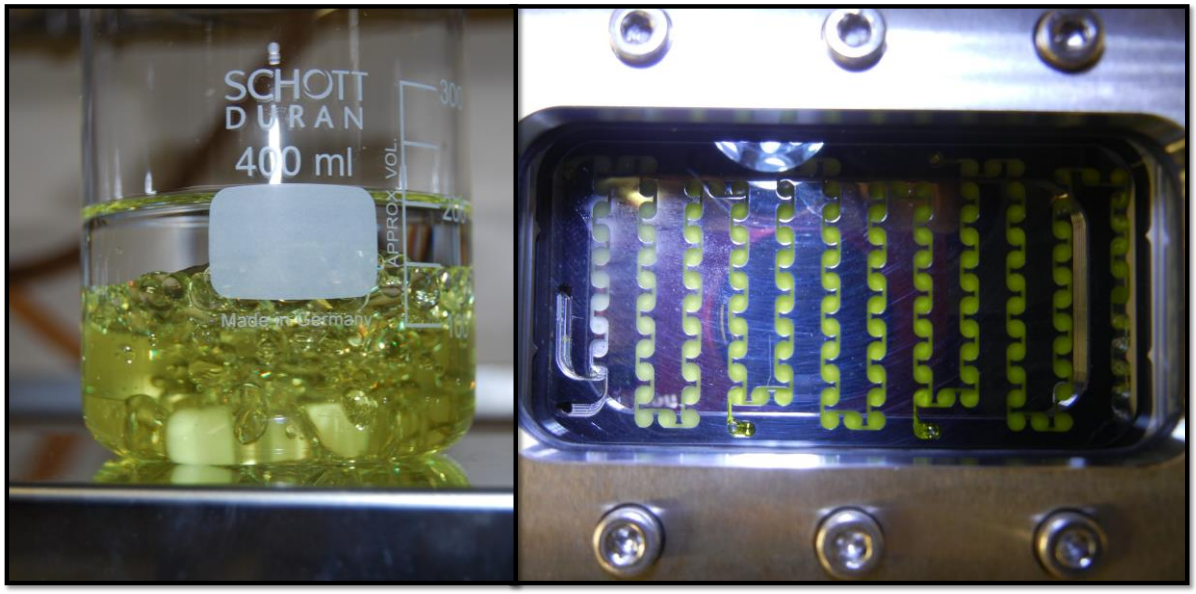

Figure 1.1 Demonstration of a liquid-liquid reaction performed batch-wise and continuously.

1.2 Motivation and research objectives

The production rates of the earlier clinical trials, if manufactured continuously, usually require a reactor with an internal diameter in the order of hundreds of micrometers to maximize the Reynolds number, mixing, and heat transfer while maintaining a reasonable pressure drop. Those are referred to as micro-reactors.

Due to their small internal diameter, they have a high area to volume ratio for heat transfer that allows better control of the temperature, and they can more easily handle high pressures. The heat and mass transfer coefficients are also increased because of shorter diffusional distances. This allows reactions to be intensified by operating them at higher concentrations, temperature and pressure.

High performance heat exchangers made of micro-channels have been successfully scaled and used at the industrial size [5]. Micro-reactors have demonstrated comparable yields to full scale industrial processes [6] and are also of interest for the development and intensification of non-medicinal and bulk chemical manufacturing [7–10]. Continuous flow technology and micro-reactors entered the laboratories of the fine

chemical and pharmaceutical industries with the help of systems like those sold by Syrris Ltd, ThalesNano Inc, Vapourtec Ltd, etc., but their broad use still remains limited. This is because determining the configuration of the continuous reactor (required internal diameter, length, feed configuration) and the best operating conditions is still a somewhat new and lengthy exercise. Moreover, the available reactors are usually a variant of coiled tubes and are not suitable for some classes of reactions like multiphase systems. The objective of this work is thus to better define reactor design for continuous systems within a toolbox framework by taking into account the parameters of the reaction and the transport phenomena occurring inside the reactor, and more specifically to study the design of micro-reactors for liquid-liquid reactions.

1.3 Thesis outline

Section 2 of this thesis presents a modular tool-box approach for the systematic selection of a reactor based on different reaction parameters. More specifically, the kinetics of the reaction, the reacting phases, and the reaction network are considered. Three scenarios are also discussed to provide an example of the application – and of the limits – of the toolbox approach. It has been published under the title "**From batch to continuous chemical synthesis – a toolbox approach**" and identifies the differences between single and multi-phase systems.

Sections 3, 4 and 5 build on the single phase work of Holvey et al. [11] and focus on the development of the reactor module for fast liquid-liquid reactions. This class of reactions was chosen because conclusions for liquid-liquid systems can be later extrapolated to gas-liquid systems. Moreover, reactors designed for fast reactions can also be adapted for slower reactions. These three studies share the same test reaction for the characterization of mass transfer in liquid-liquid systems, but evaluate the impact of different parameters. The test reaction is the alkaline hydrolysis of 4-nitrophenyl acetate, as shown on **Scheme 1.1**. The reaction had to be sufficiently rapid such that there would be no accumulation of the acetate in the aqueous phase and that the reaction would be limited only by mass transfer. This molecule was chosen because the aromatic ring and its nitro group accelerate the hydrolysis compared to alkyl esters.

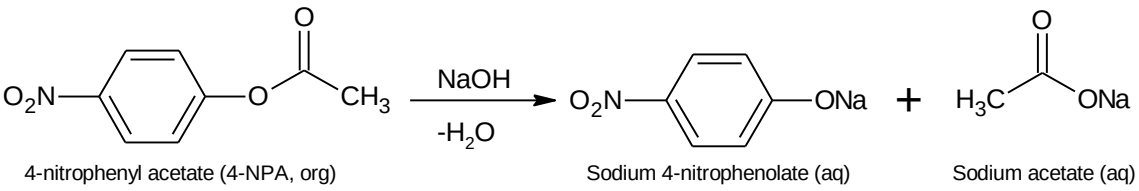

Scheme 1.1 Alkaline hydrolysis of 4-nitrohenyl acetate

Section 3 investigates the effect of physical properties by varying the organic phase such to have systems with different interfacial tensions, viscosities and densities. The micro-reactor used is adapted from a high performing mixing structure in single phase systems that utilizes serpentine channels. The results have been submitted for publication in a paper entitled "**Liquid-liquid mass transfer in a serpentine micro-reactor using various solvents**".

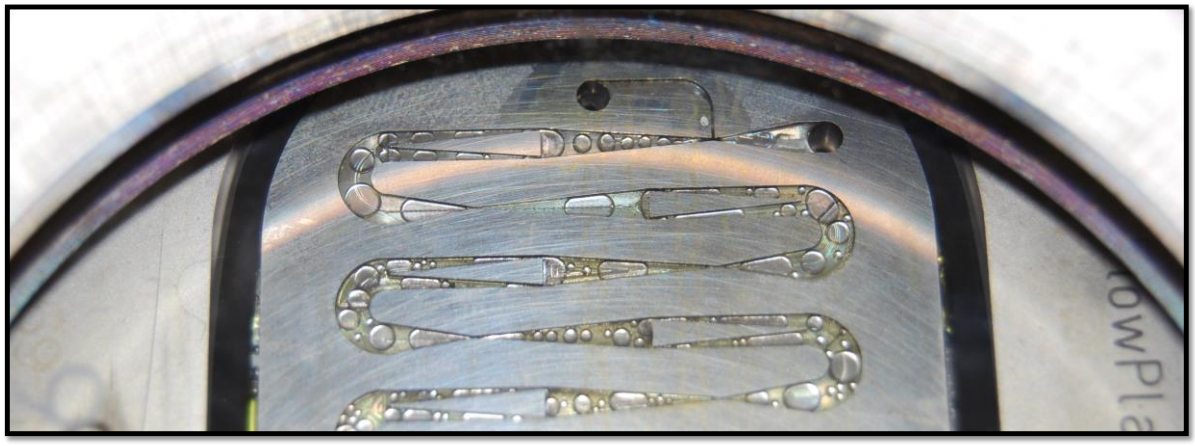

Figure 1.2 Hydrolysis of 4-nitrophenyl acetate in an obstacle based mixing structure

Section 4 investigates the effect of geometry using five mixing structures. Curvature-based mixing techniques, like the serpentine structure used in Section 3, are compared to obstacle-based mixing techniques like the one presented in **Figure 1.2** in order to identify the most energy efficient way to obtain high mass transfer rates in liquid-liquid systems. The work was published under the title "**Liquid-liquid flow regime and mass transfer in micro-reactors**".

Section 5 investigates the scale-up of micro-reactors. A sizing-up approach is derived to ensure the conservation of the energy dissipation through different reactor sizes. The

approach is tested on a micro-reactor using a novel mixing structure based on the previous studies' results. The performance of a small scale micro-reactor designed for early clinical trials and process development (1-15 mL/min) is compared to that of a larger design for flow rates one order of magnitude greater. The sizing-up approach and its limits with respect to heat transfer are then discussed. The study also compares the larger scale reactors (with diameters in the millimeter rather than micrometer) with some commercial static mixers. The publication of this material will be done under the title "**On the scale-up of micro-reactors for liquid-liquid reactions**". The mixing structure that was used is undergoing a patent application, for which details can be found in the appendix.

In conclusion, the results are summarized to develop a methodological approach for the selection of micro-reactors as depicted on **Figure 1.3**. The approach, combined with the tool-box, accelerates the determination of reactor configuration, operating conditions, mixer size and volume required for multiple reaction networks, physical properties, and scales.

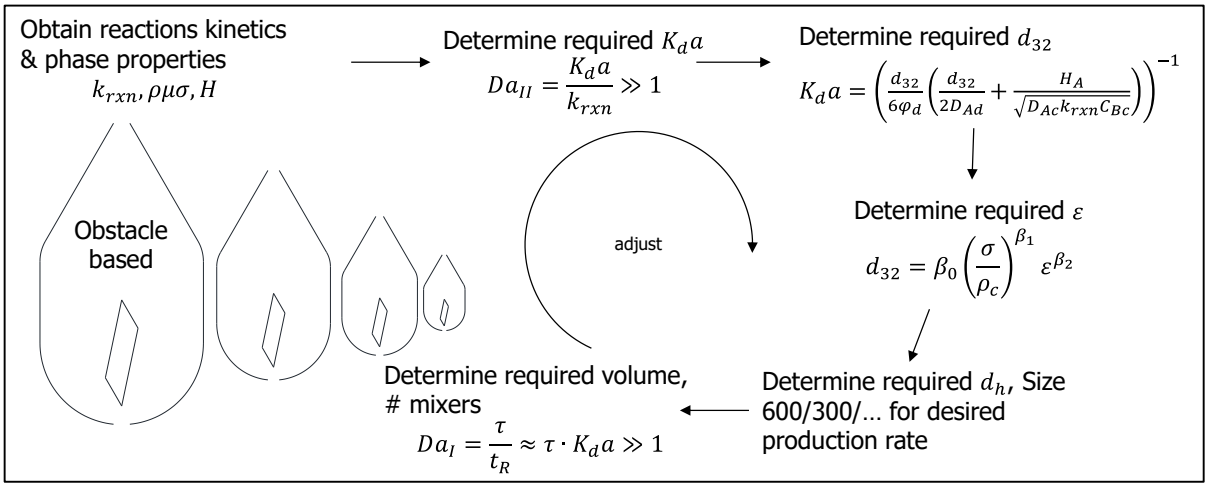

Figure 1.3 Determination of reactor size and length for liquid-liquid reactions.

2 From batch to continuous chemical synthesis – a toolbox approach

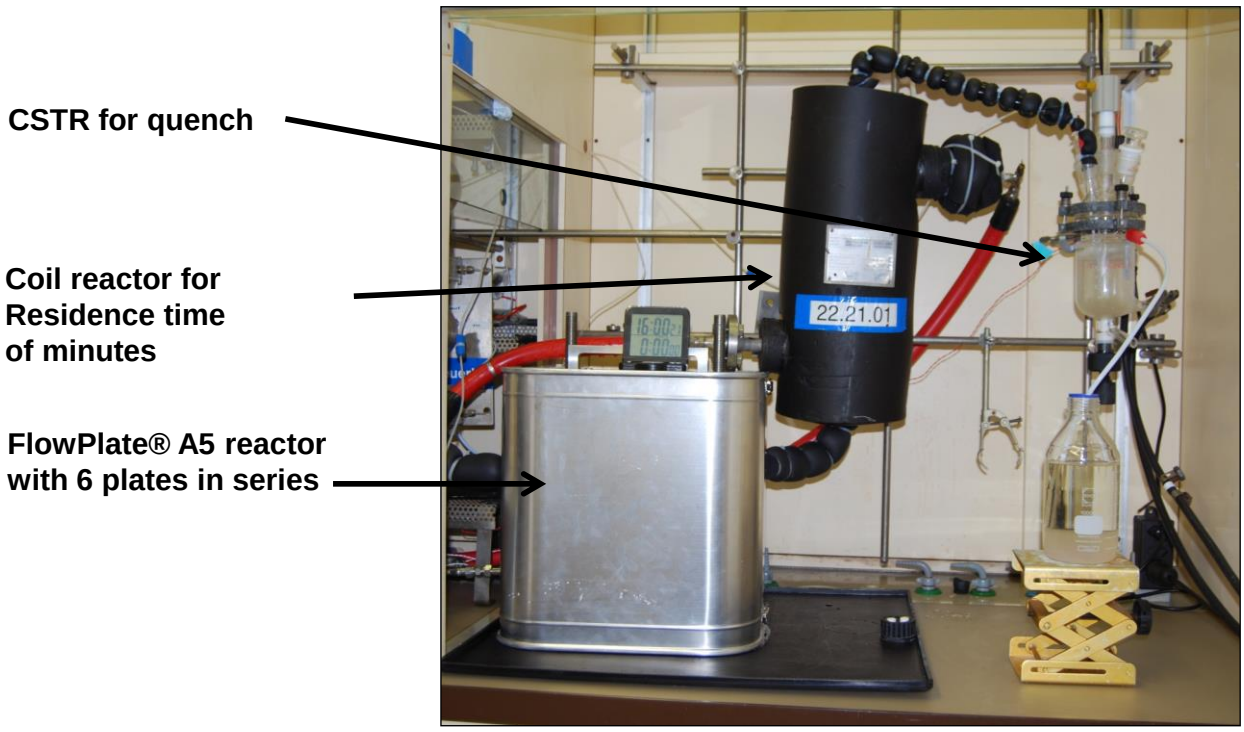

Table of Contents Graphic

*PATRICK PLOUFFE, ARTURO MACCHI**

Centre for Catalysis Research and Innovation, Department of Chemical and Biological Engineering, University of Ottawa, K1N6N5, Ottawa, Canada

*DOMINIQUE M. ROBERGE**

Chemical Development, Lonza AG, CH-3930, Visp, Switzerland

This manuscript has been published Org. Process Res. Dev. 2014, 18, 1286.

Abstract

A toolbox approach for the transfer of batch to continuous chemical synthesis is presented. The approach considers reaction kinetics (Type A, B, C), reacting phases (single phase, liquid-liquid, gas-liquid and liquid-solid) and the reaction network (parallel and consecutive reactions) in order to select the most appropriate reactor module (Plate, Coil or CSTR) for continuous operation. Then, three case studies using these three fundamental reactors are presented, but require special considerations. For the reaction of dimethyl-oxalate with ethylmagnesium chloride, a plug-flow multi-injection technology must be used to decrease the local heat generation and improve yield. For the nitration of salicylic acid, a Plate reactor with mixing elements favoring some back-mixing followed by a plug-flow system at elevated temperatures is used instead of a tandem mixed-flow CSTR and plug-flow Coil reactors in order to minimize the risk of thermal decomposition of intermediates with a reduced volume penalty. Finally, a ring-closing metathesis reaction is discussed for which the utilization of a CSTR allows the removal of catalyst-poisoning ethylene formed during the reaction and keeps the substrate concentration low to increase the yield above that of a batch or plug-flow system.

2.1 Chemical process development and scale-up challenges

2.1.1 Batch synthesis: current profile of the pharmaceutical and fine chemical industry

In the pharmaceutical and fine chemical industry, new molecules are continually discovered, developed and investigated. Malet-Sanz and Susanne [1] describe that pharmacokinetics development at Pfizer's Medicinal Chemistry Department requires initially only a few milligrams of newly discovered drugs, which are quickly scaled to hundreds of grams for further toxicology studies. Afterwards, synthesis may progress to small-scale production; Lonza [12–14] produces kilograms of material for pre-clinical trials and up to tons for the following clinical trials phases II and III.

As depicted above, molecules will be synthesized in increasing amount when progressing in the development chain. Such scale-up is non-trivial as it covers nine orders of

magnitude from milligrams to tons. This is problematic since heat generated/required scales to the power of three with the equipment's characteristic dimension (i.e., proportional to the volume) whereas heat transferred scales only to the power of two (i.e., proportional to the area). Temperature is one of the main variables governing reaction kinetics and selectivity, and requires proper control for quality assurance. To compensate or avoid potential hazards, systems can be diluted by a solvent to dampen the temperature changes. Although this may solve heat transfer problems, it reduces reactant concentration, slowing the reaction rate, increases the amount of separation steps and generates more waste[15].

In addition to scalable processes, the industry needs versatile equipment that can be used for multiple and widely diverse reactions. While manufacturing lines have dedicated reactors in some cases, the research and development of new molecules is done in a different environment; equipment is setup for a particular synthesis for weeks before being cleaned and prepared for an alternate synthesis. Only a few of the hundreds of candidate molecules may transfer to a commercial manufacturing process.

Ultimately, if a drug progresses through all the different screening tests and reaches commercialization, it will be necessary to demonstrate that the large scale process performs similarly offering at least the same product quality as the clinical trials. This can be particularly difficult if the molecular development was performed in batch reactors whereas the commercial process is to operate in a continuous manner.

2.1.2 Flow chemistry and micro-reactor technology: a viable alternative?

The development needs of the industry have been for many years addressed using batch processes. Jacketed beakers, stirring platforms, extraction bulbs and rotavaps are part of the usual equipment of batch chemistry. They are easily assembled and cleaned, and their performances have long been established. Batch processes present however limitations that are incompatible with process intensification and scale-up [14,16].

To avoid potential dilution and scale-up problems during process development, it is desirable to use continuous processes from the early molecule discovery. This is not without challenges. Consider a typical 100 kg production campaign extending over 4

weeks. Under normal working conditions, this represents a production rate of around 10 g/min. Using a standard 1/8" tube as the reactor, the Reynolds number will be around 150 (for water at ambient conditions), which is well into the laminar flow regime with diffusion-dominated mixing, mass transfer and heat transfer rates. These modes of transport are relatively slow and undesirable as they limit the control over the mixing of reactants in the channel, reaction speed and selectivity.

For a given flow rate, reducing the diameter of a tube increases the Reynolds number, reduces diffusional distances and increases its specific heat transfer area (area-to-volume ratio). For a diameter smaller than 1 mm, it increases above 10^3 m^2/m^3, allowing high heat transfer rates and tight temperature control. Reactors with internal channels of these dimensions are referred to as micro-reactors and have received increasing attention from both academia and industry due to their capacity for process intensification [17–21]. In a trade-off for better transport properties, the pressure drop through small channels is much higher. For a given flow rate, it may thus be impractical to reduce the reactor channel dimensions to reach turbulent flow and an alternative approach must be used to further increase transfer rates.

Enhancement of advective over diffusional transport of heat and mass can be achieved using various techniques. It can be challenging to select the best approach, but fortunately they all aim at a similar objective: change the velocity vector field both in magnitude and direction in order to generate secondary flow patterns, stable or unstable, which will create off-stream movements of mass and heat within a channel, resulting in a system that behaves closer to a transitional or turbulent flow rather than laminar [11].

Mixing enhancement techniques are divided into passive and active methods [22]. Passive methods utilize part of the flow energy from the pressure provided by an upstream pump. Flow multi-lamination is a technique mostly used in laminar flow to drastically reduce the diffusion distance of incoming streams where the dimension of the microstructure dictates the size of the lamellae [23]. This approach can be enhanced by a focusing technique that further stretches the lamellae [24]. For advective methods, flow through curved channels is among the simplest of these techniques, which can generate

vortices and droplet/bubble recirculation in multi-phase systems [25–29]. Other techniques include splits and recombine, obstructed, re-entering, contracted or packed flow, irregular or rough wall surface, recirculation and colliding jets [30]. Active methods function with an external source of energy. An example is the impeller of a continuous stirred tank reactor (CSTR) that is driven by an external engine. In mini and micro-channels, actuators and pulsing walls work with mechanical energy, while ultrasounds, microwaves and piezoelectric systems have also shown mixing enhancement capabilities [31,32]. Passive techniques are generally simpler and offer lower possibility of mechanical malfunction and are thus preferred at the smaller scales over miniaturization of active techniques.

2.1.3 Modularized process intensification: use the right tool at the right place

Not all unit operations within a process may benefit from continuous flow or miniaturization. Each section of the process must be considered and optimized according to its specific operating conditions and requirements. This is known as modular flow technology and we believe it is the quintessence of process intensification. In order to successfully apply the principles of process intensification, three particular aspects (reaction kinetics/hazards, phases present and reaction network) are analyzed.

Section 2.2 below addresses the impact of reaction kinetics/hazards on the selection of reactor volume. Fast reactions will benefit most from heat and mass transfer enhancements in micro-reactors. Reactions requiring tighter temperature control or with unstable intermediates may also benefit from miniaturization, whereas safe and slow reactions needing large volumes to reach the desired conversion may still be best performed in a batch reactor because of its low cost requirement (scales with volume to the power of 0.3 [3]). To facilitate this decision, reactions are categorized into Types A, B and C based on common process requirements, kinetics and hazards as described by previous publications of this group [2,3,13,33]. Details are given in Section 2.2, but importantly Type A are very fast, Type B intermediate and Type C slow reactions. Kockmann et al. [33] described an additional Type D category for reactions not within Type A, B or C, but may still benefit from micro-reactor technology via harsher reaction conditions; typically the Type D reactions need to be intensified to at least Type C

reactions to be practically transposed into flow. Consequently, this reaction type is omitted from the present Toolbox approach.

Section 2.3 below discusses the reacting phase(s) involved in the system. Single phase operation does not require the same mixing technology as multi-phase (liquid-liquid, gas-liquid or solid-liquid) and the appropriate phases contacting strategy must be chosen accordingly.

This reaction category/mixing methodology allows to quickly identify inadequate equipment and accelerates commissioning the optimal process configuration in an environment where projects are typically performed in a time-scale of weeks. The outcome of this methodology can be summarized in a toolbox matrix depicted in **Table 2.1**. Three distinct types of continuous reactors, shown in **Figure 2.1**, are proposed to address these specific systems: namely **Plates**, **Coils**, and continuous stirred tanks (**CSTR**). Once the row and column of a given reactive system are known, the matrix indicates which reactor module is most appropriate for that combination. The key to this modular toolbox approach is to use continuous flow and/or miniaturization only where appropriate and to couple it with standard semi-batch or batch technology elsewhere.

Table 2.1 The reaction/reactor matrix: preferred flow modules for a reaction type.

Rates/Phases	Homogeneous	Liquid-Liquid	Gas-Liquid	Solid-Liquid
Type A	Plate SZ	Plate LL or HEART structures	Plate Venturi with TG mixing units	CSTR or packed bed
Type B	Plate SZ Coil	Plate LL or HEART structures Coil pulsated	Plate Venturi with TG mixing units Coil pressure	CSTRs or packed bed
Type C	Static mixer Coil	Static mixer Coil pulsated	Static mixer Coil pressure	Coil pulsated

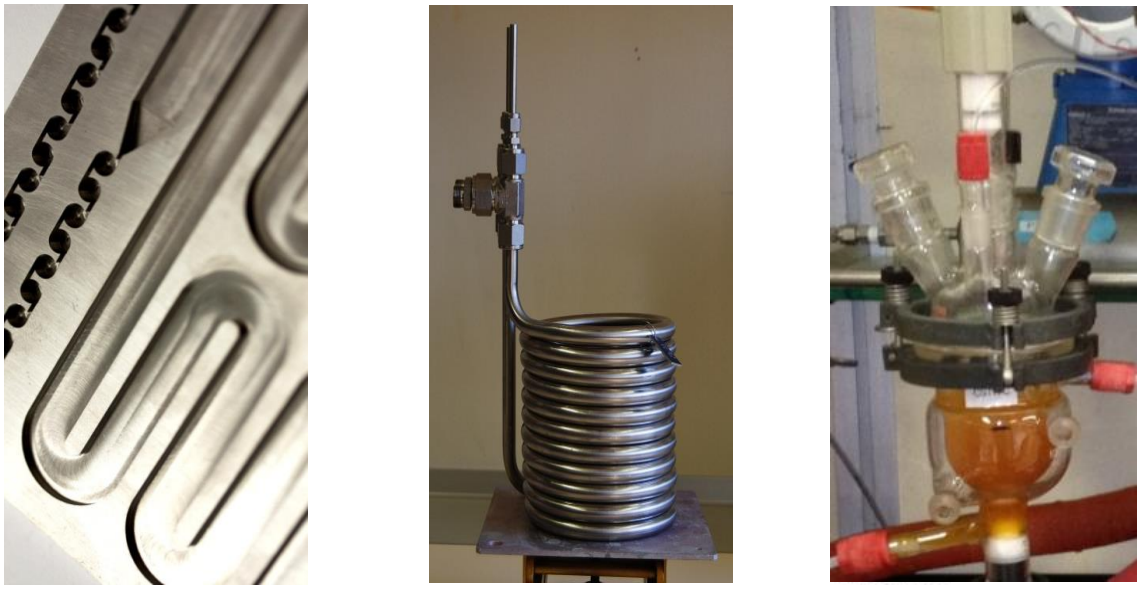

Figure 2.1 The three fundamental reactor modules.

After the proper reactor module is chosen, the required dimensions (hydraulic diameter of cross-sectional area and length) can be calculated based on transport and reaction kinetics. This is done using the different Damköhler numbers shown in **Table 2.2** [16], which are ratios of different time scales and must be greater or less than unity for satisfactory performance. For example, reactions with a large intrinsic rate constant (i.e., Type A reactions) can be satisfied by a small reactor volume (Da_I), but will likely also require a small mixing time (Da_{II}), small channels and/or high heat transfer coefficients (Da_{IV}).

If these dimensionless numbers are kept constant between research steps, the performance of the system (conversion and selectivity) should be conserved. Kockmann et al. [14,34] used these criteria to develop standard **Plate** and **Coil** sizes for the toolbox approach based on a single-channel strategy to avoid parallelization upon scale-up. At further stages of development, the specificity of the system and the approach chosen with **Table 2.1** do not change. Thus, the reactor modules previously selected don't need to be rethought, but only scaled to the new production rates.

Table 2.2 Damköhler numbers for reactor sizing and performance evaluation.

Time or Rate Ratio	Damköhler Number
Residence time/time for consumption	$Da_I = k_{rxn}C^{m-1} \cdot \frac{V_R}{Q} \gg 1$
Time for mixing/time for consumption	$Da_{II} = t_m \cdot k_{rxn}C^{m-1} \ll 1$
Rate of heat generation/removal	$Da_{IV} = k_{rxn}C^m \cdot \Delta H_{rxn} \cdot \frac{4\rho d_h}{U\Delta T_w} \ll 1$

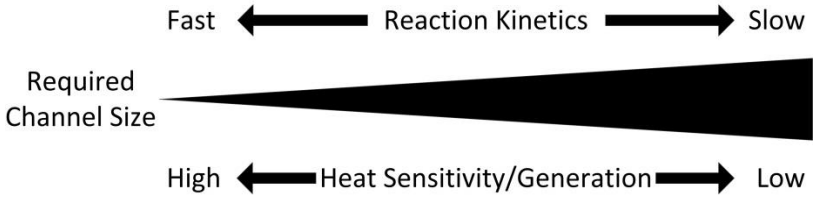

The Damköhler IV number is a difficult parameter to scale at larger flow rates. Upon scale-up, it is possible to keep the specific surface area of a reactor constant, but only in a small domain of hydraulic diameters. For commercial scale throughput, after the clinical Phase III, a compromise using the multi-injection approach will be needed to control exothermic reactions. This is analogous to a semi-batch reactor where the reaction is controlled by the addition of one reagent.

Section 2.4 below presents methods to optimize the design and operating conditions of the reactor module prescribed by the toolbox according to the reaction network in order to minimize the formation of undesired side-products.

Section 2.5 finally discusses three case-study scenarios that have particularities requiring extended flexibility and creativity from the toolbox in order to be intensified via continuous flow chemistry.

2.2 Reaction classes based on rate

While each reaction has unique features, it is possible to generalize classes that call for common process requirements. In this work, we define three reaction types as follows.

2.2.1 Type A reactions

Type A reactions are very fast, typically in the milli-second to second range, and their overall rate is mixing/mass transfer controlled. They often involve chlorine, bromide, or amines molecules, neutralizations and organometallic reactions [35]. For fast and

exothermic reactions, the use of a micro-structured reactor is necessary for proper thermal control. Small dimensions yield fast and efficient mass and heat transfer necessary to avoid hot spots, undesired products and/or run-away reactions. The industrial micro-reactors are typically **Plate** type reactors [13,33,34,36–42] in analogy to the plate type heat exchanger, where an order of magnitude greater heat transfer rate is expected compared to the shell-and-tube exchanger [43]. For Type A reactions, this means a reduction in reactor volume by a factor of ~10 leading to an important increase in space-time yield. The reactors identified in **Table 2.1** for Type A reactions are designed to provide rapid mixing and heat transfer within a small reactor volume.

2.2.2 Type B reactions

Type B reactions are slower than Type A, but still fast enough to require significant heat removal and precise mixing control. They typically need between several seconds and minutes to complete. Reaction kinetics are likely rate-limiting and thus can be accelerated via a rise in temperature, pressure and reactant concentration; although interphase mass transfer may become rate-limiting in multi-phase systems. Using conventional heat exchangers can result in large undesired temperature gradients, whereas proper selection of a micro-reactor may bring enhanced heat transfer performance with sufficient mass transfer at reasonable pressure loss as demonstrated by Palmieri et al. [44] for a Hofmann rearrangement or by Renken et al. [45] for the synthesis of an ionic liquid. A **Plate** design with different channel widths can be used to accommodate the reaction evolution, i.e., the multi-scale approach. For example in **Table 2.1**, a **Plate** with a small channel width is used at the beginning when heat generation is fast, followed by a gradual increase of the channel width and thus reactant residence time to accommodate slower reaction rates while maintaining the required rate of heat transfer for isothermal operation. Hence, with such a design, heat transfer is optimized while pressure drop is minimized and a reaction volume increase of several mL is achieved. In addition, the **Plate** can be combined with conventional **Coils** to gain volume of several liters.

2.2.3 Type C reactions

Type C reactions are typically slow and require several minutes and sometimes hours for completion, but also involve potential hazards like autocatalysis or thermal accumulation. Continuous processing may bring clear safety advantages from the beneficial thermal control at any point in space. For such reactions, **Table 2.1** suggests static mixers that can be followed by residence time modules such as **Coils**, which will provide the required reaction time in addition to thermal control. Examples of such reactions are the various protocols developed via microwave chemistry where flow can be exploited as a mean of scale-up [46]. Indeed, continuous flow micro-reactors can mimic the high pressure and temperature conditions of a microwave unit.

2.3 Reacting phases

Phase contacting pattern and intensity will impact the temperature and concentration profiles, pressure drop and ultimately reaction conversion and selectivity. Single- and multi-phase systems require different mixing approaches and the selection of the right mixer is necessary to obtain optimal reactive conditions.

2.3.1 Single phase systems – mix-then-reside

For single phase reactions, a **Plate** reactor with a "mix-then-reside" approach is usually appropriate [11,47]. That is the presence of mixing elements at the entrance of the reactor where the streams meet in order to provide fast mixing along with high heat transfer rates. It is followed by an empty rectangular serpentine channel that provides sufficient residence time for the completion of the reaction. Such an approach is depicted in **Figure 2.2**. For the slower reactions, a simple **Coil** is often sufficient for additional gain in volume. This approach maximizes transport phenomena at the initial point, where high concentration gradients and potentially high heat generation are present, but minimizes the pressure drop afterward, once the reaction rate has substantially decreased. For particular reaction networks, it is possible that a combination of multiple reactor modules will provide the maximum yield (refer to Sections 2.4 and 2.5.2).

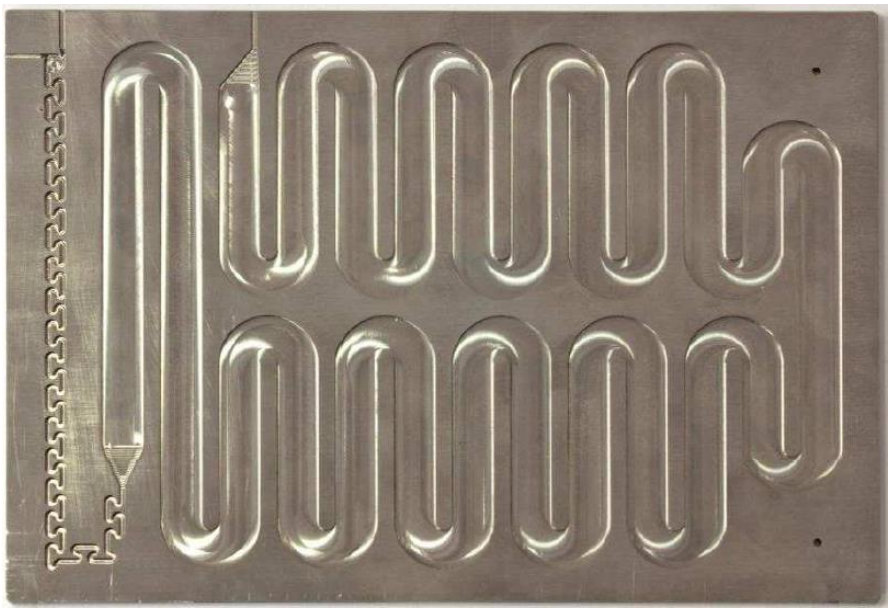

Figure 2.2 Lonza FlowPlate® A6 module for mix-then-reside with SZ mixing elements. The SZ elements enable near plug-flow conditions [11].

2.3.2 Liquid-liquid systems – mix-and-reside versus active mixing

For multi-phase reactions, a reactor with a "mix-and-reside" approach is preferable [39]. When the previous "mix-then-reside" type reactor is used, the dispersion generated in the mixing zone would likely coalesce upon entering the agitation-free residence time zone, reducing the interfacial area (mass transfer) and effectively bringing the reaction towards a halt. The balance between break-up and coalescence of the dispersed phase is a function of local agitation and energy dissipation rate [48] and, to maintain a dispersion throughout a reactor, it is often necessary to continuously mix the phases (e.g., see **Figure 2.3**). The **Plate** channels must then compromise between being small enough for fast and intense mixing (i.e., rendering the interphase mass transfer resistance low) and large enough to obtain sufficient residence time for the desired conversion.

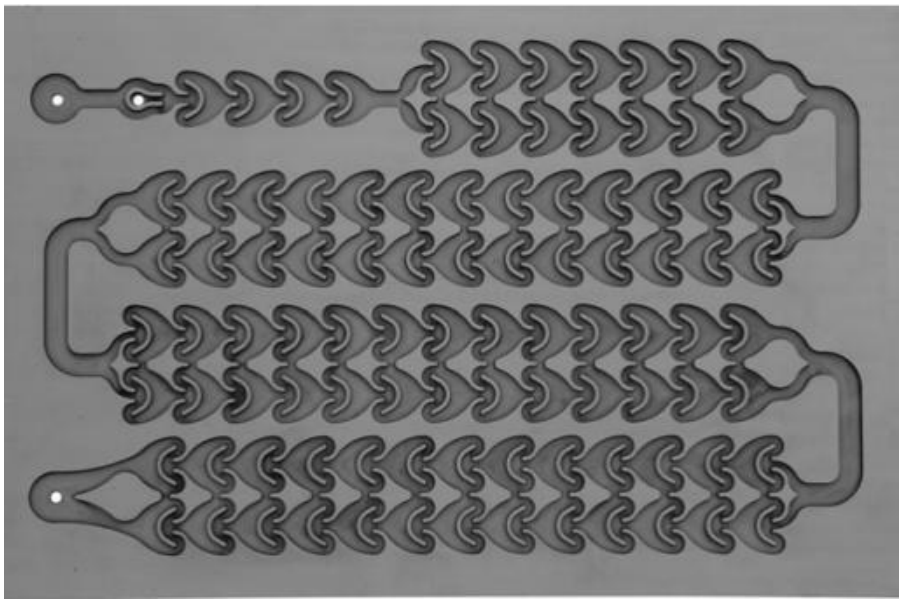

Figure 2.3 Corning® Advanced-Flow™ Reactor for mix-and-reside with HEART-shape mixing elements [38,39].

For the slower multi-phase reactions, the "mix-and-reside" approach is still appropriate, but not with **Plate** reactors. For such systems, interphase mass transfer rates do not need to be rapid, but rather sustained over a large volume to achieve conversion. Keeping with the passive mixing techniques, this can be completed by a **Coil** coupled with static mixing elements. However, at larger equipment scales, active mixing techniques might also be suitable. The mixing intensity of active techniques is decoupled with the fluid residence time, making it possible to adjust these two parameters independently. A promising technology is to pulse the flow, which has been implemented in reactors by NiTech Solutions Ltd (see **Figure 2.4** [49,50]) and by AM Technology [51]. The oscillation (amplitude/frequency) changes the velocity and shear field in direction and magnitude, as with other mixing techniques, and generates a dispersion throughout the reacting volume.

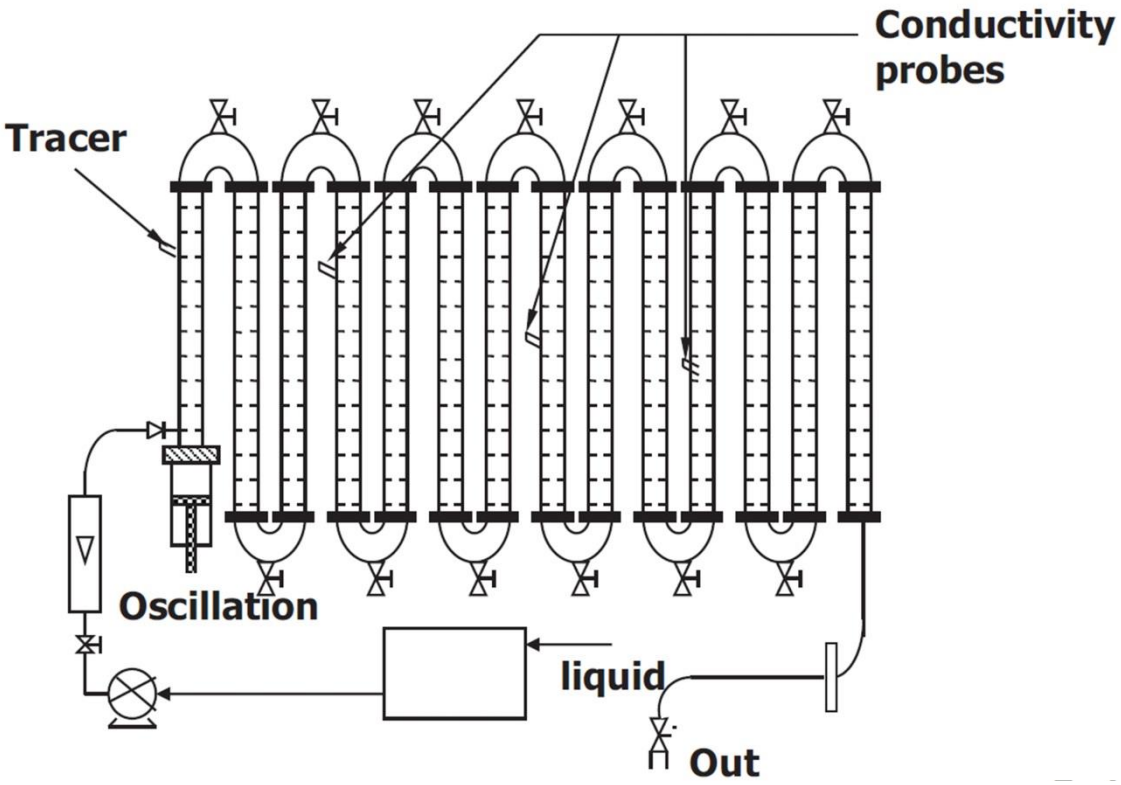

Figure 2.4 A pulsating reactor from NiTech [49,50].

2.3.3 Gas-liquid systems – use of pressure

For gas-liquid reactions, harsher reaction conditions, particularly greater pressures, can be used in tandem with **Plate** or **Coil** reactors to improve performance. At elevated pressures, smaller bubbles can be generated resulting in greater interfacial area for mass transfer [52]. Smaller bubbles also result in greater mass transfer coefficients due to reduced diffusional distances. This is particularly useful in the case of fast gas-liquid reactions by minimizing the interphase mass transfer resistance. Furthermore, the partial pressure of the gaseous reactant also increases, resulting in a greater solubility and thus driving force for mass transfer. For slower gas-liquid reactions, it essentially accelerates the kinetics. In the most ideal case, the gas is pressurized and the mass transfer increases to an extent where the liquid phase saturates and the reaction is considered homogeneous.

The initial gas-liquid dispersion can be created in a Venturi type mixer [53], which enables the formation of small gas bubbles that can react or saturate the liquid rapidly.

Such a structure can be followed by tangential (TG) mixing units that favor the back-mixing of gas in the center of the mixer so that it can be "held" to further react with the liquid recirculating within each element, as demonstrated by the referenced video.

2.3.4 Liquid-solid systems

Reactions involving solids and precipitations usually cannot be reliably performed in small-scale channels and micro-reactors due to the risk of plugging. A **CSTR** is a pragmatic approach to overcome the problem associated with solids handling, but its mixed-flow pattern has disadvantages relative to the near plug-flow pattern of some **Coil** and **Plate** reactors (refer to Section 2.4). The **CSTR** is quite useful when the reaction is very fast and the selectivity is not negatively influenced by the mixed-flow pattern, such as for acid-base precipitations [54]. In other cases, pulsated flow may be a viable alternative, since its reciprocating nature reduces the chance of plugging in small channels while maintaining near plug-flow conditions.

A special case for liquid-solid or even gas-liquid-solid systems is the use of a packed bed for heterogeneous catalysis such as in Suzuki or Heck reactions or frequently in hydrogenations. Our experience has shown that this kind of reaction in flow can often be intensified to such an extent that they can become mass transfer limited (Type A/B as shown in **Table 2.1**).

2.4 Reaction network

A reaction rarely occurs individually and is usually part of a network of parallel and consecutive reactions. The reactor design will influence the distribution of compounds and affect the network in various ways. Pursuant to Section 2.3.4, limiting flow patterns within reactors are ideally classified as mixed-flow (**CSTR**) or plug-flow (**Coil**). Intermediate flow patterns can be modeled by deviations of the limiting cases such as tanks-in-series and dispersion models [55,56].

2.4.1 Concentration profile

In a mixed-flow reactor, the concentration is constant throughout the entire volume and equal to that at the outlet, resulting in a relatively low reactant concentration. In a plug-flow reactor, the reactant concentration is highest at the entrance and gradually

decreases along the reactor, resulting in a greater volume-averaged concentration and thus conversion for reaction orders above zero. In **Table 2.3**, a steady state mass balance on a compound A is used to model the concentration profile through an isothermal reactor with a constant volumetric flow rate. Batch reactors behave similarly to plug-flow reactors, but the reaction time replaces residence time in the reactor (V_R/Q).

Table 2.3 Steady state mass balance on A for a mixed-flow and plug-flow reactor

General	Mixed-flow	Plug-flow
$Q\frac{dC_A}{dV_R} = r_A$	$C_A = C_{A0} + \frac{r_A V_R}{Q}$	$\int_{C_{A0}}^{C_A} \frac{dC_A}{r_A} = \frac{V_R}{Q}$

2.4.2 Increasing selectivity

Undesired reactions can be minimized by changing the design and operating conditions of a reactor. Consider a reaction network where a compound A reacts to produce either a desired (D) or undesired product (U) as depicted in **Table 2.4**. The instantaneous selectivity of D over U is obtained by the rate of formation of D over that of U.

Table 2.4 Parallel reaction network and expression for selectivity

Scheme	Rate and Selectivity
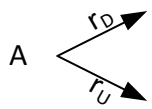	$r_A = -(r_D + r_U)$ $r_D = k_D C_A^{m_D} = A_D \exp\left(-\frac{E_D}{RT}\right) C_A^{m_D}$ $r_U = k_U C_A^{m_U} = A_U \exp\left(-\frac{E_U}{RT}\right) C_A^{m_U}$ $S_{D/U} = \frac{r_D}{r_U} = \left(\frac{A_D}{A_U}\right) \exp\left[-\frac{(E_D - E_U)}{RT}\right] \left[C_A^{(m_D - m_U)}\right]$

When the order of reaction for D is greater than for U, a high volume-averaged concentration of A is preferred and a plug-flow reactor is likely the best approach. Alternatively, when the order of reaction for D is lower than for U, a low volume-averaged concentration of A is necessary to minimize side-reactions and a mixed-flow reactor should perform better [55,56].

If the reaction activation energies are known, the temperature can also be adjusted to favour one reaction or the other. The reaction with the highest activation energy will be most affected by temperature and thus advantaged by elevated temperatures.

2.5 Case studies

The toolbox approach described earlier selects the best flow chemistry approach for a given reaction by considering its rates, phases and network. However, reactions do not always fit into such idealized categories and sometimes have case-specific particularities that present a challenge for flow chemistry and process intensification. The section below presents three case studies (a Type A and two Type B reactions) with individual transport, flow pattern, or reaction network characteristics that require additional consideration for their transfer to continuous operation.

2.5.1 Intense exothermicity - Grignard reaction

Grignard reactions are an important synthesis method to create C-C bonds. This work presents a class of Grignard reactions that is very rapid and exothermic where the organometallic molecules acting as a base react with electrophilic carbonyl groups. Undesired reactions can occur when the Grignard reacts further with the initial product to form other molecules in a consecutive reaction network. The rate at which the Grignard is mixed with the raw material is ideally much greater than the intrinsic reaction rate. This is usually accomplished by using cold or cryogenic conditions, which decrease the reaction kinetics and allow relative faster mixing. In addition to high mixing rates, the reaction must ideally be operated under high heat transfer rates in order to avoid hot spots, which will decrease the selectivity. This class of Grignard reaction is thus a single phase Type A reaction that is mixing and heat transfer limited.

The synthesis of methyl 2-oxobutanoate (2-MOB, **3**) was performed in a micro-reactor using dimethyl-oxalate (DMO, **1**) and the Grignard reagent ethylmagnesium chloride (**2**). The effect of temperature, initial DMO concentration and Grignard distribution was investigated on the yield. The reaction network (main and potential side/consecutive reactions) is shown in **Scheme 2.1**.

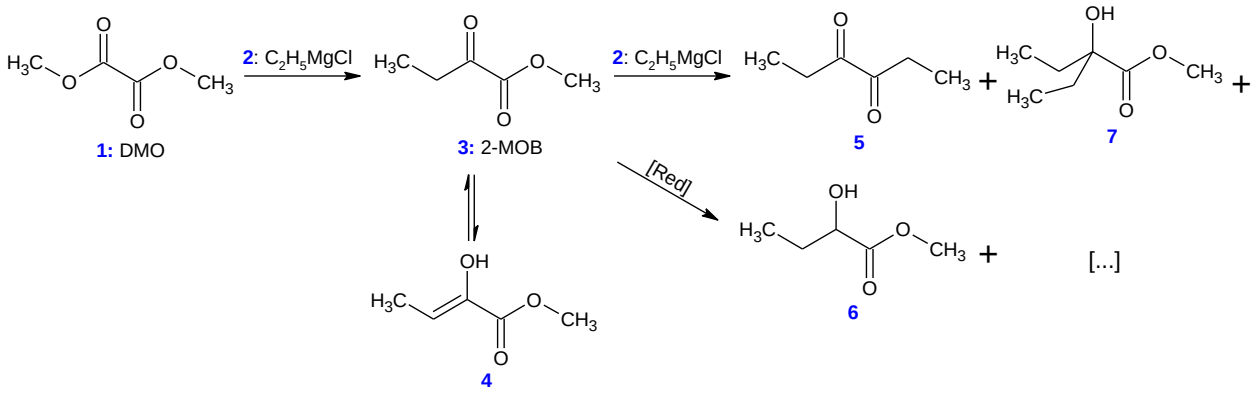

Scheme 2.1 Reaction network for the synthesis of methyl 2-oxobutanoate.

The DMO feed was a 10, 15 or 20 wt% solution in dimethoxyethane. The Grignard feed was a 19 wt% solution in THF (58 wt%) and dimethoxyethane (23 wt%). Each feed flow rate was adjusted to obtain a stoichiometric ratio of 1.05 mol **2**/mol **1**. The reactor was a glass micro-reactor **Plate** by Corning [40,57] with an internal volume of 3 mL and the average residence time was approximately 4 seconds (total flow rate 40 g/min). The Grignard feed was contacted with the DMO feed either all at once (1-injection) or divided in four and distributed along the reactor (4-injections). The feeds and the reactor were cooled to 5°C, -5°C or -15°C. The reaction mixture was quenched at the outlet with a 1 mol/L HCl solution.

The yield, calculated as the GC area% of **3** and of the conjugated enol (**4**), is shown on **Figure 2.5** for the different experimental conditions. Experiments operated at higher temperatures had lower yield, as expected, due to mixing limitations resulting in the formation of other compounds (**5**, **6** and **7**). The yield also decreased at higher initial DMO concentrations. Concentrated solutions produced more intense hot spots due to heat transfer limitations, which adversely affected the yield. Distributing the Grignard reactants through multiple inlets (4-injections) rather than all at once (1-injection) increases the yield significantly by reducing the local heat generation.

Multi-injection of the reactants in a plug-flow reactor limits local concentrations and dampens the local heat release. This approach is analogous to a semi-batch reactor where one of the reagents, in this case the Grignard compound, is dosed to control the heat release [57]. For some Type A reactions, even with micro-reactors, the mixing

process (which is volume based) will be faster than the heat exchange process (which is surface controlled) leading ultimately to a hot spot. Upon scale-up, this multi-injection approach can also be utilized to cope with the loss of specific surface area of a larger reactor [40].

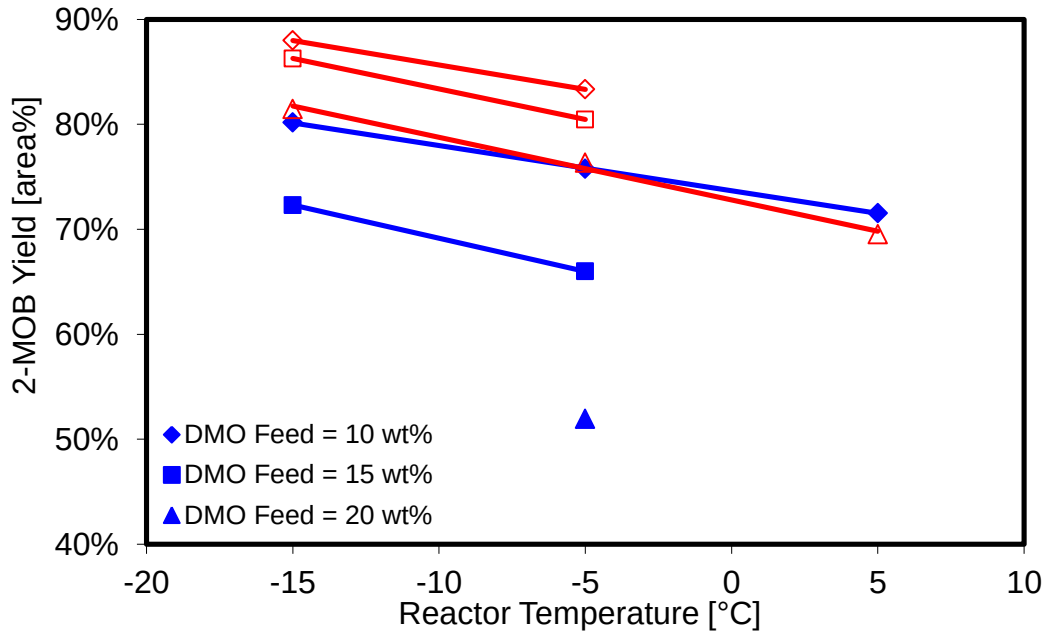

Figure 2.5 2-MOB yield for the various experimental conditions (blue/solid points: 1-injections, red/empty points: 4-injections. Total flow rate of 40 g/min

2.5.2 Decomposition hazard - salicylic acid nitration reaction

The reaction of salicylic acid (SA, **8**) with nitric acid (**9**) to form 5-nitrosalicylic acid (5-NSA, **10**), an intermediate for chemical and pharmaceutical processes (eg. 5-aminosalicylic acid), presents a challenging selectivity and temperature control. The nitration reaction network, shown in **Scheme 2.2**, can produce other compounds such as 3-nitrosalicylic acid (**11**), 2-nitrophenols (**12**) and 3,5-dinitrosalicylic acid (**13**). Amongst these by-products, picric acid (2,4,6-trinitrophenol, TNP, **14**) presents the potential for violent thermal decomposition [58].

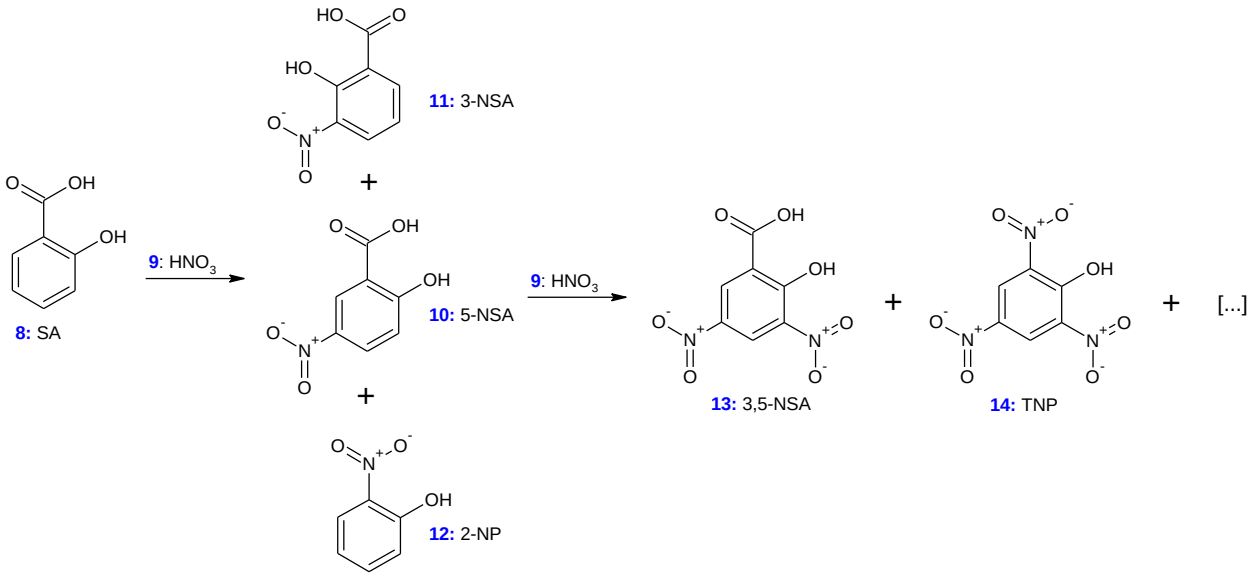

Scheme 2.2 Reaction Network for the synthesis of 5-nitrosalicylic acid.

The synthesis can be performed in a solution of nitric and acetic acid under intensified conditions in order to avoid waste disposal and hazards associated with traditional mixtures of nitric and sulfuric acids [59]. The nitration of aromatic compounds has the potential for autocatalytic behavior and run-away scenarios due to their high exothermicity [18,58,60]. Consequently, a continuous process using a micro-reactor brings added safety by reducing the working volumes associated with the synthesis as well as increasing the specific heat transfer area.

The reaction network producing 5-NSA acid has a reaction half-life of 0.5 seconds under undiluted conditions at 65°C [60]. Presence of water, however, has been shown to reduce the activity of the nitric acid by preventing the formation of the nitronium ion (NO_2^+) [59,61]. The homogenous reaction is thus considered a Type A or B at different water concentration and temperatures. The nitration of aromatic compounds follows generally a zero or first order reaction rate with the organic molecule and the literature shows no indication that dilute or high concentrations should favour 5-NSA over by-products [61]. Since polynitration can occur, however, reaction time should be limited to prevent these consecutive reactions.

A solution of salicylic acid (10 wt%) and acetic acid (90 wt%) was contacted with an aqueous solution of nitric acid (65 wt%) in a glass micro-reactor **Plate** by Corning [40,57] with an internal volume of approximately 3 mL. For additional residence time, the plate was followed by a **Coil** with an internal diameter of 1.59 mm and volumes of 10 or 20 mL. The plate and coil were submerged in a thermal bath of constant temperature.

The conversion of salicylic acid is shown on **Figure 2.6** as a function of residence time and temperature. At 45°C, there is a lag period of approximately 50 seconds during which there is no conversion. This profile is observed typically for autocatalytic reactions, where the reaction rate is close to zero instead of maximum at zero conversion. For such cases, a mixed-flow reactor at low conversion followed by a plug-flow reactor after the lag period usually minimizes the required volume to achieve a given conversion (see Section 6.4 from Levenspiel [55] for details on autocatalytic reactions).

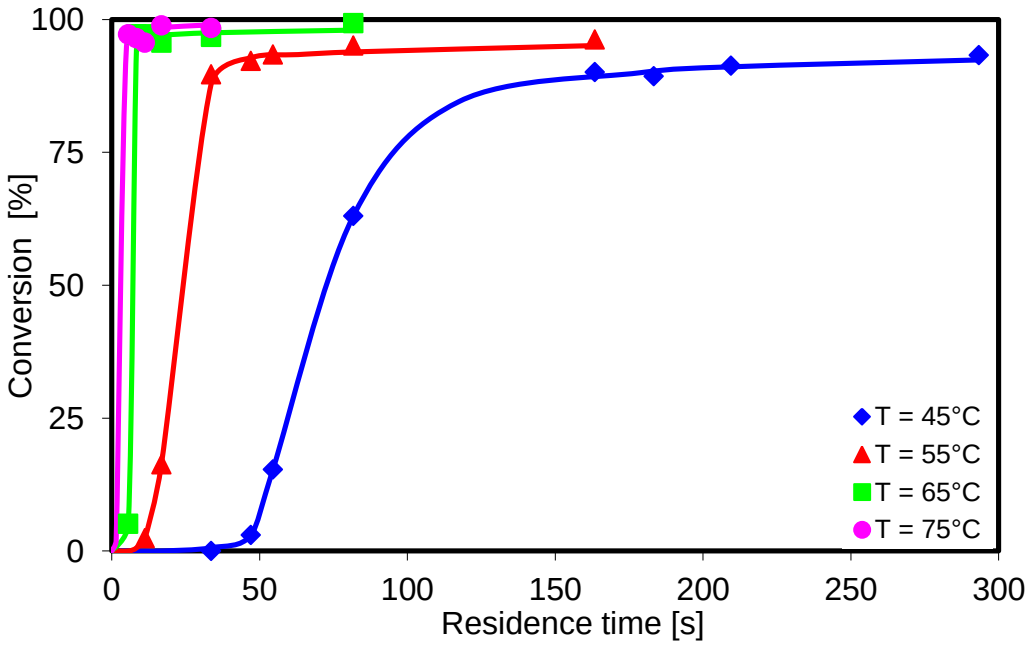

Figure 2.6 Conversion of salicylic acid as a function of residence time showing auto-catalytic behavior.

For this case however, the possibility of thermal run-away caused by unstable intermediates complicates the use of tandem reactors. For safety reasons, the reaction is preferred to be performed all within a plate type reactor for optimal heat exchange performance. The formation of intermediates or catalytic compounds can be accelerated

and the lag period diminished by increasing the reaction temperature. At 55°C, the lag time was 10 seconds and practically disappeared at 65°C and higher. The utilization of a few mixing elements favoring recirculation and producing a flow similar to a mixed-flow reactor, such as TG elements, would be more robust to initiate auto-catalysis, which could then be continued in a plug-flow reactor to allow sufficient residence time for a desired conversion.

2.5.3 Catalyst poisoning - ring closing metathesis reaction

Macro-cycles (**17**) can be synthesized from diene molecules (**15**) via ring closing metathesis (RCM, **Scheme 2.3**). Monfette et al. [62] investigated a RCM reaction in continuous flow using a homogenous ruthenium complex catalyst (**16**). Unfortunately, the catalyst deactivates due to the formation of ethylene (**18**) as a by-product, effectively stopping the reaction under certain conditions. Undesirable side reactions where the diene isomerizes (**19**) or polymerizes (**20**) into different oligomers are also present.

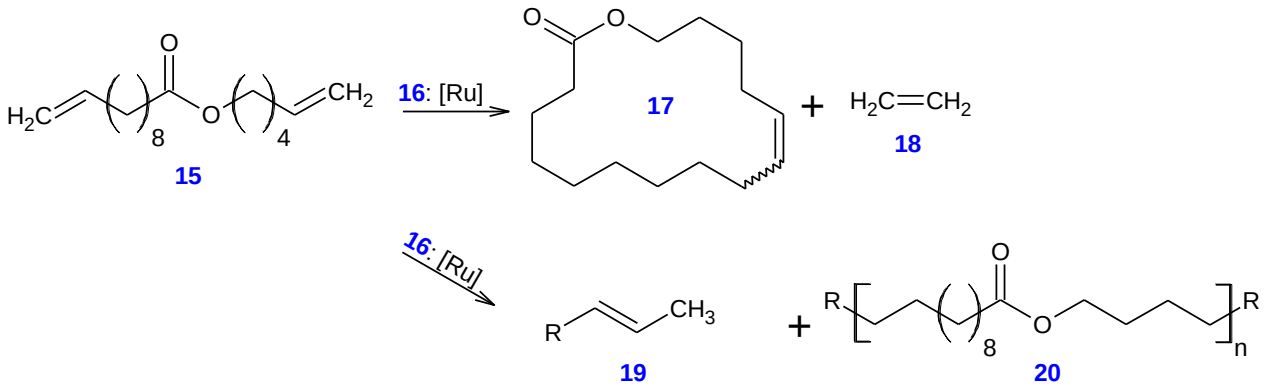

Scheme 2.3 Reaction Network for a Ring Closing Metathesis.

The experiments were conducted in toluene at 40°C, 60°C and 80°C under different reaction or residence times and catalyst and substrate concentrations. A mixed-flow stirred round bottom flask operated in batch or continuous flow (**CSTR)** and a **Coil** (plug-flow) were used to compare the effect of different flow patterns on the reaction's yield and selectivity.

Using a coil with **16** = 5 mol% and **15** = 5 mM, the reaction at 40°C was incomplete after 30 minutes, but achieved its maximum conversion at 80°C after 1.5 minutes, classing the

homogenous reaction as Type B. The reaction also showed improved selectivity at higher temperatures, suggesting that the activation energy of the desired reaction is greater than that of the undesired reactions.

Under the same catalyst and substrate concentration, reaction time and temperature, the batch reactor had a yield of 84% before the catalyst deactivated while the coil reactor obtained 79%. In the coil reactor, the ethylene product was entrapped in gas slugs and accelerated the deactivation of the ruthenium catalyst, thus limiting the maximum yield.

The coil reactor was also tested at different substrate concentration and showed decreased selectivity from 5 to 20 mM, suggesting that side reactions are favoured by higher concentrations likely due to a higher order of reaction and that a CSTR could perform better[63].

The reaction was tested using a CSTR, which allowed purging of the ethylene gas from the head space. At 80°C with **16** = 1 mol% and **15** = 5 mM, a yield above 99% was achieved. The decreased specific heat transfer area of the CSTR did not adversely affect isothermal conditions as the reaction is strongly diluted (5 mM). However, decreased concentrations slowed the reaction and the maximum yield was achieved only with a residence time of 20 minutes, while it was obtained in half the time with the coil reactor.

From these results, the RCM reaction operated into continuous flow benefits from elevated temperatures and the residence times should be in the order of minutes. The reaction could be operated under a plug-flow pattern in a Coil or Plate reactor, but the entrapment of ethylene and the presence of side reactions require instead the use of gas purging and of a low concentration reactor, for which a CSTR is best suited, although at the cost of a slower reaction.

2.6 Conclusions

Several reactions within the fine chemical and pharmaceutical industry are being conducted batch or semi-batch wise and would potentially economically and environmentally benefit from continuous flow and intensification via miniaturization. Moreover, process development and scale-up would be facilitated by the adoption of continuous flow reactors in the initial stages of molecule discovery and synthesis.

A methodology is introduced to select reactor type (**Plate**, **Coil**, or **CSTR**) and size based on the reaction kinetics/hazards and phases involved. The reactor design is also discussed in terms of operating conditions, including flow patterns, when optimizing product yields in a reaction network. Importantly, not all reactions benefit from continuous flow or miniaturization and thus process intensification should be implemented modularly as reactor geometry and operating conditions invariably affect transport-reaction kinetics interactions and their relative time scales (i.e., Damköhler numbers).

Three different reaction classes are presented and categorized according to their process requirements. Type A reactions are mass and heat transfer limited and will greatly benefit from reactor miniaturization and intense energy dissipation. Type B reactions are slower but can be accelerated by more severe reactor operating conditions (e.g., elevated temperature, concentration, and pressure) and enhanced by moderate miniaturization and mixing while maintaining sufficient reactor volume. Hazardous Type C reactions require close thermal control, which can be provided by continuous flow and volume reduction via process intensification.

High yields can be achieved for reactions involving miscible fluids through the combination of a shorter energy intensive region, followed by a longer residence time zone where the mixed-flow fluids are allowed to react to completion. However, this approach is subject to significant limitations when applied to immiscible fluids as the phases can coalesce downstream of the mixer, reducing interphase mass transfer and slowing the reaction rate. In this case, balancing continuous energy dissipation and residence time via repeated mixing arrangements is the preferred approach. The

dynamic nature of multi-phase flow, coupling of heat and mass transfer, and incorporation of solids within these systems will be topics of increasing interest to both industry and academia in the years ahead.

Finally, three case scenarios requiring special considerations are presented to demonstrate the flexibility and limitations of the proposed toolbox approach. Heat and mixing limitations required the homogenous Type A Grignard reaction to be performed via a plug-flow multi-injection **Plate** for best results. The homogenous Type A/B nitration of salicylic acid was found to be best suited for a tandem mixed-flow (**CSTR**)-plug-flow (**Coil**) reactor that is incompatible with the thermal decomposition hazard it presents. The temperature was thus increased in order to minimize the volume penalty of the used setup. Optimally, a **Plate** reactor combining initial mixing elements that provide back-mixing and a mixed-flow flow pattern followed by a plug-flow channel would be used. The homogenous Type B ring closing metathesis was found to be best operated in a mixed-flow reactor (**CSTR**) where the ethylene gas product, which poisons the catalyst, could be removed.

2.7 Author Information

Corresponding Author

* arturo.macchi@uottawa.ca; dominique.roberge@lonza.com

2.8 Acknowledgements

We acknowledge the financial support from the Natural Sciences and Engineering Research Council of Canada (IPS2-#435165) and from Lonza AG for this project. Also we would like to thank Sjoerd van Nispen for the nitration results and Norbert Kockmann for the design of structures and videos.

2.9 Nomenclature

Variables

A	Pre-exponential frequency factor (s^{-1})
C	Reactant concentration (mol/m^3)
D	Diameter of the channel (m)

d_h	Hydraulic diameter of channel (m)
E_i	Activation energy for r_i (J/mol)
k_i	Reaction rate constant of r_i (m^3/mol/s)
m	Order of reaction (-)
Q	Volumetric flow rate (m^3/s)
R	Universal ideal gas constant (J/mol/K)
r_i	Rate of formation of i (mol/m^3/s)
$S_{D/U}$	Instantaneous selectivity of D with respect to U (mol/mol)
T	Temperature (K)
t_m	Time of mixing (s)
U	Overall heat transfer coefficient (W/m^2/K)
u	Average superficial velocity of the fluid (m/s)
V_R	Volume of reactor (m^3)
ΔH_{rxn}	Heat of reaction (J/mol)
ΔT_w	Fluid-to-wall temperature difference (K)
μ	Fluid viscosity (Pa·s)
ρ	Fluid density (kg/m^3)

Acronyms

CSTR	Continuously Stirred Tank Reactor
LL	Liquid-Liquid Microstructure by Lonza
SZ	Serpentine Microstructure by Lonza[11]
TG	Tangential Microstructure by Lonza[11]

2.10 References

See thesis references.

3 Liquid-liquid mass transfer in a serpentine micro-reactor using various solvents

By *Patrick Plouffe*[a], *Dominique M. Roberge*[b], *Jonas Sieber*[b], *Michel Bittel*[b], and *Arturo Macchi*[a]

[a] Centre for Catalysis Research and Innovation, Department of Chemical and Biological Engineering, University of Ottawa, K1N 6N5, Ottawa, Canada

[b] Chemical Manufacturing Technologies, Lonza AG, CH-3930, Visp, Switzerland

This manuscript has been submitted to Chemical Engineering Journal on April 25th, 2015.

Abstract

The flow regimes are identified and mass transfer rates measured in a serpentine micro-reactor with a hydraulic diameter of 0.7 mm using the two-phase alkaline hydrolysis of 4-nitrophenyl acetate between flow rates of 0.8 to 32 mL/min. Four different organic solvents (n-butanol, n-hexanol, MTBE and toluene) were used in order to investigate the effect of phase physical properties. The continuous phase overall volumetric mass transfer coefficient, $K_c a$, was greatest in the drop flow regime and for organic solvents with lower interfacial tension resulting in larger interfacial area, a. In the parallel flow regime, $K_c a$ values increased linearly with the continuous phase capillary number. In the drop flow regime, two correlations for the prediction of the drop size were developed with fitted parameters falling within the expected values for turbulent break-up of drops in conventional static mixers.

Keywords

Micro-reactor; liquid-liquid; interfacial tension; mass transfer; flow regime; drop size

Highlights

- A liquid-liquid reaction was performed in a serpentine micro-reactor
- Four organic solvents were used: nBuOH, nHeOH, MTBE and toluene
- Slug flow, parallel flow and drop flow regimes were observed through a sight glass
- The diameter of the droplets was calculated from the experimental results
- Correlations are presented for predicting the conversion with other solvents

3.1 Introduction

In recent years, the pharmaceutical and fine chemical industries have intensified batch-wise processes using continuous flow micro-reactors and have performed multi-step synthesis of many complex organic molecules and medicinal candidates [1,15,21,64–66]. Using a modular approach [67], each stage of a reaction is analyzed and performed in a reactor with characteristics (channel size, residence time, pressure drop, mass transfer, heat transfer, flow pattern, etc.) that provide optimal conditions under safe operations. For fast reactions involving reactants in multiple phases (e.g., liquid-liquid reactions), the performance of the reactor is dependent on the overall interphase volumetric mass transfer coefficient. In order to ensure fast and efficient process development, the mass transfer rate of a reactive system is ideally predictable from a benchmark performance.

This requires a good understanding of the effect of hydrodynamics and phase physical properties on mass transfer. Past publications have focused mostly on the effect of fluid velocity or reactor dimension for a particular pair of fluids [19,20,39,47,68–75]; few have studied the impact of using various solvents with different interfacial tensions, viscosities and densities. For slug flow in a straight micro-channel, the work of Guo and Chen [76] investigated the impact of interfacial tension using surfactants, and the work of Su et al. [77] used glycerol in water to generate different aqueous/organic phase viscosity ratios. In micro-mixers however, there is a sustained dispersion of energy that can create a drop flow regime. Kockmann et al. [78] performed the liquid-liquid hydrolysis of three pure alkyl acetates (ethyl, isopropyl and n-butyl acetate), but the reaction rates were too slow to be limited only by mass transfer. At the macroscopic level, studies predicting the effect of phase physical properties are well summarized by Paul et

al. [79] for traditional unit operations (e.g., stirred vessels and mixers in pipes). However, the force ratios between gravity, inertia, viscosity and interfacial tension differ and it has not been demonstrated under which conditions traditional larger-scale correlations are accurate for micro-mixers.

The purpose of this study is thus to investigate how different liquid physical properties affect the interphase mass transfer in a micro-mixer. The chosen reactor uses a curvature-based mixing geometry producing a serpentine design. The utilization of meandering channels as mixers for micro-reactors is widely used in industry (for example see the *Art® Reactor* and the *FlowPlate® SZ or TG* [80], or the Labtrix® reactors [81]), and in academia [26,27,29,68]. They are relatively easy to design and can be manufactured using various methods in various materials (3D printing, chemical etching, mechanical machining, etc.) In this work, the mass transfer rate in a micro-reactor is measured using a test reaction and four different pairs of solvents over a range of flow rates. The results are then compared based on common flow regimes and correlated using dimensionless groups when applicable.

3.2 Experimental setup

The experimental set-up is displayed on **Figure 3.1**. SyrDos (HiTec Zang) or ISCO (Teledyne) piston pumps were used depending on flow rate and pressure requirements. The flow rate was measured by an Endress-Hauser Coriolis flowmeter and the pressure drop across the micro-reactor was measured using 6 or 20 bar Keller pressure sensors. The temperature of the feed was measured by a PT100 sensor and the micro-reactor was kept at ambient temperature using a thermal bath (23°C).

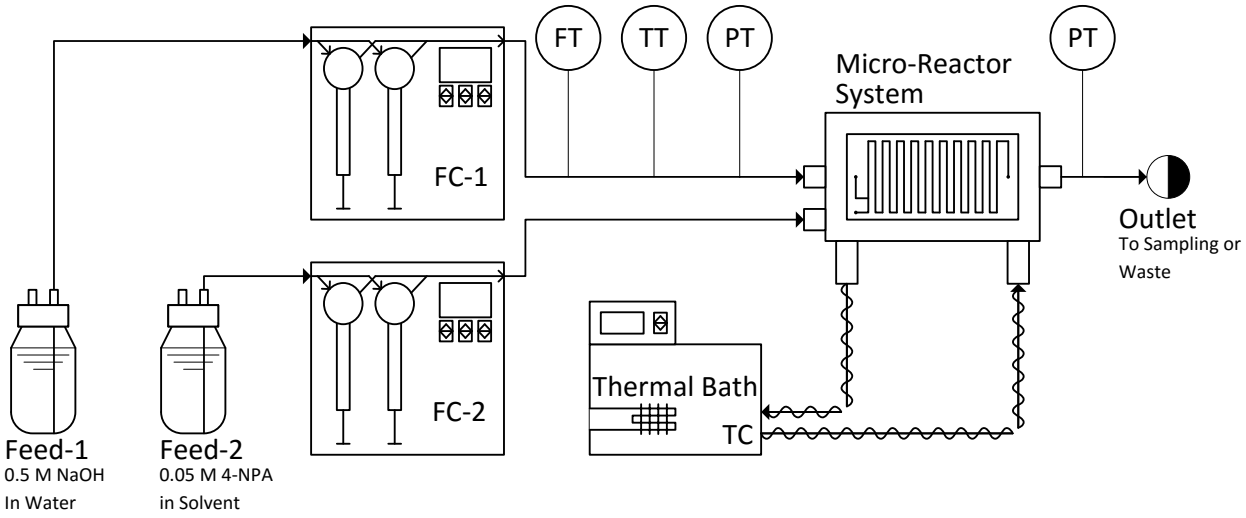

Figure 3.1 Experimental setup. Instruments identified are flow controllers (FC), flow transmitter (FT), temperature transmitter (TT) and pressure transmitter (PT).

The micro-reactor system was the Ehrfeld MMRS combined with a FlowPlate® Lab SZ reactor (see **Table 3.1**). The plate was made of Stainless Steel 316 and preferentially wetted by the aqueous phase, such that the dispersed phase was the organic solution.

Table 3.1 Micro-reactor characteristics.

Micro-mixer Geometry*	Contraction Size (mm)	Number of Mixers	Micro-Reactor Volume (mL)
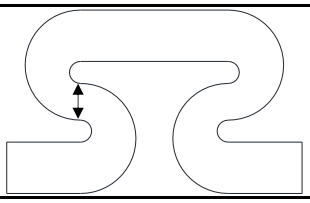	0.50 x 1.25	137.5	1.05

*Double arrows identify the contraction zone.

The chemical reaction used to assess the mass transfer rate was the two-phase alkaline hydrolysis of 4-nitrophenyl acetate (4-NPA, **Scheme 3.1**). This reaction has been used in the past and determined to be a single step second order hydrolysis in water. Compared to standard ester hydrolysis reactions [19,78,82], the presence of an aromatic ring and of a nitro group makes this reaction even more rapid with an intrinsic rate constant as high as 14.0 L/mol/s [83–85]. The reactant is not very soluble in water (less than 2.5

mmol/L at 23°C), but the product of the reaction, sodium 4-nitrophenolate, colors the aqueous phase yellow and allows visual distinction between the two phases. The molar concentrations of the main reactant and product were determined using an HP Agilent 1100 series HPLC system, which included a G1322A degasser, a G1311A quaternary pump, a G1313A autosampler, a G1316 column compartment and a G1315B diode array detector. A sample volume of 5.0 µL was injected into a 250 mm x 4.6 mm i.d. Agilent Zorbax SB-C8 column to separate the compounds. The separation was performed at room temperature. A pre-screening showed that a wavelength of 294 nm was best suited for the simultaneous detection of the product and unconverted reactant. Two mobile phases were used and composed of a 0.1 wt% trifluoroacetic acid solution in HPLC-grade water and in a mixture of HPLC-grade water (24.1 wt%) and acetonitrile (75.8 wt%).

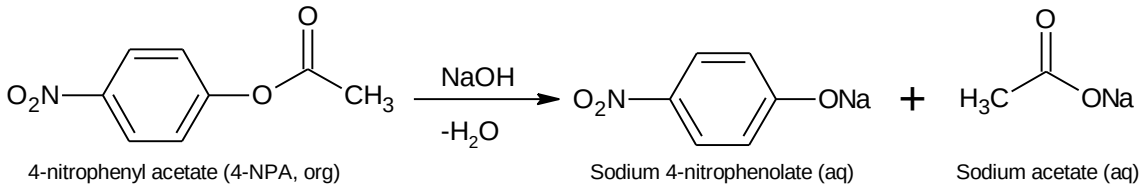

Scheme 3.1 Alkaline hydrolysis of 4-nitrophenyl acetate

The organic phase was a 0.05 mol/L solution of the acetate in either n-butanol, n-hexanol, methyl tert-butyl ether (MTBE) or toluene. These solvents were chosen due to their distinct physical properties (**Table 3.2**). The aqueous phase was a 0.5 mol/L sodium hydroxide (NaOH) solution. The molar ratio of NaOH to 4-NPA 10:1 was chosen to ensure a pseudo-first order reaction with a half-life of 0.1 seconds. Both phases were fed to the reactor at equal flow rates of 0.40 to 16 mL/min. Photographs of the flow were taken at each run from a sight glass using a Nikon CoolPix™ S8100 camera to determine the flow regime. Samples were taken at the reactor outlet by quenching the two-phase mixture in an agitated solution that homogenized and neutralized the reacting mixture. The quench composition varied depending on the organic solvent: 0.7 wt% acetic acid, 26.5 wt% water and balance acetonitrile was used for toluene and MTBE, and 1.8 wt% acetic acid, 26.2 wt% water and balance acetonitrile for n-butanol and n-hexanol. A molar ratio 6:1 acetic acid:NaOH was used for dosing the quench. The stability of the quenched samples was measured over a week and resulted in a conversion drift of about 0.2% per day

around pH 5.2-5.3. Samples were analyzed immediately when possible and at most within 24 hours.

Table 3.2 Physical and thermodynamic properties of solvents at ambient temperature (23°C).

Solvent	σ (mN/m)	ρ (kg/m³)	μ (mPa·s)	H_A (-)	D_A (m²/s)
n-Butanol [86–88]	1.8	806	2.571	31 ± 2	3.6E-10
n-Hexanol [86,88,89]	6.6	815	4.539	40 ± 7	2.3E-10
MTBE [90–92]	10.5	737	0.369	115 ± 24	25E-10
Toluene [86–88]	35.4	862	0.552	230 ± 7	17E-10
0.5 M NaOH in Water [93]	-	1020	1.124	-	6.1E-10

The partition coefficients of 4-NPA (H_A) were experimentally determined by contacting each 0.05 mol/L organic solution with pure water and are presented with a 95% confidence interval using the mean squared residual. The mixtures were stirred overnight to achieve equilibrium and then both phases were analyzed via HPLC to determine the equilibrium concentrations. This was performed for different volumetric ratios of water and organic solution and the partition coefficients were calculated from the slope of the different equilibriums (see **Figure 3.11** in Section 3.8.1). The diffusion coefficients of 4-NPA (D_A) were estimated using the Wilke-Chang correlation with an estimated molal volume for 4-NPA of 176.6 cm^3/mol [94].

3.3 Experimental results

3.3.1 Flow regimes

Three distinct flow regimes were observed throughout the micro-reactor as the flow rate increased: slug flow (SF), parallel flow (PF), and drop flow (DF) as shown on **Figure 3.2**. DF is defined herein as when the dispersed phase no longer occupies the full width of the channel as in SF; circular drops were generally observed, but deformed/elongated drops are also included in this flow regime. Upon increasing the flow rate, the size of the drops decreased and the mixture eventually became opaque due to light scattering from the elevated interfacial area. The transition to an opaque mixture has been defined as a dispersed flow regime in a previous publication [75], but it is merged for this work with the drop flow regime for modeling purposes. Except when noted otherwise, no

significant entrance effect was observed and the flow regime was fully developed within the first eight of 137.5 mixing elements.

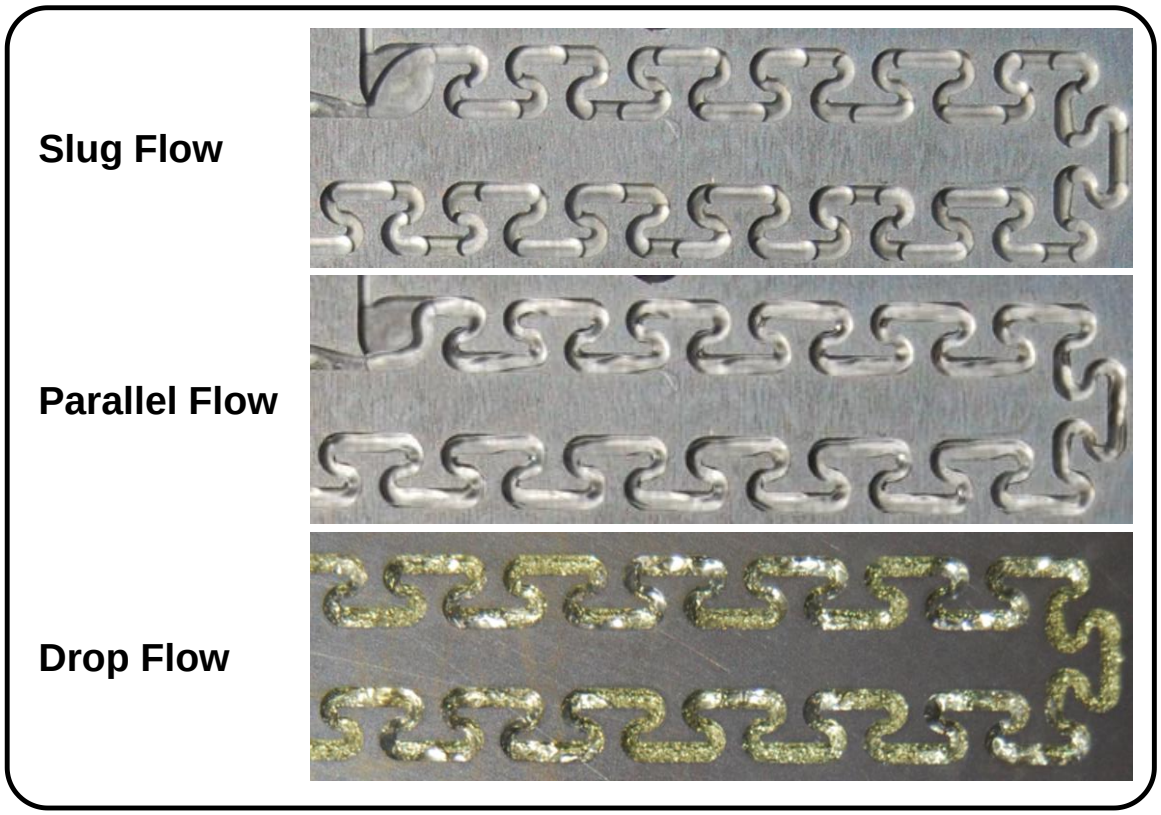

Figure 3.2 Flow regimes observed. Fluids are injected separately and meet in the circular section (see top left).

3.3.2 4-NPA conversion

The flow regimes and the conversion of 4-NPA as a function of flow rate are plotted on **Figure 3.3**. The conversion followed a general U-shaped trend and is consistent with literature [28,75,78]. SF, observed at the lowest flow rates, resulted in a decrease of conversion upon increasing the flow rate. A transition to PF was observed for n-butanol, n-hexanol and MTBE and resulted in a further decrease of the conversion. The transition for n-butanol occurred gradually; PF was initially formed, but broke down into SF further in the reactor due to instabilities [95]. The transition point was pushed forward with increasing flow rate until the whole reactor was under PF at 12.6 mL/min. Finally, SF or PF broke down into DF at the higher flow rates and resulted in an increase of conversion.

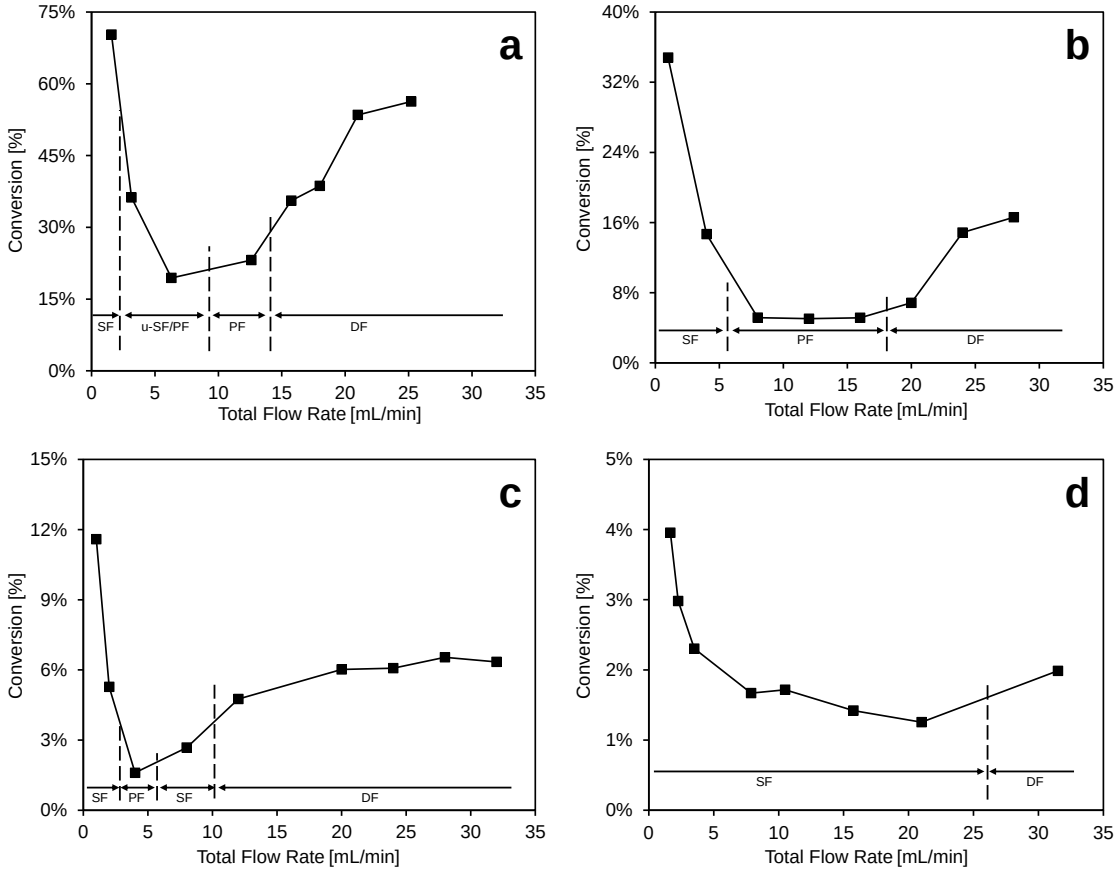

Figure 3.3 Hydrolysis conversion of 4-nitrophenyl acetate using n-Butanol (a), n-Hexanol (b), MTBE (c) or Toluene (d) as the organic solvent. Flow regimes are identified by SF (slug flow), PF (parallel flow) and DF (drop flow) with sometime the prefix "u-" (unstable).

3.4 Discussion

3.4.1 Mass transfer coefficient calculation

The conversion of 4-NPA is a function of the mass transfer rate and the residence time in the reactor. These two variables generally change in an opposed manner upon increasing the flow rate: the mass transfer coefficient increases, but the time spent in the reactor decreases. In SF, the net effect is a decreasing conversion because the increase in mass transfer is not sufficient to compensate for the loss in residence time. A change in flow regime can result in a significant variation of the mass transfer coefficient due to a change interfacial area and in the transport mechanism.

The overall volumetric mass transfer coefficients, $K_d a$ (based on the dispersed phase concentration gradient) and $K_c a$ (based on the continuous phase concentration

gradient), are calculated by decoupling the residence time, τ, from the conversion results using a reactive extraction mass balance (Equation (3.1) to Equation (3.4) assume a dilute plug flow).

$$Q_{tot}\varphi_d \cdot \frac{dC_{Ad}}{dV_R} - r_A'''' = Q_{tot}\varphi_d \cdot \frac{dC_{Ad}}{dV_R} - K_d a \cdot C_{Ad} = 0 \quad (3.1)$$

$$\eta = 1 - \frac{C_{Ad}^{out}}{C_{Ad}^{in}} = 1 - \exp\left(-K_d a \frac{\tau}{\varphi_d}\right) \quad (3.2)$$

$$K_d a = -\frac{\varphi_d}{\tau}\ln(1-\eta) \quad (3.3)$$

$$K_c a = H_A \cdot K_d a \quad (3.4)$$

The continuous phase overall volumetric mass transfer coefficient for each solvent is plotted as a function of flow rate on Figure 4. An increase in $K_c a$ is observed by increasing the flow rate due to stronger secondary flow patterns that enhances mass transfer. Kashid et al. [72] reported that upon transition from SF to PF in various T-junction micro-reactors, the slope of $K_d a$ with flow rate decreased or became negative. Likewise, Plouffe et al. [75] reported this trend in more complex tortuous micro-reactors. **Figure 3.4** a, b, and c also illustrate that a transition from SF to PF produces a decrease in $K_c a$. Upon transition into DF, a sudden increase in the slope of $K_c a$ with flow rate is observed in comparison with SF or PF due to a decrease in the size of the dispersed phase, which positively impacts both K_c and a.

The data was further analyzed specifically for each flow regime to account for the differences in transport mechanisms. This hydrolysis reaction is considered as a pseudo-first order fast reaction occurring completely within the continuous phase film. The continuous phase overall volumetric mass transfer coefficient in such a system can then be modeled as shown in Equation (3.5) (adapted from Levenspiel [55]).

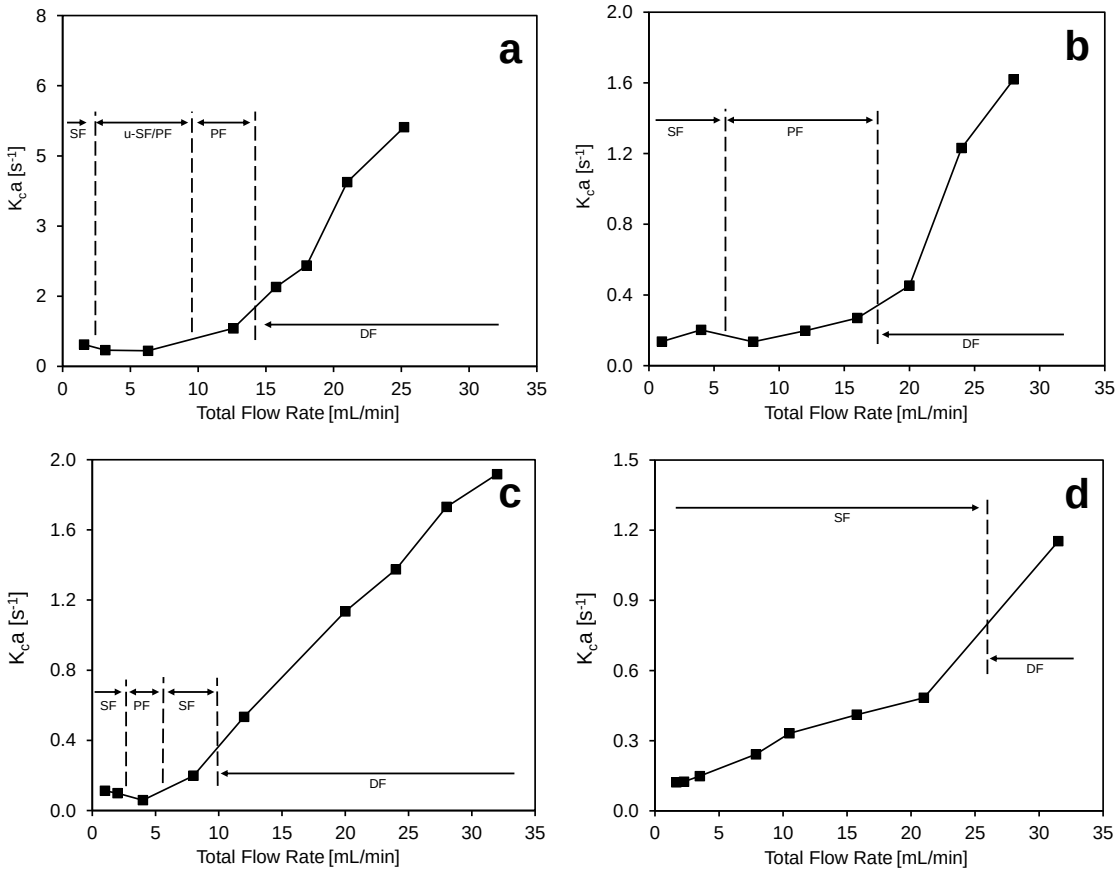

Figure 3.4 Continuous phase overall volumetric mass transfer coefficient using n-Butanol (a), n-Hexanol (b), MTBE (c) or Toluene (d) as the organic solvent. Flow regimes are identified by SF (slug flow), PF (parallel flow) and DF (drop flow) with sometime the prefix "u-" (unstable).

$$\frac{1}{K_c a} = \frac{1}{H_A k_d a} + \frac{1}{a\sqrt{D_{Ac} k_{rxn} C_{Bc}}} \tag{3.5}$$

The changes in interfacial area and mass transfer resistances with flow rate and solvents used within a flow regime are first reviewed. Afterwards, correlations of $K_c a$ as a function of flow rate and phase physical properties are presented and compared with experimental data when possible.

3.4.2 Mass transfer in slug flow

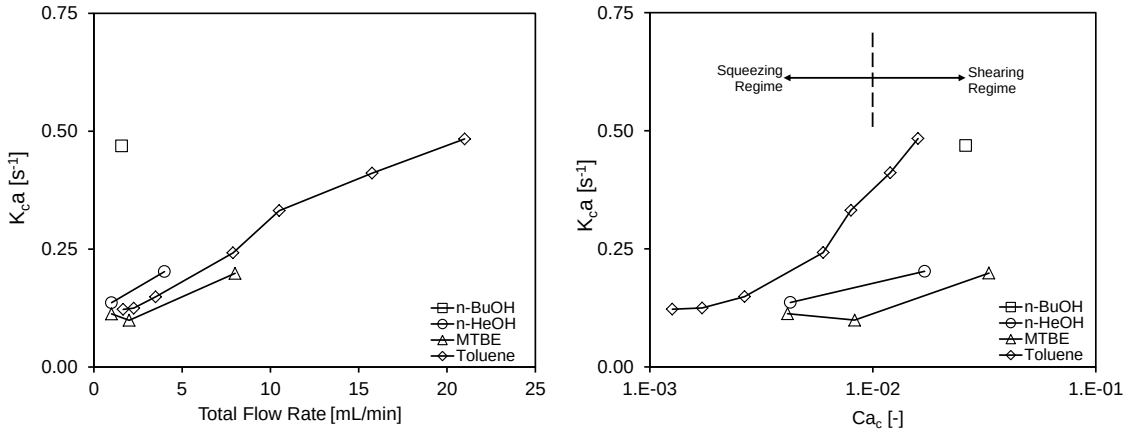

Figure 3.5 Continuous phase overall volumetric mass transfer coefficient in the slug flow regime against total flow rate (right) or against the continuous phase capillary number (left).

The continuous phase overall volumetric mass transfer coefficients for slug flow are shown on **Figure 3.5**. A greater velocity increases the rate of internal recirculation within slugs and the convective transport coefficients [96], but the effect on the interfacial area depends on how the slug shape is affected. The diameter of a slug travelling through a channel is constricted by the presence of a continuous film. The film thickness is generally correlated with the continuous phase capillary number (calculated with Equation (3.6)) as proposed by Bretherton [97] and applied by Ghaini et al. [19]. Systems with a greater Ca_c (lower interfacial tension or greater flow rate) will have a thicker film and a greater specific interfacial area. The difference, however, is marginal and its effect on $K_c a$ likely negligible over the range investigated here.

$$Ca_c = \frac{\mu_c u_{tot}}{\sigma} \tag{3.6}$$

$$u_{tot} = \frac{Q_{tot}}{A_h} = \frac{Q_d + Q_c}{A_h} \tag{3.7}$$

The length of a slug depends on its mechanism of formation when both fluids meet in a tee junction or other contacting point as analyzed by Garstecki et al. [98], Leclerc et al. [99], Kashid et al. [20], and Tice et al. [100]. They defined a squeezing regime when the surface forces dominate the viscous forces at Ca_c below 10^{-2} and a shearing regime at

greater values of Ca_c. Under the squeezing regime, the slugs length is predicted to remain constant upon increasing the flow rate if the volumetric feed flow ratio remains constant [101,102]. However, this may no longer be the case under the shearing regime, as demonstrated by the work of Guo and Chen [76] on air slugs in water. As shown with **Figure 3.5**, the slugs of toluene were apparently formed mostly within the squeezing regime and n-butanol within the shearing regime, while those of n-hexanol and of MTBE could be formed in either regime. In the squeezing regime, the interfacial area is not expected to vary, thus the observed increase in $K_c a$ should be due to enhanced slug recirculation and convective mass transfer.

The utilization of a meandering channel has shown to produce asymmetrical recirculation patterns within slugs that homogenizes them and enhances the mass transfer coefficient [27]. Therefore, the mass transfer coefficient is expected to be greater than for slugs travelling in a straight channel [103]. Correlations by Skelland and Wellek [104], Di Miceli Raymondi et al. [105], Sobieszuk [106–108], or Kashid et al. [72] could be used as a comparison, but a better knowledge of the slugs geometry is required to apply them. The resolution of the pictures presented in this work is not high enough to accurately measure the slug length, especially for the faster slugs in the shearing regime. It was thus not possible to correlate and consolidate the different overall volumetric mass transfer coefficient data points as a function of operating conditions.

3.4.3 Mass transfer in parallel flow

When two liquids flow parallel in a straight direction, mass transfer occurs perpendicularly to the flow and mostly via diffusion. In fully developed laminar flow, constant values for the convective mass transfer coefficients on either side of the interface would be observed. Additionally, the interfacial area is also expected to be constant. Consequently, the overall volumetric mass transfer coefficient would not change with flow rate. However, the results of **Figure 3.6**a demonstrate an increase in $K_c a$ with flow rate that may be due to a distortion of the interface and to secondary flow patterns generated by the curves and contractions of the micro-mixer. Secondary flow patterns, which increase in strength with increasing velocity similarly to Dean vortices in single phase curved channels, increase mixing in the radial direction within each phase

and reduce the boundary layer thickness at the interface [27,96,109]. It was observed that $K_c a$ increases linearly with the continuous phase capillary number as depicted on **Figure 3.6**b.

$$K_c a = 3.78 \cdot Ca_c \tag{3.8}$$

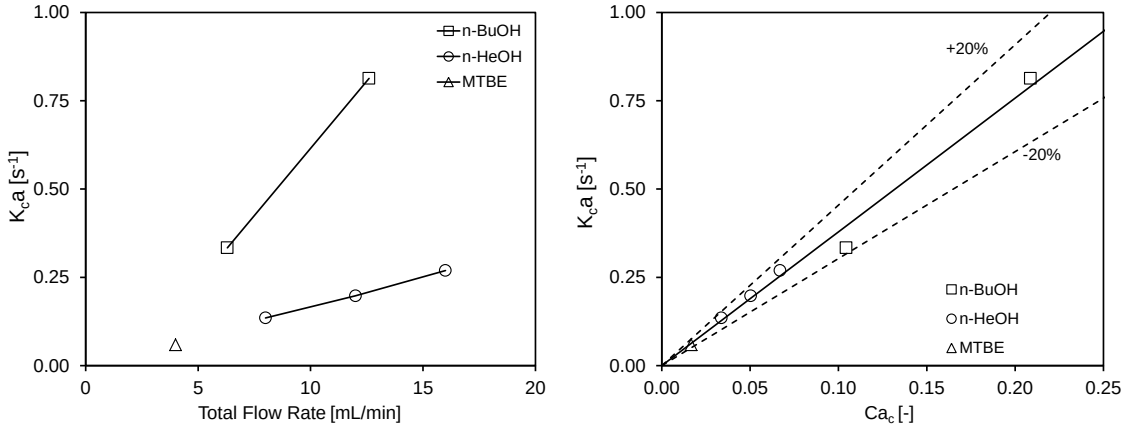

Figure 3.6 Continuous phase overall volumetric mass transfer coefficient in the parallel flow regime against total flow rate (right) or against the continuous phase capillary number (left).

In Equation (3.8), the proportionality constant has units of s^{-1} and is empirical. Further investigation of the velocity profile and of the interface is needed to develop a mechanistic model and render the equation dimensionless.

3.4.4 Mass transfer in drop flow

In the drop flow regime, the interphase mass transfer is modeled as the reactive extraction of a stagnant sphere and is depicted on **Figure 3.7**. This model assumes that the drops have a size equal to the surface-volume average diameter, d_{32}, used for the calculation of the specific interfacial area in the continuous phase overall volumetric mass transfer coefficient (rewritten in Equations (3.9) and (3.10)).

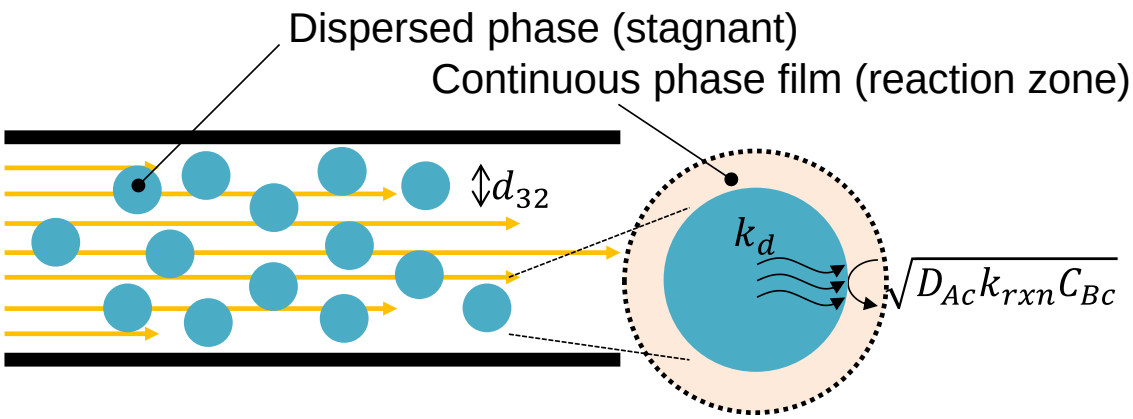

Figure 3.7 Drop flow reactive extraction model.

$$a = \varphi_d \frac{6}{d_{32}} \tag{3.9}$$

$$\frac{\sqrt{D_{Ac}k_{rxn}C_{Bc}}}{K_c a} = \frac{d_{32}}{6\varphi_d}\left(\frac{\sqrt{D_{Ac}k_{rxn}C_{Bc}}}{H_A k_d} + 1\right) \tag{3.10}$$

The dispersed phase convective coefficient, k_d, is calculated from the dispersed phase Sherwood number in Equation (3.11), which was assumed to be equal to that for drops with a fully developed concentration profile, i.e., 2 (see Section 3.8.2 for more detail). This causes Equation (3.10) to become quadratic in terms of d_{32}. The size of the drops can then be calculated as the positive root of that function as shown in Equation (3.12). The obtained drop diameters are plotted against flow rate for the various solvents on **Figure 3.8**. The magnitude, between 360 and 30 μm, is appropriate when compared with the dimensions of the reactor and with photographic observations.

$$k_d = Sh_d \frac{D_{Ad}}{d_{32}}, \quad Sh_d \approx 2 \tag{3.11}$$

$$d_{32} = \frac{H_A D_{Ad}}{\sqrt{D_{Ac}k_{rxn}C_{Bc}}}\left(\sqrt{1 + \frac{12\varphi_d}{K_c a}\frac{D_{Ac}k_{rxn}C_{Bc}}{H_A D_{Ad}}} - 1\right) \tag{3.12}$$

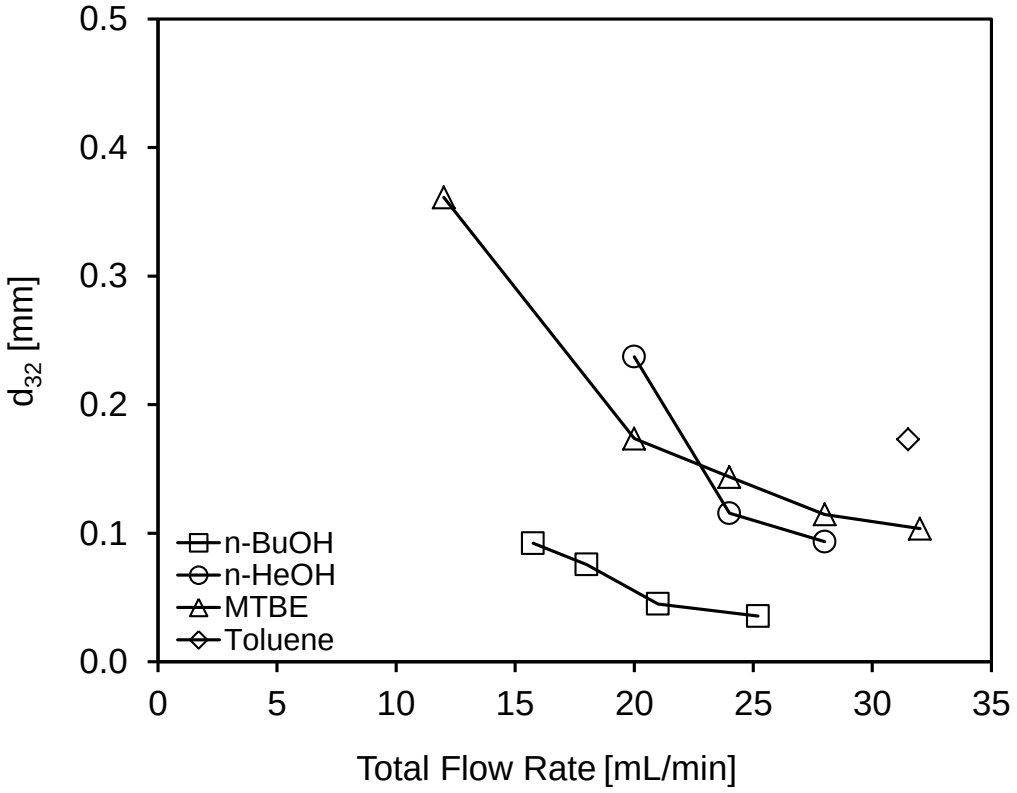

Figure 3.8 Estimated drop size for each organic solvent in the drop flow regime.

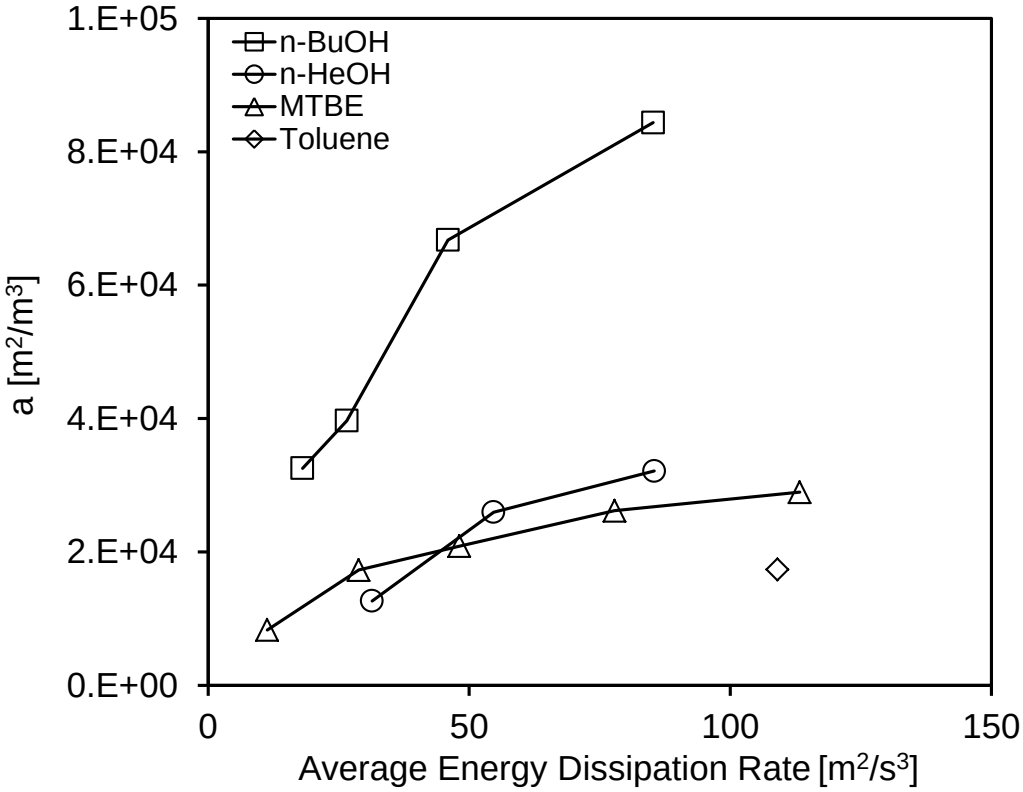

Figure 3.9 Specific interfacial area for drop flow against the average rate of energy dissipation.

From Equation (3.9), the specific interfacial area is calculated from the size of the drops. It is plotted on **Figure 3.9** as a function of the average rate of energy dissipation calculated from pressure drop measurements (Equation (3.13)). The energy dissipation of a system relates the size, frequency and kinetic energy of eddies that impact and break-up the dispersion [110,111]. It can be used in turbulent flow to calculate the maximum stable droplet diameter [112,113] and was used to derive a first model to correlate the drop size. A second model uses the Weber and Reynolds dimensionless numbers (Equations (3.14) and (3.15)).

$$\varepsilon = \frac{\Delta P Q_{tot}}{\rho_c V_R} \tag{3.13}$$

$$We_c = \frac{\rho_c d_h u_{tot}^2}{\sigma} \tag{3.14}$$

$$Re_c = \frac{\rho_c d_h u_{tot}}{\mu_c} \tag{3.15}$$

The proportionality coefficients and exponents shown in **Table 3.3** were fitted using the method of the least squares and a 95% confidence interval is estimated based on the mean squared residual.

Table 3.3 Drop diameter models parameters.

Parameter	Model 1 Energy dissipation based	Model 2 Dimensionless numbers based
Base Model	$d_{32} = \beta_0 \cdot \left(\frac{\sigma}{\rho_c}\right)^{\beta_1} \cdot \varepsilon^{\beta_2}$	$\frac{d_{32}}{d_h} = \beta_0 \cdot We_c^{\beta_1} \cdot Re_c^{\beta_2}$
Fitted Model	$\ln(d_{32}) = \ln(\beta_0) + \beta_1 \ln\left(\frac{\sigma}{\rho_c}\right) + \beta_2 \ln(\varepsilon)$	$\ln(d_{32}/d_h) = \ln(\beta_0) + \beta_1 \ln(We_c) + \beta_2 \ln(Re_c)$
$\ln(\beta_0)$	1.432 ± 2.209	0.974 ± 0.735
β_1	0.657 ± 0.151	-0.713 ± 0.183
β_2	-0.646 ± 0.287	≈ 0
s_{res}^2	0.039	0.055
R^2	0.918	0.873

The results of Lobry et al. [48] and of Theron et al. [114] suggest that the volume-surface average drops in static mixers is a constant fraction of the maximum stable diameter.

Then, the exponents β_1 and β_2 of model 1 are expected to be approximately 0.6 and -0.4 which are within the 95% confidence intervals (see Section 3.8.3 for details).

For model 2, the Weber number exponent is expected to be -0.6 and the Reynolds number exponent is expected to be between 0.4 and 0 for laminar and turbulent flow, respectively (see Section 3.8.3 for details). The confidence interval for β_1 includes the expected value, while that of β_2 showed it was not statistically significant and suggest that the drop generation is done via turbulent-like mechanism. This is consistent with Plouffe et al. [75] which described how secondary flow patterns generated by complex micro-mixers grow in strength and frequency with greater energy dissipation, similar to turbulent eddies.

An ANOVA shows that both models are statistically significant, and the coefficient of determination and the mean squared residual show that model 1 fits better than model 2. This is expected because model 1 is based on the experimentally obtained energy dissipation rate, which requires knowledge of the pressure drop for the experimental system. However, the pressure drop can be difficult to predict at high dispersed phase concentrations in liquid-liquid systems. Alternatively, model 2 offers a practical predictive purpose as it is based on parameters which can be calculated without specific experimental data. Using both models, the conversion within the drop flow regime is predicted and compared with that obtained experimentally on **Figure 3.10** for the different solvents.

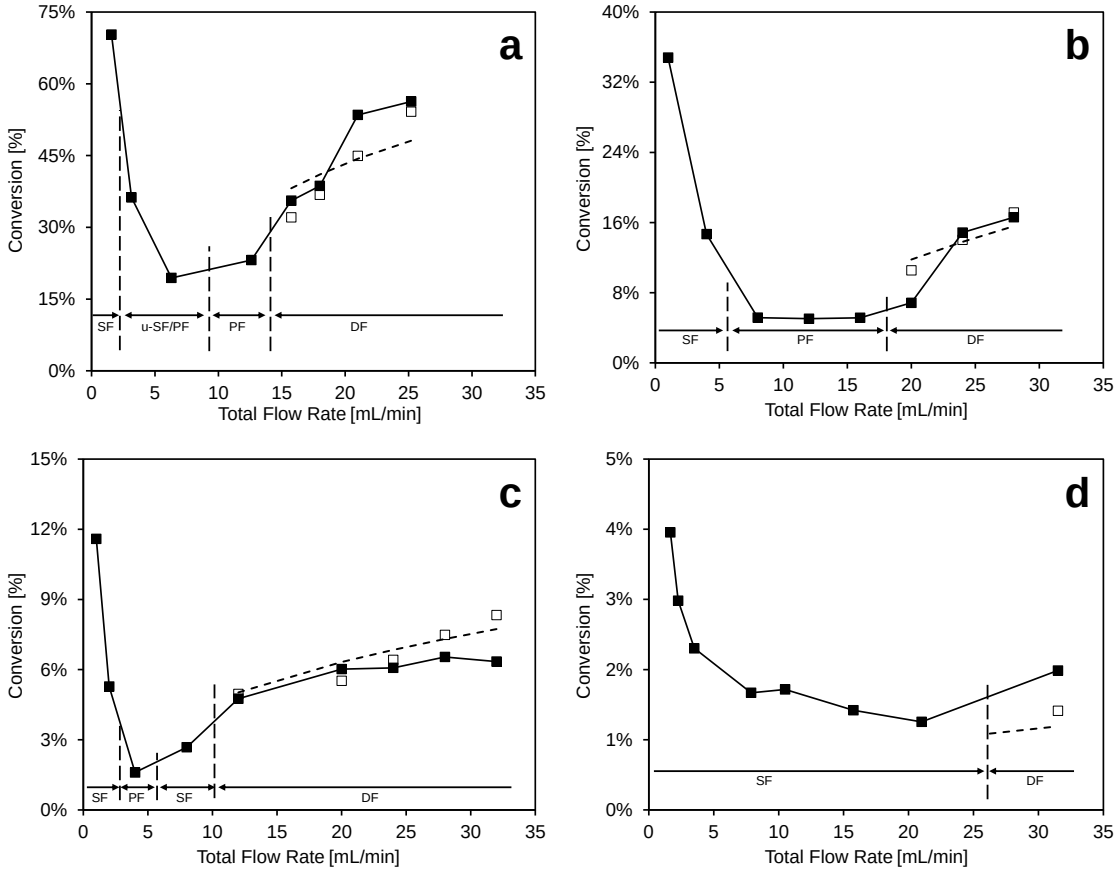

Figure 3.10 Experimental (■) and predicted (Model 1: □, Model 2: ---) conversion of 4-nitrophenyl acetate during drop flow using n-Butanol (a), n-Hexanol (b), MTBE (c) or Toluene (d) as the organic solvent.

3.5 Conclusion

The characterization of the overall mass transfer coefficient in a serpentine micro-reactor using various solvent pairs demonstrated that it is strongly affected by the flow regime and is greatest in the drop flow regime.

In slug flow, the utilization of meandering channels typically increases mass transfer compared to straight channels. $K_c a$ was found to increase with increasing flow rate. In the squeezing slug formation regime, the interfacial area is not reported to change significantly with increased flow rate in the literature, but the convective mass transfer coefficients are greater due to an accelerated internal fluid recirculation within the slugs. Correlations already exist for the convective mass transfer coefficients within and

outside of the dispersed phase, but an adequate prediction of the slug dimensions is still required for the modeling of $K_c a$, especially within the shearing slug formation regime.

The transition from slug to parallel flow decreases the mass transfer coefficient. In parallel flow, $K_c a$ increased with flow rate due to secondary flow patterns generated by the curvature of the mixer that created advection over the interface and increased mass transfer beyond diffusion. Within the range investigated, $K_c a$ increased linearly with Ca_c. Additional experiments studying the velocity profile and interface should be conducted to further generalize the correlation into a dimensionless form.

In drop flow, a reactive extraction over drops model was successfully applied to the data. The volume-surface average diameter of the drops was determined from the conversion results of the pseudo-first order reaction, and modeled with the system's interfacial tension and average rate of energy dissipation in the reactor as well as with the dimensionless Weber and Reynolds numbers. Both models were found to be statistically significant and their parameters close to expected values derived from macroscopic static mixers. The first model is more accurate than the second, but requires the determination of the energy dissipation rates for the liquid-liquid system of interest. The successful correlation of the drop flow regime means that results from a benchmark system can be used to predict the performance of a reactive system, hopefully resulting in faster continuous flow process development.

In conclusion, during process development, the pair of solvents should be chosen to optimize the rate of mass transfer for fast liquid-liquid reactions. A system with a low interfacial tension should be chosen to obtain small drops at low flow rates and with a low partition coefficient, H, to favour penetration of the organic reactants.

3.6 Acknowledgement

The authors would like to thank the Natural Sciences and Engineering Research Council of Canada and Lonza AG for their financial contribution. Also Ehrfeld Mikrotechnik BTS is acknowledged for the reactor manufacturing and Sébastien Mongeon for his help.

3.7 Nomenclature

General

Symbol	Description	Units
a	Specific interfacial area	m^2/m^3
A_h	Cross-sectional area of the channel at the contraction	m^2
Bi	Biot number	-
Ca	Capillary number	-
C_n	Infinite sum "n"th coefficient	-
C_{ij}	Concentration of molecule "i" in phase "j"	mol/m^3
d_{32}	Volume-surface average droplet diameter	m
d_h	Hydraulic diameter at the channel contraction	m
D_{ij}	Molecular diffusion coefficient of molecule "i" in the phase "j"	m^2/s
Fo	Fourier number	-
H	Organic/aqueous concentration distribution coefficient	-
k	Local convective mass transfer coefficient	m/s
k_{rxn}	Second order reaction rate constant	$m^3/mol/s$
K	Overall convective mass transfer coefficient	m/s
ΔP	Pressure drop across the reactor	Pa
Q	Volumetric flow rate	m^3/s
r''''	Reactive volumetric extraction rate	$mol/m^3/s$
R	Drop radius	m
R^2	Coefficient of determination	-
Re	Reynolds number	-
s_{res}^2	Mean squared residual	-
Sh	Sherwood number	-
u	Superficial velocity at the contraction	m/s
V_R	Reactor volume	m^3
We	Weber number	-
X	Dimensionless position	-

β	Fitting parameter	*
ε	Average rate of energy dissipation	m^2/s^3
ζ	Infinite sum "n"th characteristic values	-
η	Conversion of 4-NPA	%
μ	Dynamic viscosity	Pa·s
ρ	Density	kg/m^3
σ	Interfacial tension	J/m^2
τ	Average residence time	S
φ	Volumetric phase fraction	-
θ	Dimensionless concentration	-

Indices

A	Of the 4-nitrophenyl acetate
B	Of the sodium hydroxide base
c	Of the continuous phase
d	Of the dispersed phase
tot	Total of the continuous and dispersed phase

3.8 Appendix

3.8.1 Appendix A: Determination of the partition coefficient

Organic solutions of 4-NPA at 50 mmol/L were contacted with HPLC water over night in an agitated vessel. Afterward, the equilibrium concentrations of 4-NPA in the organic and aqueous phase were determined via HPLC. The partition coefficient was then calculated from the slope of the different equilibriums (forced through the origin).

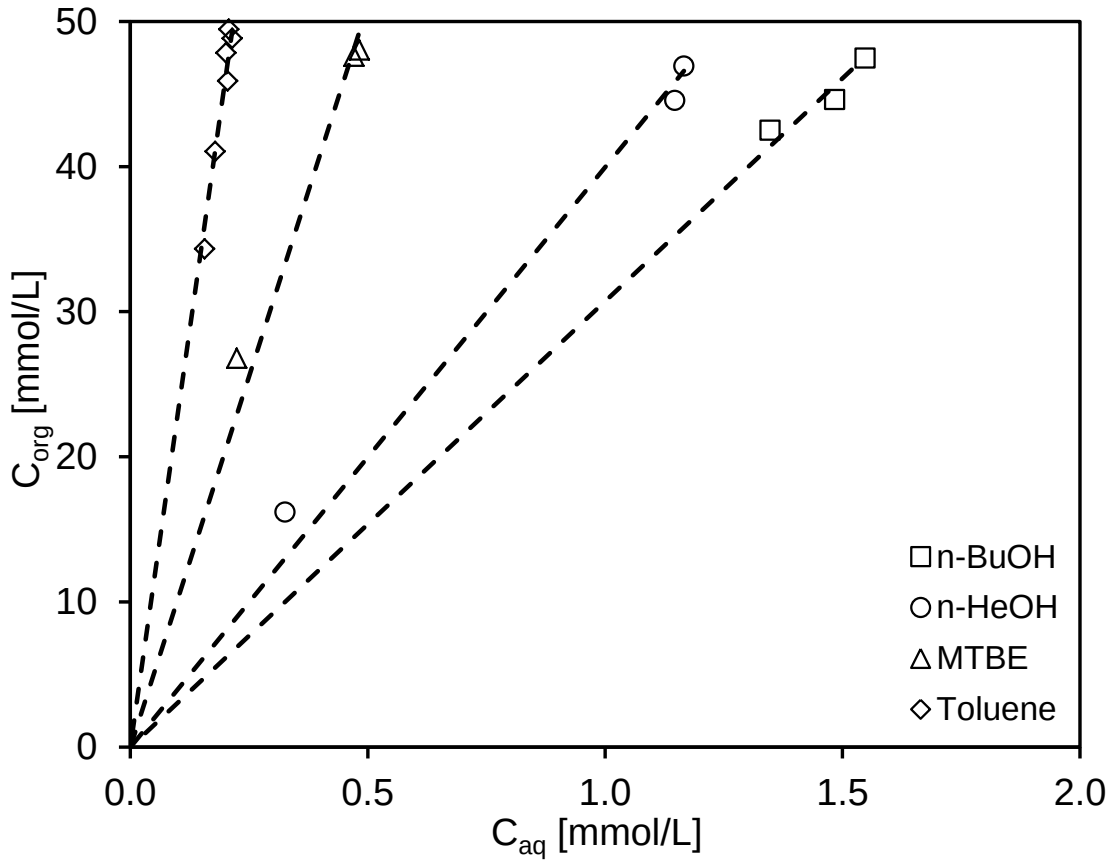

Figure 3.11 Experimental equilibrium concentrations for the determination of the partition coefficients, H_A.

3.8.2 Appendix B: Concentration profile and conversion in a drop

The calculation of the drop size is performed in this work via approximation of the internal convection coefficient. Alternatively, a plug flow mass balance could be performed on differential volume elements to derive the concentration profile within the drops (assuming a constant diffusion coefficient):

$$\frac{1}{r^2}\frac{\partial}{\partial r}\left(r^2 D_{Ad}\frac{\partial C_{Ad}}{\partial r}\right) = \frac{\partial C_{Ad}}{\partial \tau} \tag{3.16}$$

The equation is rendered dimensionless using the drop's radius (R), the diffusion constant and the initial concentration:

$$X = \frac{r}{R} \tag{3.17}$$

$$Fo = \frac{D_{Ad}\tau}{R^2} \tag{3.18}$$

$$\theta = \frac{C_{Ad}}{C_{Ad}^{in}} \tag{3.19}$$

$$\frac{1}{X^2}\frac{\partial}{\partial X}\left(X^2\frac{\partial \theta}{\partial X}\right) = \frac{\partial \theta}{\partial Fo} \tag{3.20}$$

Which has the general solution

$$\theta(X, Fo) = \sum_{n=1}^{\infty} C_n \cdot \frac{\zeta_n X}{\sin(\zeta_n X)} \cdot \exp(-\zeta_n^2 Fo) \tag{3.21}$$

$$C_n = 4\frac{\sin(\zeta_n) - \zeta_n \cos(\zeta_n)}{2\zeta_n - \sin(2\zeta_n)} \tag{3.22}$$

And the values for the coefficients ζ_n are the positive roots of

$$Bi = 1 - \zeta_n \cot(\zeta_n) \tag{3.23}$$

Where Bi is the Biot number and represents the ratio between the internal and the external resistance to mass transfer. In the case of a fast pseudo-first order reactive extraction, the external resistance is a function of the reaction kinetics and not of convection in the continuous phase. It can then be shown that the Biot number is equal to

$$Bi = \frac{\sqrt{D_{Ac} k_{rxn} C_{Bc}}}{H_A D_{Ad}} R \tag{3.24}$$

The conversion as a function of residence time can be calculated by integrating the concentration profile throughout the whole drop volume:

$$\eta = 1 - \frac{\int C_{Ad} dV}{C_{Ad}^{in} V} = 1 - 3\int_0^1 \theta(X, Fo) X^2 dX \tag{3.25}$$

$$\eta = 1 - 3\sum_{n=1}^{\infty} C_n \cdot \frac{\sin(\zeta_n) - \zeta_n \cos(\zeta_n)}{\zeta_n^3} \cdot \exp(-\zeta_n^2 Fo) \quad (3.26)$$

$$\eta = f(Fo, Bi) = f(D_{Ad}, D_{Ac}, k_{rxn} C_{Bc}, H_A, \tau, R) \quad (3.27)$$

Using a numerical root solving method, it is possible to find the value of the drop radius resulting in the observed experimental conversion. The surface-volume average drop diameters approximated by $Sh_d \approx 2$ using Equation (3.12) were on average 0.02 mm smaller than those determined from the infinite sum on Equation (3.27). It was decided that Equation (3.12) is sufficiently accurate and simple to be used for the determination of the d_{32} within the range investigated.

3.8.3 Appendix C: Drop size correlation

Correlations for the dispersion size are generally a derivation of the maximum stable droplet diameter in a turbulent flow as a function of the average rate of energy dissipation [48,111]. Presuming that the average droplet diameter is equal to a fraction of the maximum stable diameter, the derivation in a straight tube is as follow:

$$d_{max} = C_1 \left(\frac{\sigma}{\rho_c}\right)^{0.6} (\varepsilon)^{-0.4} \quad (3.28)$$

$$d_{32} = C_2 \cdot d_{max} = C_1 C_2 \left(\frac{\sigma}{\rho_c}\right)^{0.6} (\varepsilon)^{-0.4} \quad (3.29)$$

Equation (3.29) can be rendered dimensionless as follows:

$$d_{32} = C_1 C_2 \left(\frac{\sigma}{\rho_c} \cdot \frac{d_h u^2}{d_h u^2}\right)^{0.6} (\varepsilon)^{-0.4} = C_1 C_2 We_c^{-0.6} \left(\frac{d_h^{0.6} u^{1.2}}{\varepsilon^{0.4}}\right) \quad (3.30)$$

$$\frac{d_{32}}{d_h} = C_1 C_2 We_c^{-0.6} \left(\frac{u^{1.2}}{d_h^{0.4} \varepsilon^{0.4}}\right) = C_1 C_2 We_c^{-0.6} \left(\frac{u^3}{d_h \varepsilon}\right)^{0.4} \quad (3.31)$$

$$\varepsilon = \frac{\Delta P Q}{V_R \rho_c} = \frac{\left(f \cdot \frac{L}{d_h} \cdot \frac{\rho_c u^2}{2}\right) \cdot \left(\frac{\pi}{4} d_h^2 \cdot u\right)}{\left(L \cdot \frac{\pi}{4} d_h^2\right) \cdot \rho_c} = \frac{f}{2} \cdot \frac{u^3}{d_h} \quad (3.32)$$

$$\frac{d_{32}}{d_h} = C_1 C_2 \cdot We_c^{-0.6} \cdot \left(\frac{2}{f}\right)^{0.4} \quad (3.33)$$

In laminar flow, the friction factor is usually proportional to the inverse of the Reynolds number, while in turbulent flow it is constant. Consequently, correlations for the average droplet diameter usually take the form

$$\frac{d_{32}}{d_h} = \beta_0 \cdot We_c^{\beta_1} Re_c^{\beta_2} \tag{3.34}$$

With the exponent β_1 being equal to about -0.6 and the exponent β_2 varying between 0.4 (laminar flow) and 0 (turbulent flow).

3.9 References

See thesis references.

4 Liquid-liquid flow regime and mass transfer in micro-reactors

*PATRICK PLOUFFE, ARTURO MACCHI**

Centre for Catalysis Research and Innovation, Department of Chemical and Biological Engineering, University of Ottawa, K1N6N5, Ottawa, Canada

*DOMINIQUE M. ROBERGE**

Chemical Development, Lonza AG, CH-3930, Visp, Switzerland

This manuscript has been published as *Chem. Eng. J.* **2014**. DOI: 10.1016/j.cej.2014.10.072

Abstract

The flow regimes and mass transfer rates in five complex micro-reactors with different mixing mechanisms were investigated using the two-phase alkaline hydrolysis of 4-nitrophenyl acetate. n-butanol and toluene were used as organic solvents. Using n-butanol in curvature-based micro-mixers, the flow regime evolved from slug to parallel to drop/dispersed flow with increasing flow rates. In obstacle-based micro-mixers, no parallel flow was observed. Using toluene, no parallel flow was observed for all reactors. The conversion of 4-nitrophenyl acetate was found to be strongly dependent on the flow regime. In slug and parallel flow, the conversion generally decreased with an increase in flow rate whereas it typically increased in drop flow and was constant or slightly decreased in dispersed flow. The different micro-mixers were compared using the overall volumetric mass transfer coefficient, $K_{org}a$, which was primarily a function of the rate of energy dissipation within the dispersed flow regime. The geometry itself impacts the resulting flow regime and rate of energy dissipation at a given flow rate. The micro-reactors were then compared using modified Damköhler's numbers. Curvature-based reactors were found to be inadequate for liquid-liquid reactions under the studied conditions, as they favour parallel flow patterns and yield relatively low interphase mass transfer rates.

Keywords

Micro-reactor; liquid-liquid reaction; mass transfer; mixing; slug and parallel flow; dispersed flow.

4.1 Introduction

Process development and intensification in the fine chemical and pharmaceutical industry can be achieved by using continuous flow micro-reactor technology instead of traditional batch operations [1,64,65]. The small scale of these reactors increases their surface-to-volume ratio, which enhances wall-fluid heat transfer rates allowing more severe reaction conditions [115]. This advantage can potentially be extended to multiphase reactions by allowing intimate contact between the reacting streams [6,17,18,20,21]. However, synthesis rates in such small reactors often result in a laminar flow regime where transport phenomena are diffusion driven and thus relatively slow.

Mixing enhancement techniques are used to generate secondary flow patterns resulting in a flow field that resembles transitional or turbulent flow rather than laminar [11]. This can be done by modifying the internal geometry of the micro-reactor to include, amongst others, curvatures [116], contractions and expansions, splits and recombination of streams [117], and obstacles. These are referred to as passive mixing techniques in contrast to active methods that utilize external forms of energy such as mechanical actuators [22,30].

For single phase applications, a contacting element such as a T-junction can be used to mix the reacting streams and then followed by an empty channel to add residence time and complete the reaction [11,47,118,119]. In multiphase applications, this approach generally leads to a slug or parallel flow pattern after the contacting element. Recirculatory motion within the slug homogenizes the interior and reduces the boundary layer thickness at the interface, thus increasing mass transfer rates [19,83,96]. When parallel flow occurs, the mass transfer is dependent on the lateral diffusion of molecules and high transfer rates are achieved only in smaller geometries where diffusional distances are short and the relative surface area is large [120,121].

Alternatively, more complex micro-reactors that incorporate multiple consecutive micro-mixers and micro-channels can be used. They dissipate energy continuously throughout the reactor's volume and generate a dispersion smaller in size than slugs [39,48,122]. The drawback of this approach is a generally greater pressure loss and/or lower residence time.

Commercially available micro-reactors for multi-phase systems generally rely on one or more of the passive mixing techniques stated previously. Curvatures are exploited by the *Art® Reactor* and the *Lonza FlowPlate® SZ or TG* micro-reactors [80] in the form of meandering, serpentine, and recirculating channels. Contraction and expansion effects are utilized by the *IMM orifice microreactor* [123,124]. The *Kenics® static mixer by Chemineer™* [125,126] uses a ribbon like structure to split streams and recombine them with others. This approach is also used by the *IMM Caterpillar Micromixer*. The *Advanced-Flow™ reactor by Corning®* [39] utilizes most of the previous techniques, but also focuses the flow on an obstacle to disrupt it.

Confronted to the variety of types, shapes, and sizes of micro-reactors available, the most appropriate choice for fast liquid-liquid reactions is complex. It is not straightforward to extrapolate results of single phase reactions to predict the performance in multi-phase flow for the purpose of technology transfer and process intensification.

In this context, this study first analyzes the different mixing techniques using five differently shaped micro-mixers with solvents (relatively low/high interfacial tension) and production rates (1-50 mL/min) relevant to the fine chemical and pharmaceutical industry. Two curvature-based (SZ, TG) and three obstacle-based/hybrid micro-mixers (Spade, Venturi, Sickle) are used and are detailed further. Using photographs and a test liquid-liquid reaction, the flow regimes and mass transfer rates are obtained as a function of flow rate and the performance of the different mixing techniques compared with the purpose of identifying the most efficient. Then, the study compares the different reactors using the dimensionless Damköhler timescales to determine which is the most effective.

4.2 Experimental setup

The experimental set-up is displayed in **Figure 4.1**. SyrDos (HiTec Zang) or ISCO (Teledyne) piston pumps were used depending on flow rate and pressure requirements. The flow rate was measured by an Endress-Hauser Coriolis flowmeter and the pressure drop across the micro-reactor was measured using 6 or 20 bar Keller pressure sensors. The temperature of the feed was measured by a PT100 sensor and the micro-reactor was kept at ambient temperature using a thermal bath.

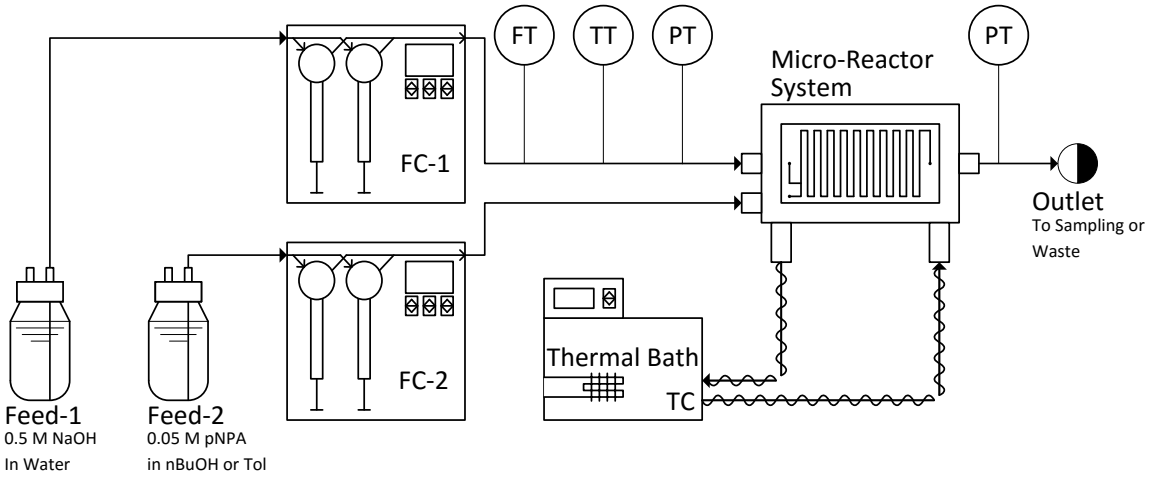

Figure 4.1 Experimental setup. Instruments identified are Flow Controllers (FC), Flow Transmitter (FT), Temperature Transmitter (TT) and Pressure Transmitter (PT).

The five different micro-mixers are detailed in **Table 4.1** and **Figure 4.2**. The micro-reactor system was the Ehrfeld MMRS combined with the Lonza FlowPlate® Lab plate reactor. The plate micro-reactors, one for each mixer, were made in stainless steel 316 or in Hastelloy C22™ and preferentially wetted by the aqueous phase so that the dispersed phase is the organic solution. The SZ, TG, Venturi and Sickle micro-mixers are designs by Lonza while the Spade micro-mixer resembles Corning®'s Advanced-Flow™ reactor. The contraction size is defined as the smallest cross-section through which all the flow passes.

Table 4.1 Micro-reactor and micro-mixer characteristics.

Name	Micro-mixer*	Contraction Size (mm)	Number of Mixer	Reactor Volume (mL)
SZ	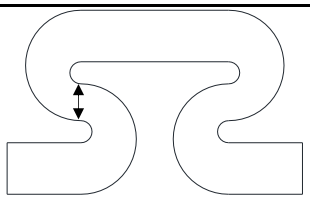	0.50 x 1.25	137.5	1.05
TG	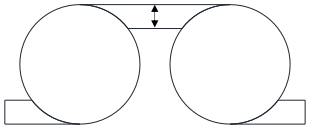	0.50 x 1.25	69.5	1.07
Venturi		0.20 x 0.50	18	0.40
Sickle	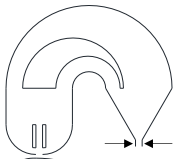	0.20 x 0.50	71	0.48
Spade	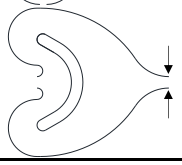	0.50 x 1.00	12	0.31

*Elements are not to scale, flow is from left to right, and double arrows identify the contraction zone.

The SZ mixer is a serpentine channel that generates secondary flow patterns via Dean vortices [109]. Although simple in design, it can efficiently mix single phase mixtures [11]. The TG mixer is similar, but will generate recirculation flow in its corners [see Video 1 in Section 4.7] that favours local backmixing and may be an advantage for certain reaction types like auto-catalysis. The Venturi mixer lowers the pressure at the injection point using a smooth contraction and expansion and is followed by a triangular obstacle. It creates an initial fine dispersion for gas-liquid mixtures [53]. The Sickle mixer was specifically designed for multiphase systems. These last two micro-mixers were developed for low flow applications and were thus built with the smallest hydraulic diameters.

The chemical reaction used to assess the performance of the different micro-mixers was the two-phase alkaline hydrolysis of 4-nitrophenyl acetate (**Scheme 4.1**). The product of the reaction, sodium 4-nitrophenolate, colors the aqueous phase yellow and allows visual distinction between the two phases. The molar concentrations of the main

reactant and product were determined by a pre-calibrated HPLC surface response method for quantitative analysis. An HP Agilent 1100 series HPLC system, which includes a G1322A degasser, a G1311A quaternary pump, a G1313A autosampler, a G1316 column compartment and a G1315B diode array detector, was used. A sample volume of 5.0 µL was injected into a 250 mm x 4.6 mm i.d. Agilent Zorbax SB-C8 column to separate the compounds. The separation was performed at room temperature. A pre-screening showed that a wavelength of 294 nm was best suited for the simultaneous detection of the unconverted reactant and product. Two mobile phases were used and composed of a 0.1 wt% trifluoroacetic acid solution in HPLC-grade water and in a mixture of HPLC-grade water (24.1 wt%) and acetonitrile (75.8 wt%).

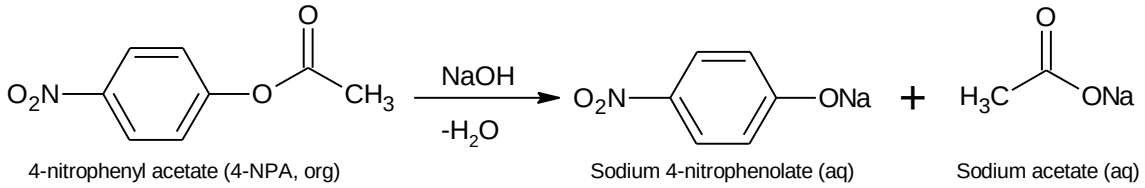

Scheme 4.1 Alkaline hydrolysis of 4-nitrophenyl acetate.

The organic phase was a 0.05 mol/L solution of the acetate in either n-butanol or toluene. These two solvents were chosen due to their distinct differences in interfacial tension and solubility in water (**Table 4.2**). The aqueous phase was a 0.5 mol/L sodium hydroxide (NaOH) solution. Both phases were fed in the reactor at equal flow rates of 0.40 to 22.15 mL/min. Photographs of the flow and 120 FPS videos were taken at each run from a sight glass using a Nikon CoolPix™ S8100 camera and the flow regime noted. Samples were taken at the reactor outlet by quenching the two-phase mixture in an agitated solution of 72.8 wt% acetonitrile, 26.5 wt% water and 0.7 wt% acetic acid that homogenized and neutralized the reacting mixture. The stability of the quenched samples was measured over a week and resulted in a conversion drift of about 0.2% per day around pH 5.2-5.3. Samples were analyzed immediately when possible and at most within 24 hours.

Table 4.2 Physical properties of fluids at ambient temperature [86,87].

Fluid	Density (kg/m^3)	Viscosity (mPa*s)	Interfacial tension with water (mN/m)	Solubility in water (mol%)
Toluene	862	0.552	35.4	0.01
n-Butanol	806	2.571	1.8	1.88
0.5 M NaOH	1020	1.124	-	-

4.3 Flow regimes

Four distinct flow regimes were identified from visual observations and photographs taken: slug flow; drop flow where the dispersed phase was segmented into generally spherical drops of diameter equal to or slightly smaller than the channel largest width; dispersed flow where the dispersed phase was segmented into a quasi-emulsion of diameter an order of magnitude smaller than the channel width; and parallel flow where both phases flow side-by-side in the channel. Examples of each flow regime are displayed in **Figure 4.2**.

Unstable slug flow where drops are sheared off the main slugs and unstable parallel flow where the parallel flow breaks into slug, drop or dispersed flow downstream in the reactor were also observed – those were considered transitional regimes. In the dispersed flow regime, droplets could not be clearly identified due their relatively high velocity and small size, and the mixture started to become opaque due to light scattering from the resulting elevated interfacial area.

4.3.1 Experimental results

The **SZ micro-mixer** produced slugs at 2 mL/min for the n-butanol/aqueous NaOH system (**Figure 4.2**c). From 2 to 15 mL/min, an unstable parallel flow formed at the feed contacting point and transitioned to slug flow further into the channel. As the flow rate was increased, the breaking point shifted downstream until the complete reactor was in parallel flow. Above 15 mL/min, the parallel flow broke into a drop/dispersed flow (**Figure 4.2**k). For the toluene/aqueous NaOH system, the flow regime was mostly slug flow, but some small drops were sheared off from the main slugs above flow rates of 20-25 mL/min

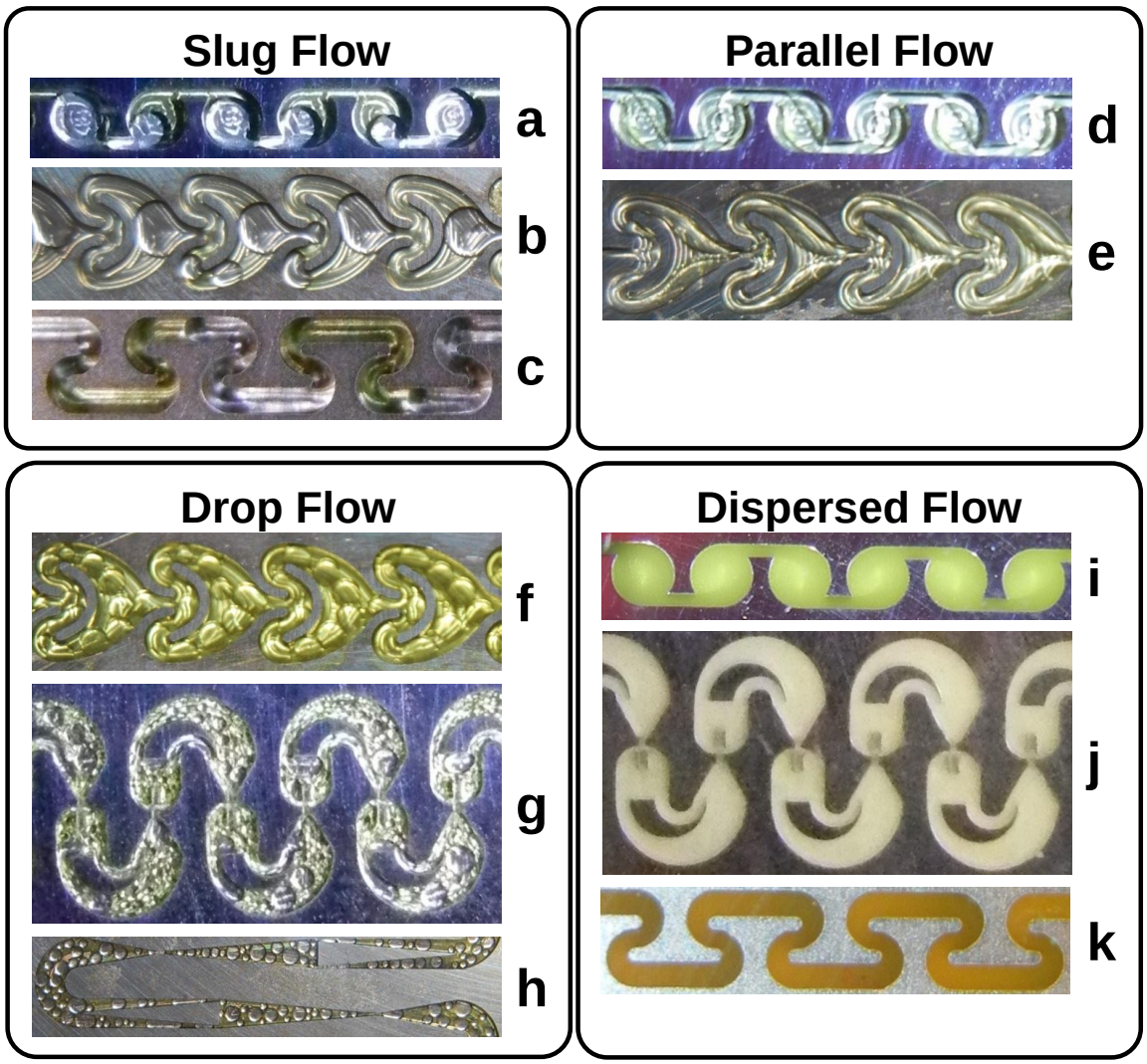

Figure 4.2 Flow regimes observed (mixers are not to scale).

The **TG micro-mixer** produced slugs at 1.6 mL/min for the n-butanol/aqueous NaOH system (**Figure 4.2**a), but transitioned to parallel flow abruptly (**Figure 4.2**d) as opposed to progressively as in the SZ micro-mixer. The parallel flow seemed stable, regardless of the directional change in the mixer. The aqueous solution, being the denser phase, was always adjacent to the outside curve. The change in rotational direction caused both sides of the parallel flow to cross such that phases initially side-by-side were now stacked below-and-above. A further rotation of the interface caused both sides to exit the transfer channel in alternated positions without breaking-up the parallel flow. However, the rotational motion at the interface will affect the boundary layer and may significantly increase the overall mass transfer coefficient in comparison to a non-rotating parallel

flow in a straight micro-channel. Above 10 mL/min, the parallel flow breaks in the corner micro-mixers only and small droplet recirculation is observed [see Video 1 in Section 4.7]. These secondary flow patterns gain in strength as the flow rate is increased. After 16.5 mL/min, parallel flow breaks down completely and the flow becomes dispersed (**Figure 4.2**i). Using the toluene/aqueous NaOH system, slugs were initially formed. Above 12 mL/min, the slugs were pushed against the outside wall of the circular zone by inertia and some fine drops were sheared off.

The **Venturi micro-mixer** produced initially drops for the n-butanol/aqueous NaOH system (**Figure 4.2**h), but they coalesced through the micro-reactor and sometimes exited in the form of slugs. The coalescence was mostly observed for synchronized drops on each side of the triangular obstacle when entering the 180^{o} curve, because the inertia pushed the inside drop towards the outside one. Higher flow rates produced a smaller initial drop size, but also increased coalescence in the curve due to greater inertia [see Video 2 in Section 4.7]. Above 8 mL/min, the flow was considered dispersed. Drop coalescence was less pronounced for the toluene/aqueous NaOH system. Above 6 mL/min, a jet was formed in the expansion zone and occasionally broke down into drops at higher flow rates due to instabilities [Video 3 in Section 4.7].

The **Sickle micro-mixer** was made as an improvement of the Venturi. The triangular obstacle and the curve were combined to desynchronize drops and avoid coalescence, while the contraction was reshaped to favor jetting and subsequent jet break-up by lateral eddies. For both liquid-liquid systems, drop flow was initially obtained (**Figure 4.2**g). The flow regime was considered dispersed by 3 mL/min for the n-butanol/aqueous NaOH system and 6 mL/min for the toluene/aqueous NaOH system. Only the Sickle achieved dispersed flow with the toluene/aqueous NaOH system (**Figure 4.2**j).

The **Spade micro-mixer** initially produced drops for the n-butanol/aqueous NaOH system (**Figure 4.2**f). At 6 mL/min, a regime similar to parallel flow where the flow is divided into lamellas was observed (**Figure 4.2**e), but it was not stable and broke down into drops approximately halfway through the reactor. The presence of the unstable parallel flow

regime for the n-butanol/aqueous NaOH system was investigated more closely and could be repeated for flows of 6-10 mL/min [see Video 4 in Section 4.7]. Above 18 mL/min, drop flow transitioned to dispersed flow. For the toluene/aqueous NaOH system, large slugs (**Figure 4.2**b) were initially observed and became unstable slugs/drops after 8 mL/min.

4.3.2 Discussion

Published literature has not clearly explained the transition from slug to parallel flow. It is often reported that interfacial tension curves the interface and helps maintain a slug shape, but both the inertial or viscous forces are sometimes deemed responsible for extending and dragging the interface downwards. A thorough mechanism of transition from slug to parallel flow still needs to be developed in order to define if the transition should be expressed using the Weber number (inertia/surface forces) or the Capillary number (viscous/surface forces). Guillot and Colin [95] observed transitions between slug and parallel flow in a straight micro-channel at $Ca < 1$ using a system of water dispersed in silicon oil or n-hexane. Similar observations were reported by Dessimoz et al. [120] for toluene dispersed in water. On the other hand, Zhao, Chen and Yuan [41,127,128] studied water and kerosene flow through a T-junction followed by a micro-channel and described the flow regimes using different Weber number criteria.

The formation of parallel flow is reported to be favored in rectangular shaped channels [95] and for high phase viscosity ratios [129]. The contact angle of the continuous phase also impacts the stability of parallel flow and may change the flow regime at equal Capillary number [120,130,131]. The transition to parallel flow reduces the overall pressure drop through a channel due to a lubrication effect by the less viscous liquid. Russell and Charles [132] analyzed this reduction in friction by presuming applicability of the Navier-Stokes equation for incompressible liquids and found that the position of the interface was a function of only the viscosity ratio when ignoring interfacial tension effects. For liquids systems with an elevated interfacial tension, Pohar et al. [133] showed that the flow ratio also affects the position of the interface. This suggests that systems with a relatively low interfacial tension will be less affected by the flow ratio and enter a parallel flow regime more easily.

In the present study, parallel flow was observed for the n-butanol/aqueous NaOH system ($\mu_d/\mu_c = 2.29$, $\sigma = 1.8$ mN/m) and not for the toluene/aqueous NaOH system ($\mu_d/\mu_c = 0.49$, $\sigma = 35.4$ mN/m). This is consistent with reported observations since the viscosity ratio of the n-butanol/aqueous NaOH system is greater, its interfacial tension lower and n-butanol better wets the metal than toluene.

Additionally, parallel flow was observed only for curvature-based micro-mixers (i.e., the SZ and TG) and the Spade micro-mixer. The latter is at some extent also based on symmetrical curvatures and it produced a transitional parallel flow for a specific range of flow rates (6-10 mL/min), which may be outside the recommend operating range for a similar-sized commercial Advanced-Flow™ reactor by Corning®.

In curves, the centrifugal force pushes the denser fluid towards the outside perimeter, which may favour the segregation of phases into a parallel-like flow pattern. At the higher flow rates, eddies and instabilities across the interface will eventually cause the parallel flow to break down, as observed in our experiments. However, the range of flow rates over which parallel flow is observed in the TG and SZ micro-mixers is relatively large since their geometry locally increases the interfacial forces via a forced curvature of the interface that dampens short wavelength instabilities. In contrast, obstacle-based micro-mixers (e.g., the Venturi and Sickle) generated drop flow from the onset of flow conditions and avoided parallel flow.

4.4 Liquid-liquid hydrolysis

Suitable test reactions for mass transfer investigations must be fast enough to be considered not kinetically limited [19,55,82,134]. The conversion of the reactants is then proportional to the mass transfer rate and allows straightforward calculation of the interphase mass transfer coefficient. The two-phase alkaline hydrolysis of 4-nitrophenyl acetate has been used previously in the literature due to its fast intrinsic kinetics and ease of analysis [20,83,84]. The intrinsic reaction rate constant has been estimated at 14 L/mol/s, [85] which is sufficient to be modeled as an instantaneous or a very-fast reaction in most multiphase systems. An excess of NaOH was used and the reaction is considered pseudo-first order. All of the 4-nitrophenyl acetate transferring into the

aqueous solution is consumed ($C_{aq} = 0$) and the overall volumetric mass transfer coefficient, $K_{org}a$, is calculated using Equations (4.1) to (4.3).

$$Q_{tot}\varphi_{org} \cdot \frac{dC_{org}}{dV_R} = -K_{org}a\left(C_{org} - E \cdot C_{aq}\right) = -K_{org}a \cdot C_{org} \quad (4.1)$$

$$\eta = 1 - \frac{C_{org}^{out}}{C_{org}^{in}} = 1 - \exp\left(-\frac{K_{org}a}{\varphi_{org}} \cdot \tau\right) \quad (4.2)$$

$$K_{org}a = -\frac{\varphi_{org}}{\tau}\ln(1-\eta) \quad (4.3)$$

4.4.1 Experimental results

The hydrolysis conversion of 4-nitrophenyl acetate for each reactor and liquid-liquid system is shown in **Figure 4.3**. The conversion using the n-butanol/aqueous NaOH system was between 9% and 100%. Using the toluene/aqueous NaOH system, it was significantly lower and below 7%. The observations specific to each micro-reactor are described below.

The **SZ micro-reactor** showed a large decrease in conversion (from 70% to 19%) upon transition to parallel flow when using the n-butanol/aqueous NaOH system. Once the parallel flow broke down into drop/dispersed flow, the conversion increased to 56%. Using the toluene/aqueous NaOH system, the conversion decreased from 4.0% to 1.3% in the slug flow regime and increased to 2.0% when the slugs became unstable after 20-25 mL/min.

The **TG micro-reactor** initially yielded a 50% conversion under slug flow at 1.6 mL/min for the n-butanol/aqueous NaOH system and the transition to parallel flow decreased it to 9.0%. In the parallel flow with corner recirculation, the conversion increases up to 24% at 16.5 mL/min. Upon transition to dispersed flow, the conversion reached 54% at 22 mL/min before slowly decreasing afterward. Using the toluene/aqueous NaOH system, the conversion decreased from 3.5% to 1.3% in the slug flow regime and increased slightly at flow rates above 12 mL/min. It reached only 2.1% at 42.5 mL/min.

The **Venturi micro-reactor** yielded an initial conversion of 81% for the n-butanol/aqueous NaOH system at 1 mL/min. Due in part to drop coalescence [see Video 2 in Section 4.7], the conversion decreased to 63% at 2 mL/min and remained constant until 8 mL/min when the flow was considered dispersed. Afterwards, the conversion slowly decreased and reached 35% at 28 mL/min. For the toluene/aqueous NaOH system, the initial conversion was 4.2% and decreased upon increased flow rate. It stabilized around 1.5% when jets at the contraction started to form.

The **Sickle micro-reactor** achieved 100% conversion at 0.8 mL/min for the n-butanol/aqueous NaOH system. The conversion decreased to 85% upon increasing the flow rate and kept decreasing slowly upon transition from drop to dispersed flow, but distinct slopes are clearly identifiable for each flow regime. A conversion of 6.6% was obtained initially for the toluene/aqueous NaOH system and decreased to 2.9% at 4 mL/min due to a decrease in residence time. Upon transition from drop to dispersed flow, the conversion increased to 4.6% before gradually decreasing again.

The **Spade micro-reactor** had an initial conversion of 51% at 1 mL/min for the n-butanol/aqueous NaOH system. The transition to parallel flow decreased it to 14%. Upon re-entering drop flow, the conversion increased to 21-23% and stabilized once the flow was considered dispersed. For the toluene/aqueous NaOH system, the initial conversion was 1.5% in the slug flow regime. After 8 mL/min, large drops were observed, and the conversion decreased below analytical precision beyond 16 mL/min due to insufficient residence time. The available area of this reactor plate was not completely covered with the Spade micro-mixer yielding a lower volume and residence times relative to the other micro-reactor plates.

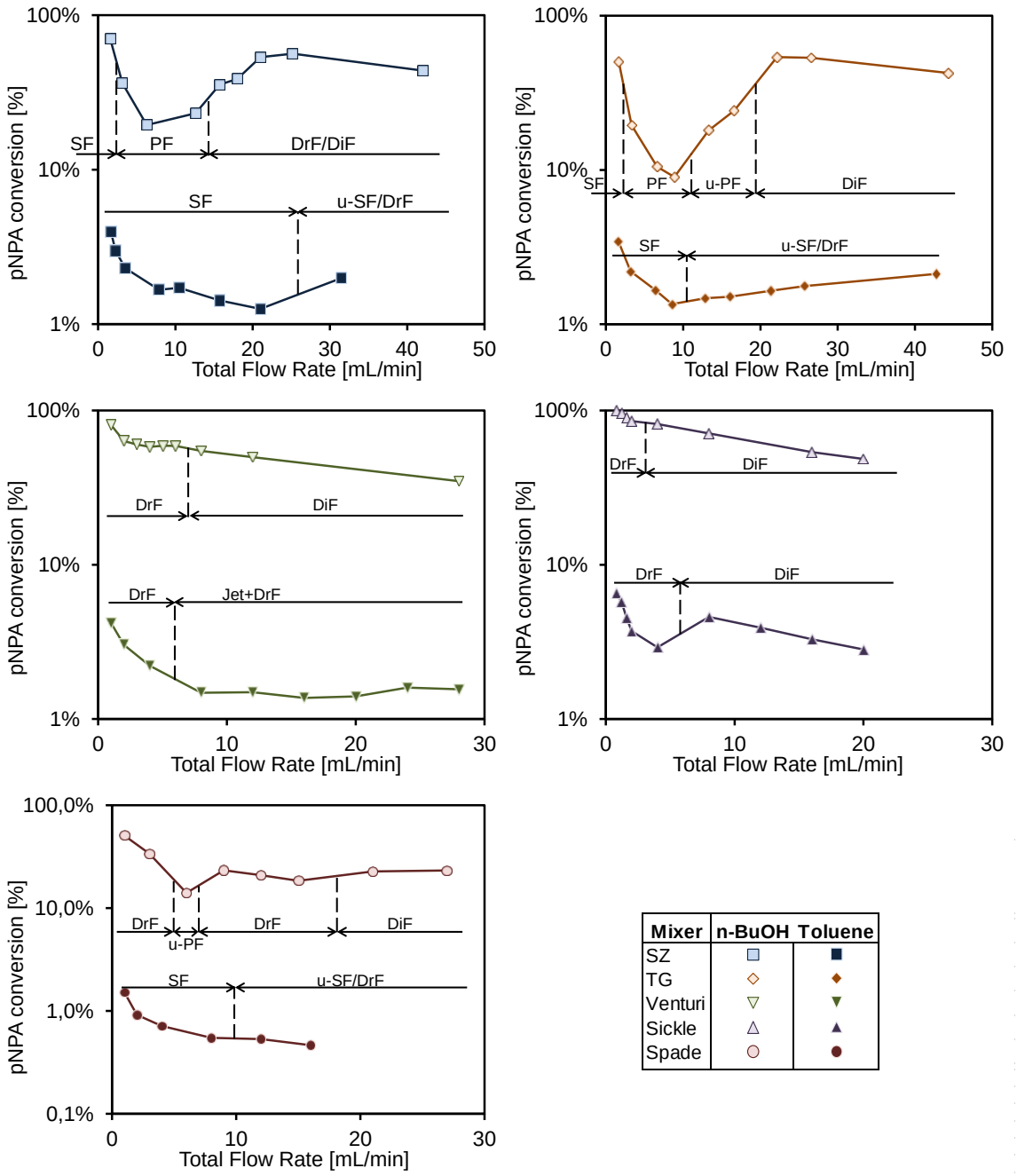

Figure 4.3 Hydrolysis conversion of 4-nitrophenyl acetate in the SZ, TG, Venturi, Sickle and Spade micro-reactors. Flow regimes are identified by SF (slug flow), PF (parallel flow), DrF (drop flow), DiF (dispersed flow) and sometimes the prefix "u-" (unstable).

4.4.2 Discussion

For both liquid-liquid systems, a similar trend of conversion against flow rate was observed. Initially, in the slug flow regime, the conversion decreases with increasing flow rate since the impact of lower residence time is greater than the increase in interfacial

area or slug internal recirculation. For the n-butanol/aqueous NaOH system, the conversion dropped further upon entering a parallel flow regime for certain reactors. At higher flow rates, a transition occurs where instabilities and stronger secondary flow patterns reduce the dispersion size and an increasing conversion with flow rate trend is observed. A plateau and slight decrease of conversion is observed at the highest flow rates once the flow is fully dispersed. This overall trend has been previously observed in literature [28,78,84] and is further supported by **Figure 4.4** where the overall volumetric mass transfer coefficient ($K_{org}a$) is plotted against the total flow rate. In the dispersed flow regime for the n-butanol/aqueous NaOH system, the overall volumetric mass transfer coefficient of each micro-mixer converges to a similar value. Furthermore, results obtained with the Sickle micro-mixer show that $K_{org}a$ values for the toluene/aqueous NaOH system differ from those for the n-butanol/aqueous NaOH system and indicate that, within the dispersed flow regime, $K_{org}a$ depends primarily on the fluids' physical properties, such as interfacial tension, with marginal impact of geometry.

Three papers published by Kashid et al. in 2011 [47,72,73] analyzed the flow regimes, conversions, and mass transfer of five micro-reactors for liquid-liquid and gas-liquid flow. Upon transition to parallel flow, the derivative of $K_{org}a$ with respect to flow rate decreased or became negative. Only one complex micro-reactor achieved dispersed flow, yielding the highest *mixing effectiveness*, as the other four reactors were variants of a T-junction contactor.

The utilization of simpler T-junction type micro-reactors becomes problematic for scale-up. They generally operate in slug or parallel flow, since a fine dispersion can only be generated at elevated flow rates and since the energy dissipation rate is not sustained, which can result in the coalescence of the dispersion downstream. To compensate, a small channel diameter is used to generate slugs with a relatively large surface-to-volume, but at the cost of increased pressure drop. In order to increase production using T-junction type micro-reactors, while considering the limitations mentioned above, a parallelization approach is required, which is not always economically or operationally efficient and feasible [33,37,102]. Alternatively, micro-reactors relying on the

continuous break-up of the dispersed phase, such as those depicted in this article, are not bound by the same limitations.

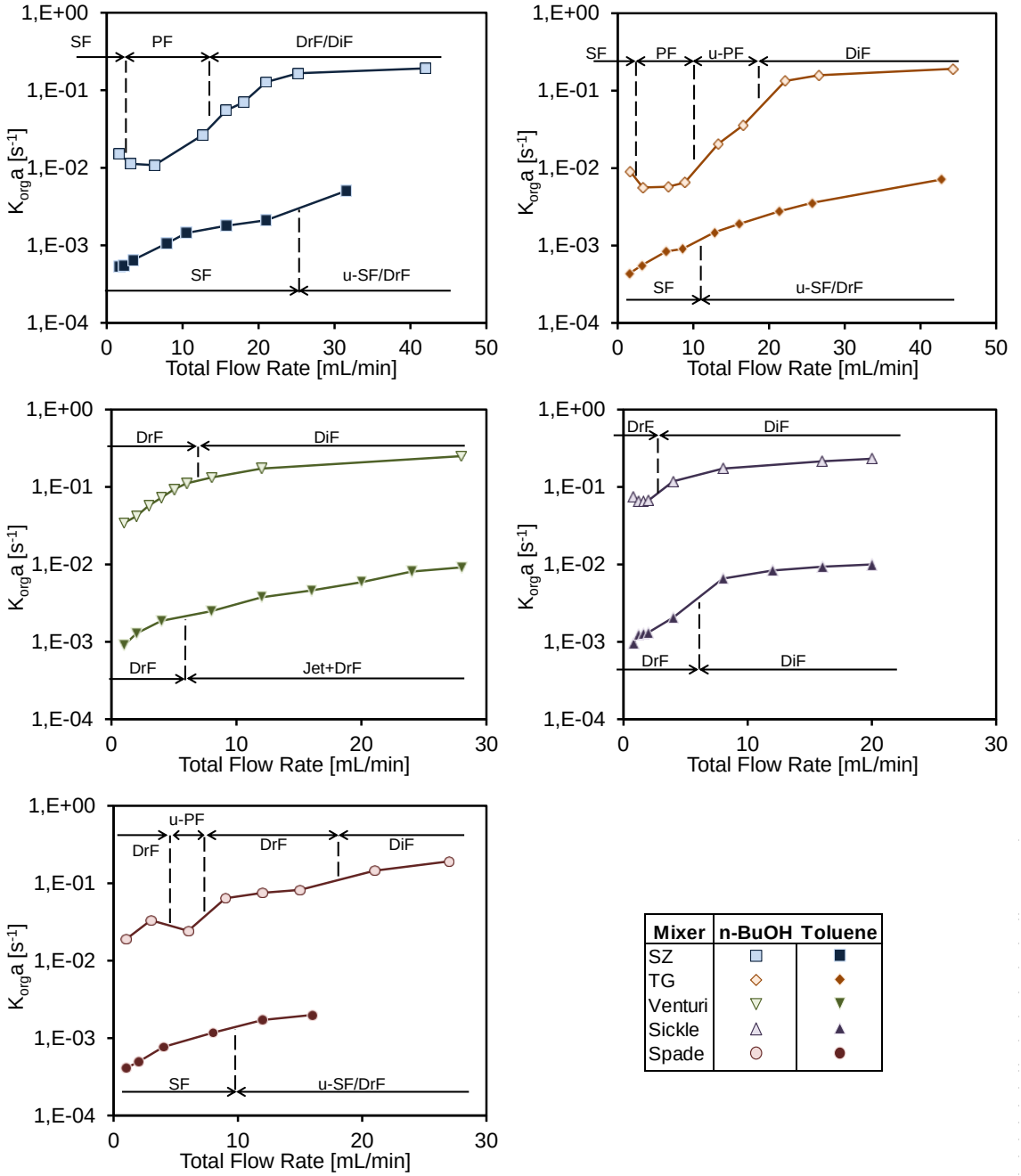

Figure 4.4 Overall volumetric mass transfer coefficient of both liquid-liquid systems at various flow rates for all micro-mixers. Legend is the same as in **Figure 4.3**.

Laminar break-up of droplets can occur via deformation of the interface by viscous shear or elongation shear. The velocity gradients generated by vortices in curves [26,29,96]

can generate such viscous shear and the contraction or expansion of channels generates elongation shear. Turbulent break-up of droplets occurs when they collide with eddies of equal or smaller size with a kinetic energy sufficient to increase the interfacial area of the system. A higher rate of energy dissipation, calculated from (4.4), increases the eddy collision frequency and kinetic energy, yielding an overall increase in break-up rate and a decrease in dispersion size [111,113]. Additionally, high energy dissipation rates reduce the boundary layer thickness around the interface, lowering the convective mass transfer resistance [135]. The overall volumetric mass transfer coefficients, $K_{org}a$, are plotted against energy dissipation rate on **Figure 4.5**.

$$\bar{\varepsilon} = \frac{\Delta P Q_{tot}}{\rho_c V_R} = \frac{\Delta P}{\rho_c \tau} \tag{4.4}$$

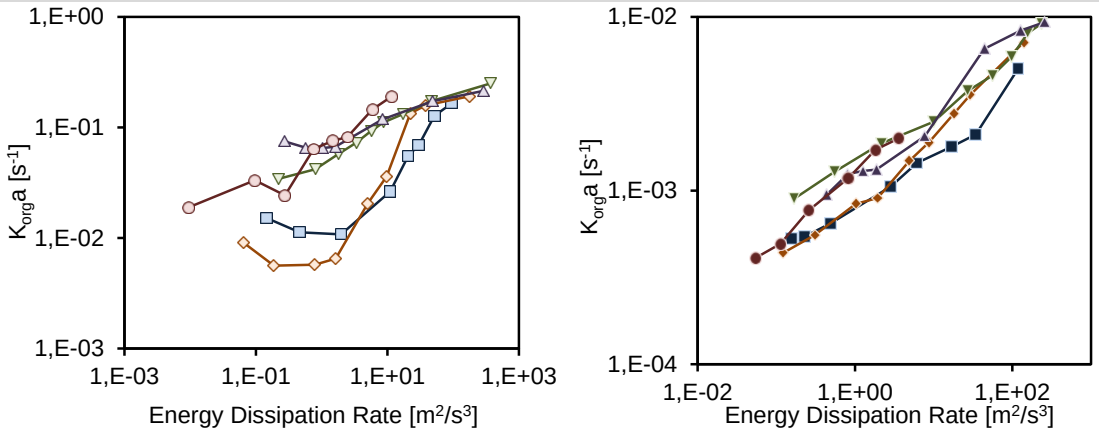

Figure 4.5 Overall $K_{org}a$ in the different micro-mixers for the n-butanol/aqueous NaOH system (left) and for the toluene/aqueous NaOH system (right). Legend is the same as in **Figure 4.3**.

In the investigated micro-mixers, the Reynolds number of the continuous phase varies between 20 and 1350 which would yield laminar flow in a single phase straight channel scenario. However, they are designed to generate secondary flow patterns and vortices that produce a gradual transition from laminar to turbulent flow as they grow in strength and become unstable. As a result, much like the collision frequency and kinetic energy of turbulent eddies, the number and intensity of these secondary flow patterns increase with the rate of energy dissipation, even at low Reynolds number [11,28]. This leads to an increasing $K_{org}a$ at higher $\bar{\varepsilon}$ for the drop and dispersed flow regimes. Similar rates of energy dissipation, within these flow regimes and a particular liquid-liquid system, result

in similar values of $K_{org}a$. A power law model was fitted using all micro-mixers to the drop and dispersed flow regime data for the n-butanol/aqueous NaOH system (Equation (4.5)). The average absolute relative deviation (Equation (4.6)) was only 14%.

$$K_{org}a = 6.55 \times 10^{-2} \cdot \bar{\varepsilon}^{0.23} \quad (4.5)$$

$$AARD = \frac{1}{N}\sum_{i=1}^{N}\left|1 - \frac{C(\varepsilon_i)^n}{(K_{org}a)_i}\right| \quad (4.6)$$

The effect of geometry is thus minor once the secondary flow patterns involved in breaking the dispersion have a characteristic length smaller than the geometrical scale of the micro-mixer. Similar to the theory of Kolmogorov, large secondary flow patterns transfer energy to smaller ones until the energy is dissipated in interface creation or heat. The micro-mixer geometry will mainly affect the minimum flow rate at which the drop or dispersed flow regime is attained. This is earliest for the Sickle micro-mixer, followed by the Venturi. Both of them have the smallest hydraulic diameter and consequently the greatest pressure drop and rate of energy dissipation at a given flow rate.

4.5 Reactor comparison

In this section, the micro-reactors are compared by considering both the intensification of mass transfer due to their micro-mixer geometry, and the residence time they provide. The comparison is plotted on **Figure 4.6** using the modified first Damköhler number, calculated from Equation (4.7), and the inverse of the second Damköhler number calculated from Equation (4.8). Data for the Spade micro-reactor is omitted as its plate was not fully covered with micro-mixers, resulting in an unfair volume penalty.

$$Da_I' = K_{org}a \cdot \tau \quad (4.7)$$

$$Da_{II}' = \frac{1}{Da_{II}} = \frac{K_{org}a}{kC^{n-1}} \quad (4.8)$$

Da_I' is a dimensionless measure of conversion and represents the residence time relative to the characteristic reaction time. For fast liquid-liquid reactions, the reaction rate is mass transfer limited and Equation (4.7) modifies Da_I by using the overall volumetric mass transfer coefficient instead of the intrinsic reaction rate constant. A large Da_I' value means that molecules have sufficient time to transfer between phases and react before exiting the reactor.

Da'_{II} is a dimensionless measure of mass transfer and represents the time required for molecules to react relative to the time for interphase transfer. For mass transfer limited reactions, it is by definition small since the intrinsic reaction rate is much greater than the rate of mass transfer. This parameter is relevant for the selectivity in certain reaction networks. A Grignard reaction, for example, will benefit from a large Da'_{II} value since a rapid transfer of reactants relative to the reaction kinetics will increase the selectivity by preventing the subsequent reaction of the product and the formation of undesired compounds, as reported by Plouffe et al [67].

For each micro-reactor, a large Da'_{I} (X-axis) is usually obtained at the cost of a small Da'_{II} (Y-axis). However, an increase in both parameters can be observed upon transition from slug or parallel flow to drop or dispersed flow, where the mass transfer rate sufficiently increases to compensate for a reduction in residence time. A decrease in both parameters is noticeable for the reactors using the SZ or the TG micro-mixers when entering parallel flow. These data points are then dominated by all others in terms of Da'_{I} and Da'_{II} and this flow regime must be avoided for optimized operation.

Reactors relying on curvature-based micro-mixers are not suited for fast liquid-liquid reactions despite their larger volume. They generated relatively low energy dissipation rates and are conducive to the formation of undesirable parallel flow patterns. Those relying on obstacles, contractions and expansions performed better. The Sickle micro-reactor produced combinations of Da'_{I} and Da'_{II} that dominated the Venturi for all data points. Thus, it would be the best suited amongst those compared for the operation of a fast liquid-liquid reaction, especially in cases where high mass transfer rates are required to obtain a high selectivity (i.e., greater Da'_{II}).

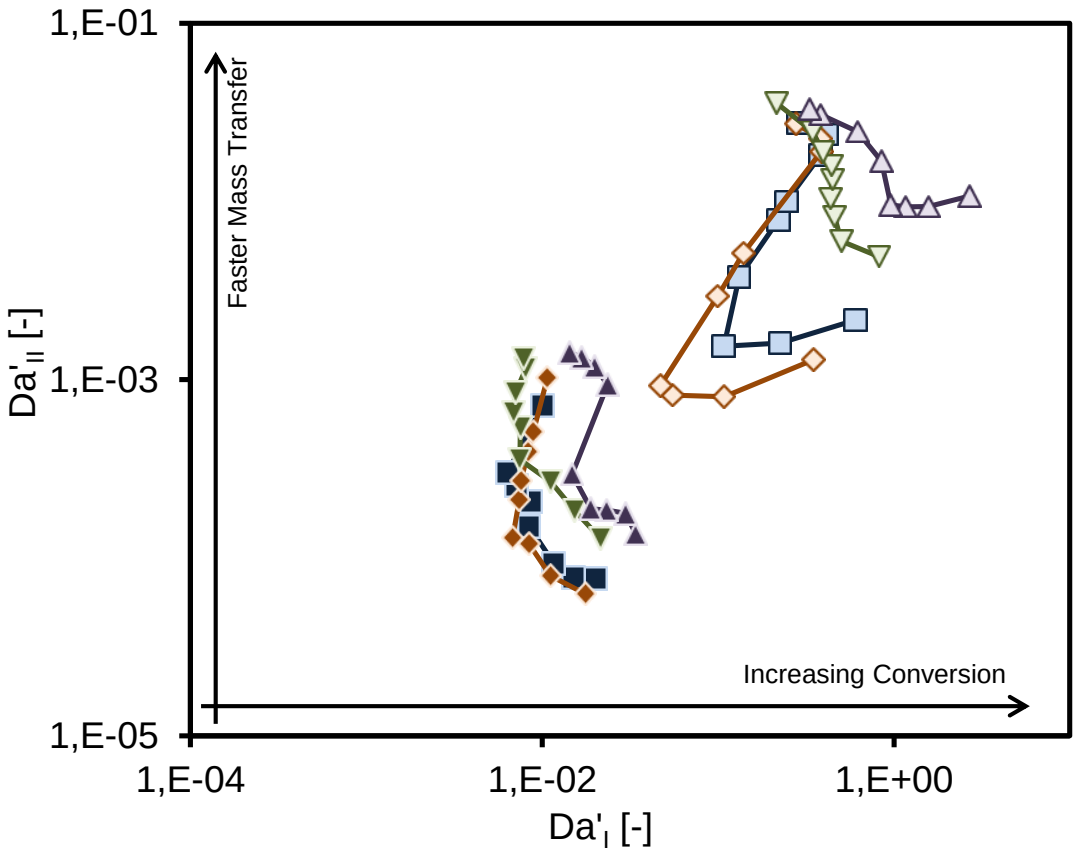

Figure 4.6 Modified Damköhler numbers for both systems for the micro-reactors. Legend is the same as in **Figure 4.3**.

4.5.1 Conclusion

An aqueous alkaline solution and a 0.05 M solution of 4-nitrophenyl acetate in toluene or in n-butanol were fed at equal flow rates in five different micro-reactors. Due to the range of flow rates investigated, multiple flow patterns were observed. The dispersed phase usually started as slugs and ended as fine droplets at higher flow rates. For the SZ, TG and Spade mixers using n-butanol/aqueous NaOH, parallel flow was obtained between the slug and dispersed flow regimes. While the mechanism for the transition of slug to parallel flow is not fully understood, it was observed in all curvature-based micro-mixers in this study. Centrifugal forces push the denser fluid to the outside of the curve and such channels may dampen the instabilities.

The hydrolysis conversion of the 4-nitrophenyl acetate was measured at the outlet of each micro-reactor. For both liquid-liquid systems, a similar trend of conversion against flow rate was observed. Initially, in the slug flow regime, the conversion decreases with

increasing flow rate, because the impact of lower residence time is greater than the gain in interfacial area or slug internal recirculation. For the n-butanol/aqueous NaOH system, the conversion decreased further upon entering a parallel flow regime for certain reactors. At greater flow rates, a transition occurs where instabilities and stronger secondary flow patterns reduce the dispersion size and an increasing conversion with flow rate trend is obtained. A plateau and slight decrease of the conversion is observed at the highest flow rates once the flow is fully dispersed.

The overall volumetric mass transfer coefficient was analyzed against the rate of energy dissipation for each micro-mixer. It showed that within the dispersed flow regime, $K_{org}a$ was primarily a function of the phases physical properties and energy dissipation rate, but not directly of the micro-mixer geometry which affects the resulting pressure drop and flow regime at a given flow rate. This could be due to the secondary flow patterns involved in the dispersed phase break-up mechanisms having a characteristic length smaller than the micro-mixers.

Select micro-reactors were compared based on different Damköhler numbers. For both liquid-liquid systems, the Sickle micro-reactor performs best and provided the greatest mass transfer rates. For both liquid-liquid systems, the TG micro-reactor performs worst due to very stable parallel flow. Micro-reactors using curvature-based micro-mixer did not perform well under the studied conditions. This is of fundamental importance when considering that many commercial micro/mini reactors presently rely on curvature-based micro-mixers to generate secondary flow patterns. Contraction-expansion and obstacle-based micro-mixers, such as those presented in this work, are better suited for fast liquid-liquid reactions.

4.6 Acknowledgement

The authors would like to thank the Natural Sciences and Engineering Research Council of Canada and Lonza AG for their financial contribution. Also Ehrfeld Mikrotechnik BTS is acknowledged for the reactor manufacturing.

4.7 Supplementary material

Available online:

Video 1 Unstable parallel flow in TG micro-reactor using n-butanol/aqueous NaOH system. Total flow is 12.8 mL/min.

Video 2 Coalescing drops in Venturi micro-reactor using n-butanol/aqueous NaOH system. Total flow is 1.0 mL/min.

Video 3 Jetting drops in Venturi micro-reactor using toluene/aqueous NaOH system. Total flow is 8.0 mL/min.

Video 4 Unstable parallel flow break point in Spade micro-reactor using n-butanol/aqueous NaOH system. Total flow is 6.0 mL/min.

4.8 Nomenclature

Definitions

Micro-Channel	A generally empty channel, straight or curved, with an hydraulic diameter below 1 mm
Micro-Mixer	A segment, of a particular geometry, with a hydraulic diameter below 1 mm and designed for mixing and interphase mass transfer
Micro-Reactor	A combination of micro-channel(s) and/or micro-mixer(s).

Symbols

a	[m2/m3]	Specific interfacial area of contact
C	[mol/m3]	Reactant's concentration
Da	[-]	Damköhler number
E	[-]	Equilibrium partition coefficient
d_h	[m]	Hydraulic diameter of the contraction
k	[1/s]	First order reaction rate constant
K_{org}	[m/s]	Overall convective mass transfer coefficient
n	[-]	Order of the reaction
ΔP	[Pa]	Pressure loss in the reactor

Q	[m3/s]	Volumetric feed flow rate
u	[m/s]	Superficial velocity at the contraction
V_R	[m3]	Volume of the reactor

Greek Symbols

ε	[m2/s3]	Energy dissipation rate
η	[%]	Conversion
μ	[Pa·s]	Fluid viscosity
ρ	[kg/m3]	Fluid density
σ	[N/m]	Fluid interfacial tension with water
τ	[s]	Average residence time
φ_{org}	[-]	Volumetric fraction of the organic phase

Subscripts

aq	-	Aqueous phase
c	-	Continuous phase
d	-	Dispersed phase
org	-	Organic phase
tot	-	Total – sum of the aqueous and organic phase

4.9 References

See thesis references.

5 On the scale-up of micro-reactors for liquid-liquid reactions

By *Patrick Plouffe*[a], *Michel Bittel*[b], *Jonas Sieber*[b], *Dominique M. Roberge*[b] and *Arturo Macchi*[a]

[a] Centre for Catalysis Research and Innovation, Department of Chemical and Biological Engineering, University of Ottawa, K1N 6N5, Ottawa, Canada

[b] Chemical Manufacturing Technologies, Lonza AG, CH-3930, Visp, Switzerland

This manuscript has been submitted to Chem. Eng. Sci. on July 17th, 2015.

Abstract

The scale-up of a micro-reactor with a mixer designed for liquid-liquid reactions is investigated using a $3/7^{th}$ approach that scales the hydraulic diameter at increased flow rates and keeps constant the average rate of energy dissipation. Smaller ($d_h = 283$ μm) and larger-scale ($d_h = 714$ μm) mixers are compared using single phase pressure drop measurements and a liquid-liquid reactive extraction. The single phase tests demonstrate that the energy dissipation rate of the larger scale mixer is accordingly comparable to the smaller scale mixer at flow rates ~8.5 times greater. The overall volumetric mass transfer coefficients of the reactive extraction, $K_c a$, of both scale mixers were also similar at equal energy dissipation rate in the drop flow regime. Finally, the upper limit of the sizing approach is discussed in terms of heat transfer limitations and comparability with commercially available static mixers.

Highlights

- A constant energy dissipation approach was used to scale-up micro-reactors.
- Two different sizes were tested using a liquid-liquid reactive extraction.
- Their energy dissipation rates and $K_c a$ were similar at designed flow rates.
- The impact of scale-up is evaluated for different heat generation rates.
- Different reactor sizes and commercial mixers are compared for scale-up.

Keywords

Micro-reactor, liquid-liquid, scale up, energy dissipation, reactive extraction, transport phenomena

5.1 Introduction

Micro-reactors have sub-millimeter characteristic lengths that enable reaction control over harsh process conditions difficult to reach with conventionally sized reactors. At relatively small flow rates, they have become essential tools for process development in flow [64]. By using them modularly [67], micro-reactors allow novel and intensified process conditions that can be carried upon scale-up [21]. As a result, they have been an attractive technology for process development and intensification in the fine chemical and pharmaceutical industries, which remain traditionally dominated by batch and semi-batch synthesis [3,12].

During the development of a new medicine [1,14], milligrams of the diverse candidates will be required for toxicological and kinetics studies. Some of these molecules may then proceed to the next development stages where an increased amount of material will be synthesized for the pre-clinical trials (grams), clinical trials (kilograms) and productions (tons). Therefore, the production process needs to be versatile and scalable over several orders of magnitude from 10^{-3} to 10^{6} grams. Additionally, it is advantageous to use a continuous process early on, i.e. to use micro-reactors, in order to establish a manufacturing process in flow. Then, scale-up of the production rate can be performed generally via one of two methods: numbering-up of micro-reactors, or sizing-up of the constituting channels and mixers.

With numbering-up, micro-reactors are added in parallel and the flow of reactants is divided amongst them. This method of scale-up can maintain the advantages of the smaller scales, but is difficult to apply in practice. The difficulty arises mainly with the dosing of the reactants; the equal and stoichiometric subdivision of the different reactant feeds into amounts greater than two or three can be challenging especially for multi-phase reactions [71]. The sizing-up approach is not similarly limited in practice, but the sized-up dimensions have to be carefully engineered to carry the advantages of miniaturization at larger production rates.

This research group has previously described a mathematical approach to the conservation of mass transfer performance for the sizing-up of micro-reactors as well as

provided some supporting evidence for single phase reactions [11,33]. The fundamental approach is derived from the scale-up of turbulent static mixer for mixing in pipes (for examples, see Etchells and Meyer (Chapter 7 of of Paul et al. [79])). An article by Woitalka et al. [136] successfully matched the extraction efficiency and mass transfer coefficient of different sized liquid-liquid micro-reactors as a function of residence time. However, no detail is provided on the approach used for scale-up and the basis of comparison, residence time, is insufficient without more information since adding mixing elements would increase time spent in the reactor for a given flow rate, but not the mass transfer coefficient. The purpose of this work is to test an energy dissipation derived sizing-up approach with a liquid-liquid system and to evaluate its impact on the inter-phase mass and wall-to-fluid heat transfer performance of a micro-reactor. Additionally, a comparison is made with traditionally sized static mixers and reactors to determine the operational boundary of both types of reactors.

5.1.1 Derivation of the Scale-Up Rule and Sizes

The size and velocity of eddies in a fluid as well as the thickness of the boundary layer at the interface with another fluid vary with the energy dissipation rate and impact mixing and mass transfer. The sizing-up approach assumes that the mass transfer performance of a sized-up reactor will stay the same if the average rate of energy dissipation is kept constant during scale-up. The average rate of energy dissipation is calculated from the total flow rate, pressure drop and volume of the reactor as shown in Equation (5.1).

$$\varepsilon = \frac{\Delta P Q}{\rho V_R} \propto f \frac{Q^3}{d_h^7} \tag{5.1}$$

From Equation (5.1), it is possible to calculate the required reactor size at a scaled flow rate to keep the energy dissipation constant, as shown in Equation (5.2). In a straight channel, the friction factor would be proportional to the inverse of the Reynolds' number for laminar flow and constant for turbulent flow. In the first case, the hydraulic diameter would scale with the ratio of the design flow rates to the power of 1/3 while in the second it would be to the power of 3/7.

$$\frac{d_{h2}}{d_{h1}} = \left(\frac{f_2 Q_2^3}{f_1 Q_1^3}\right)^{1/7} \tag{5.2}$$

It is postulated that the $3/7^{th}$ rule is adequate, because the chaotic secondary flow patterns associated with mixing and phase break-up grow in strength with energy dissipation similarly to turbulent eddies. Moreover, the scaling is applied to micro-mixers in which the transition from laminar to turbulent flow is smooth and occurs at Reynolds number that are traditionally lower than in a straight circular pipe [137]. Thus, the ratio of the friction factors should be close to unity, especially once to the power of 1/7. Therefore, it can be calculated that a 10-fold increase in flow rate should be accompanied with a sizing-up of the geometry by a factor of 2.68.

The manufacturing process of the micro-reactors in this study did not allow dimensions smaller than 200 µm wide by 500 µm deep ($d_h = 286$ µm), so this was chosen as the small scale benchmark and is referred to as "Size 600". A 10-fold scaled-up version of the micro-reactors would thus require channels 537 µm wide by 1341 µm deep ($d_h = 767$ µm). The dimensions were adjusted to standard sizes of 500 µm wide by 1250 µm deep ($d_h = 714$ µm) corresponding to an actual flow rate scaling factor of ~8.5 and is referred to as "Size 300".

5.2 Experimental Setup

The micro-reactor used in this work is made of a series of micro-mixers such to continuously agitate the phases and dissipate energy. The micro-mixer is an improvement of a previous one presented in an earlier publication [75] and is specifically designed for multi-phase systems. The structure focuses the flow onto an obstacle designed to break the dispersed phase and to desynchronize the fragments using a non-symmetrical obstacle and chambers of unequal volume. The micro-reactors were machined on a Hastelloy® ISO 216 A7 plate (74 mm wide by 105 mm long) for the Size 600 micro-mixer, and on ISO 216 A7 and A5 (148 mm wide by 210 mm long) plates for the Size 300 micro-mixer. The plates were used in a FlowPlate® Lab and A5 system (Ehrfeld Mikrotechnik BTS). On the A5 plate, only the second half of the series of mixers were used. Close-up views of the micro-mixer and plates are shown on **Figure 5.1**. The dimensions and properties of the micro-reactors are depicted in **Table 5.1**.

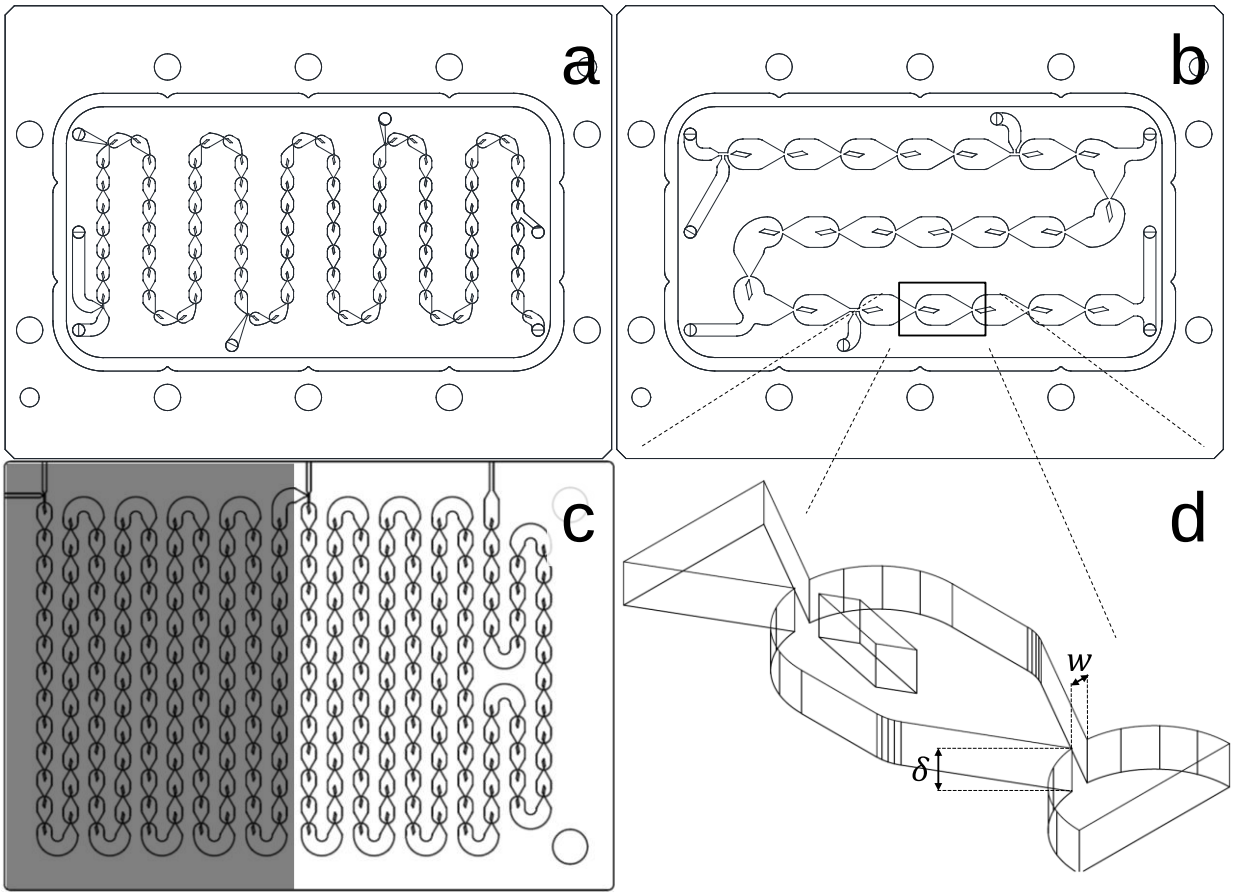

Figure 5.1 Micro-Reactor Plates A7 Size 600 (a) and Size 300 (b), A5 Size 300 (c), and Micro-Mixer (d).

Table 5.1 Micro-Reactors Properties

Scale	Contraction Size (μm)	Plate Size (mm)	Number of Mixers	Volume (mL)
Size 600	w: 200, δ: 500, d_h: 286	A7 (74 x 105)	88	0.269
Size 300	w: 500, δ : 1250, d_h: 714	A7 (74 x 105)	21	1.094
		A5 (148 x 210)	113	5.638

The experimental setup is shown on **Figure 5.2**. The flow rate was measured by an Endress-Hauser Promass A Coriolis flowmeter and the pressure drop across the micro-reactor was measured using a Wika M-11 pressure sensor. The temperature of the feed was measured by a PT100 sensor and the micro-reactor was kept at ambient temperature using a thermal bath. HiTec Zang SyrDos™2 syringe pumps, Teledyne ISCO

Series D syringe pumps or Ismatec Reglo-Z gear pumps were used depending on flow rate and pressure requirements.

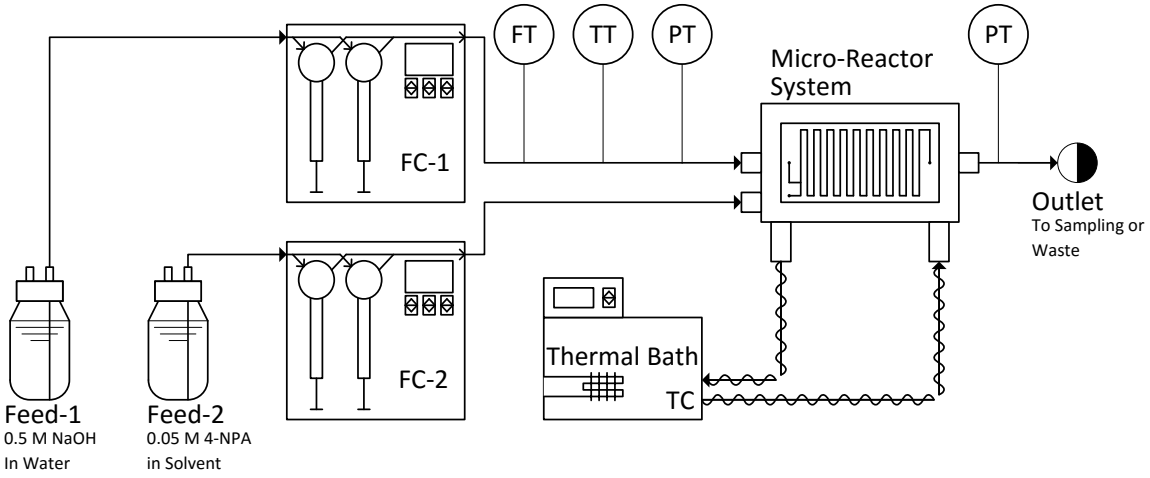

Figure 5.2 Experimental setup. Instruments identified are Flow Controllers (FC), Flow Transmitter (FT), Temperature Controller (TC), Temperature Transmitter (TT) and Pressure Transmitter (PT)

Single phase pressure drop measurements were performed by operating only FC-1 and replacing Feed-1 with distilled water. The chemical reaction used to assess the mass transfer rate was the two-phase alkaline hydrolysis of 4-nitrophenyl acetate (4-NPA, **Scheme 5.1**). This reaction has been used in the past and determined to be a single step second order hydrolysis in water with an intrinsic rate constant of 14.0 L/mol/s [83–85]. The product of the reaction, sodium 4-nitrophenolate, colors the aqueous phase yellow and allows visual distinction between the two phases.

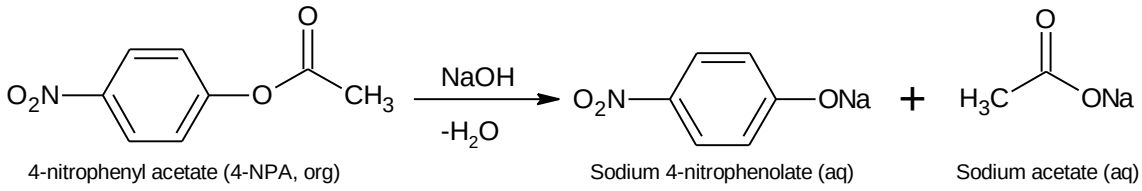

Scheme 5.1 Alkaline hydrolysis of 4-nitrophenyl acetate

The organic phase was a 0.05 mol/L solution of the acetate in either n-butanol or toluene. These solvents were chosen due to their distinct physical properties (**Table 5.2**). The partition coefficients of 4-NPA (H_A) were determined experimentally (see Section 3.8.1). The diffusion coefficients of the acetate were estimated using the Wilke-Chang

correlation [94]. The aqueous phase was a 0.5 mol/L sodium hydroxide (NaOH) solution. A molar ratio of NaOH to 4-NPA 10:1 was chosen to ensure a fast pseudo-first order reaction with a half-life of 0.1 seconds. Both phases were fed in the reactor at equal flow rates. Photographs of the flow were taken for A7 plate runs from a sight glass using a Nikon D40x "kit" camera fitted with a AF-S DX Zoom-Nikkor 18-55mm f/3.5-5.6G ED II lens and the flow regime noted. Samples were taken at the reactor outlet by quenching the two-phase mixture in an agitated solution of acetonitrile, water and acetic acid that homogenized and neutralized the reacting mixture. The stability of the quenched samples was measured over a week and resulted in a conversion drift of about 0.2% per day around pH 5.2-5.3. Samples were analyzed immediately when possible and at most within 24 hours. The molar concentrations of the main reactant and product were determined using a HP Agilent 1100 series HPLC system, which included a G1322A degasser, a G1311A quaternary pump, a G1313A autosampler, a G1316 column compartment and a G1315B diode array detector. A sample volume of 5.0 µL was injected into a 250 mm x 4.6 mm i.d. Agilent Zorbax SB-C8 column to separate the compounds at room temperature. A pre-screening showed that a wavelength of 294 nm was best suited for the simultaneous detection of the product and unconverted reactant. Two mobile phases were used and composed of a 0.1 wt% trifluoroacetic acid solution in HPLC-grade water, or in a mixture of HPLC-grade water (24.1 wt%) and acetonitrile (75.8 wt%).

Table 5.2 Physical properties of solvents at 23°C.

Solvent	ρ (kg/m^3)	μ (mPa*s)	σ (mN/m)	H_A (-)	D_A (m^2/s)
n-Butanol [86–88]	806	2.571	1.8	31 ± 2	3.6E-10
Toluene [86–88]	862	0.552	35.4	230 ± 7	2.3E-10
0.5 M NaOH in Water [93]	1020	1.124	-	-	6.1E-10

5.3 Sizing-up rule validation

The experimental results show that the size 300 micro-reactor was a successful scale-up of the size 600 for flow rates of an order of magnitude greater. This was determined first with pressure drop measurements and then by comparing the overall mass transfer coefficients and the surface-volume average drop diameter over a range of flow rates in each micro-reactor.

5.3.1 Single Phase Energy Dissipation Measurements

The single phase pressure drop throughout the micro-reactors is shown on **Figure 5.3**a. It follows an expected quadratic relationship with the flow rate that results from the gradual transition between laminar and turbulent flow in static mixers [11,74,138]. The average energy dissipation rate is then calculated from the pressure drop. The results of the Size 300 micro-reactor are expected to be the same as those of the Size 600, but at flow rates greater by a factor of 8.5. The measurements of the Size 300 are in good agreement with this, as shown on **Figure 5.3**b; the 95% confidence interval on the average experimental scaling factor was calculated to be 8.6 ± 0.3. This demonstrates that, at least in single phase flow, the 3/7 scale-up rule is valid for the selected range of operating conditions.

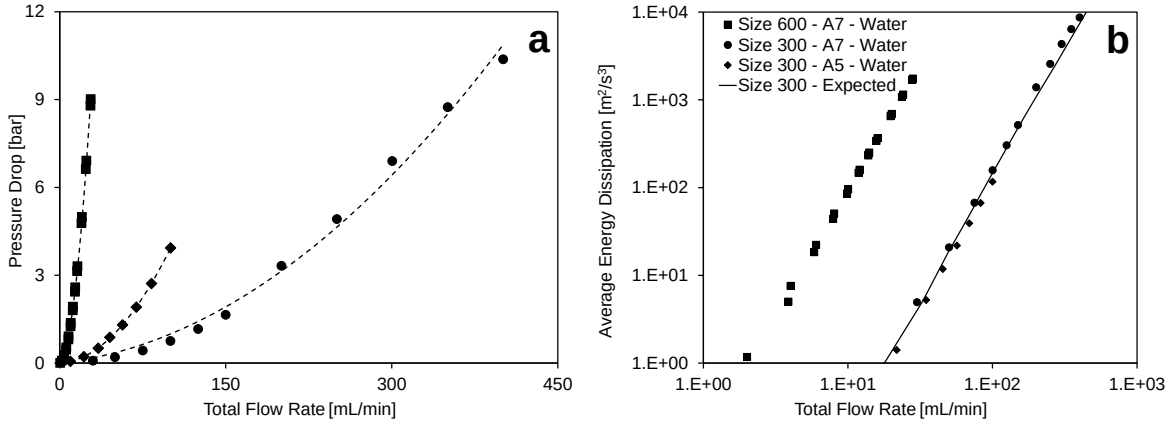

Figure 5.3 Single phase pressure drop (a) and energy dissipation rate (b) measurements in the Size 600 and 300 micro-reactors.

5.3.2 Inter-Phase Mass Transfer Coefficients

The liquid-liquid flow regimes during the reactive multiphase runs were determined visually and are consistent with previous work in complex geometry micro-reactors [75]. At low flow rates, slugs were observed in the reactors. At greater flow rates, the dispersed phase was broken down into drops. Examples are shown on **Figure 5.4**. The flow regimes are mapped on **Figure 5.5** along with the measured experimental conversion.

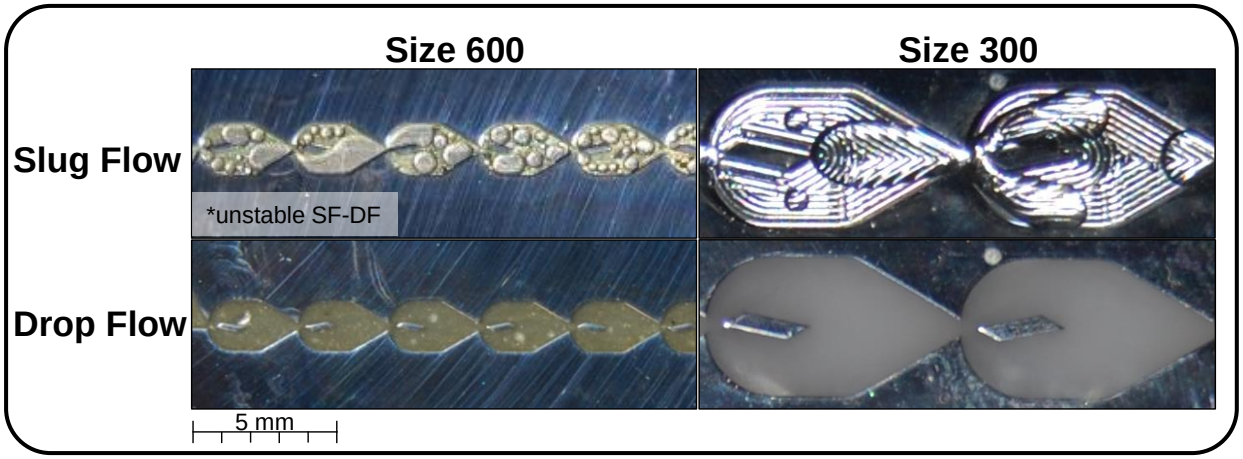

Figure 5.4 Examples of slug flow and drop flow regimes in the micro-reactors. Direction of the flow is from left to right.

The conversion was greater using n-butanol than toluene due to its lower interfacial tension, producing smaller droplets and a greater interfacial area, and to its lower partition coefficient, resulting in a better penetration of the 4-NPA into the aqueous film. While the size 300 micro-mixer is designed for flow rates ~8.5 times greater than in the size 600, the volume of the micro-reactors on A7 and A5 plates were increased by a respective factor of ~4 and of ~20.5. This explains why the conversion values are lower in the size 300 A7 reactor and greater in the size 300 A5 reactor (**Figure 5.5**b and **Figure 5.5**d).

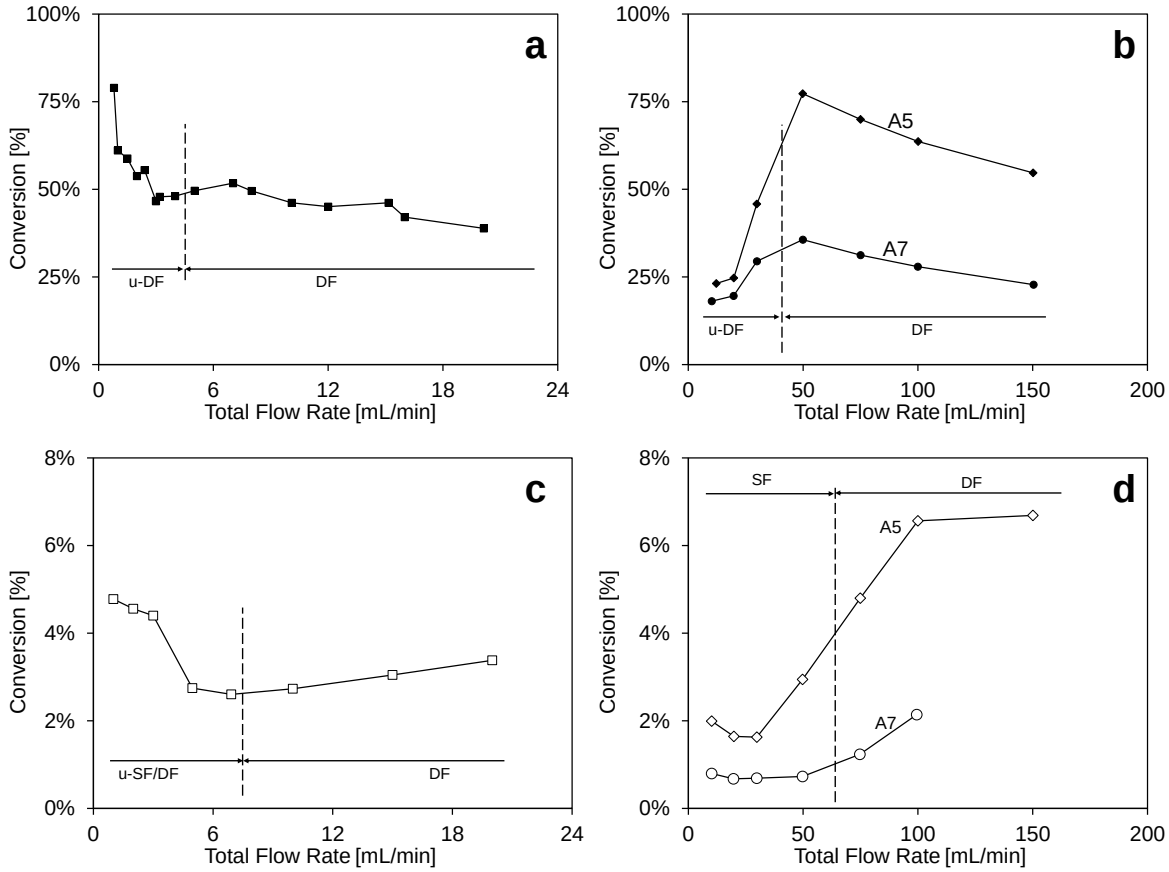

Figure 5.5 Conversion of 4-NPA using 1-butanol in the Size 600 (a) and Size 300 (b) micro-reactors, and using toluene in the Size 600 (c) and Size 300 micro-reactors (d). Flow regimes are identified by SF (slug flow), DF (drop flow), and sometime the prefix "u-" for unstable transition regimes.

By decoupling the effect of residence time from the conversion, it is possible to calculate the continuous phase overall mass transfer coefficient, $K_c a$, as shown in Equations (5.3) to (5.7). **Figure 5.6** displays $K_c a$ against the average rate of energy dissipation calculated from the experimentally measured pressure drop across the micro-reactor. The data correlated well only when a drop flow regime was reached and demonstrates that, indeed, the sizing-up approach was valid then. The similitude did not hold in the slug flow regime occurring at the lower flow rates, where a discrepancy between the reactors was observed. Under this regime, the size of slugs generally depends on the dimensions of the contacting point where they form and not of the energy dissipation [27,96,98,99]. Therefore, the slugs in the Size 300 reactor are larger and have a lower specific interfacial area. Plouffe et al. [75] reported that at elevated energy dissipation rates, the effect of

using differently shaped micro-mixers became marginal once a drop flow regime was obtained. The micro-mixers geometry influenced instead the flow rate at which the drop flow regime was obtained.

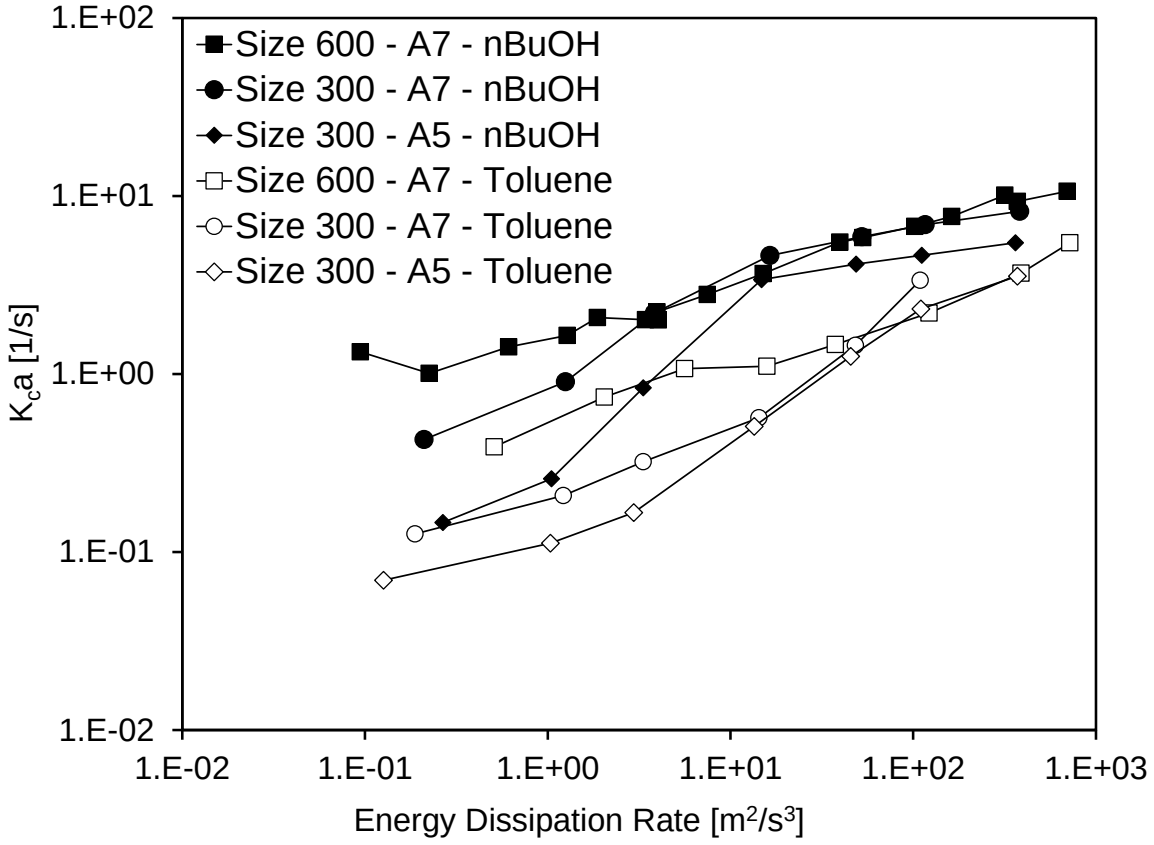

Figure 5.6 $K_c a$ against the average energy dissipation rate.

$$Q_{tot}\varphi_d \cdot \frac{dC_{Ad}}{dV_R} - r_A = Q_{tot}\varphi_d \cdot \frac{dC_{Ad}}{dV_R} - K_d a \cdot C_{Ad} = 0 \tag{5.3}$$

$$\eta = 1 - \frac{C_{Ad}^{out}}{C_{Ad}^{in}} = 1 - \exp\left(-K_d a \frac{\tau}{\varphi_d}\right) \tag{5.4}$$

$$K_d a = -\frac{\varphi_d}{\tau}\ln(1-\eta) \tag{5.5}$$

$$K_c a = H_A \cdot K_d a \tag{5.6}$$

$$\varepsilon = \frac{\Delta P \cdot Q_{tot}}{\rho_c V_R} = \frac{\Delta P}{\rho_c \tau} \tag{5.7}$$

The 4-NPA hydrolysis reaction can be modeled as a fast pseudo-first order reactive extraction [55]. The surface-volume average diameter of the dispersion, d_{32}, in the drop flow regime can be calculated from the experimental results as demonstrated in **Section 3.4.4** using Equation (5.8). It is derived from a stagnant spheres model with a fully developed concentration profile model. The surface-volume average drop diameter is correlated over the different reactor sizes and solvents using two different models. The first model is derived from the theoretical maximum stable drop diameter for turbulent flow [139–141] calculated from the energy dissipation rate in Equation (5.9) and is shown on **Figure 5.7**. The second model uses the Weber and Reynolds dimensionless numbers and is shown on **Figure 5.8**. The details of the fitted correlations are shown on **Table 5.3**. The fitted parameters are shown with a 95% confidence interval calculated from the mean squared residual.

$$d_{32} = \frac{H_A D_{Ad}}{\sqrt{D_{Ac} k_{rxn} C_{Bc}}} \left(\sqrt{1 + \frac{12 \varphi_d}{K_c a} \frac{D_{Ac} k_{rxn} C_{Bc}}{H_A D_{Ad}}} - 1 \right) \tag{5.8}$$

$$d_{max} = \beta \left(\frac{\sigma}{\rho_c} \right)^{0.6} \varepsilon^{-0.4} \, , \beta \approx 1 \tag{5.9}$$

Table 5.3 Drop diameter model parameters.

Parameter	Model 1 Energy Dissipation Based	Model 2 Dimensionless Numbers Based
Base Model	$d_{32} = \beta_0 \cdot d_{max}$	$\frac{d_{32}}{d_h} = \beta_0 \cdot We_c^{\beta_1} \cdot Re_c^{\beta_2}$
Fitted Model	$d_{32} = \beta_0 \cdot d_{max}$	$\ln(d_{32}/d_h) = \ln(\beta_0) + \beta_1 \ln(We_c) + \beta_2 \ln(Re_c)$
β_0	0.29±0.04	$e^{-0.28 \pm 0.38}$
β_1	n/a	-0.35±0.06
β_2	n/a	≈0
s_{res}^2	$2.44 \cdot 10^{-10}$ m²	0.047
R^2	0.81	0.88

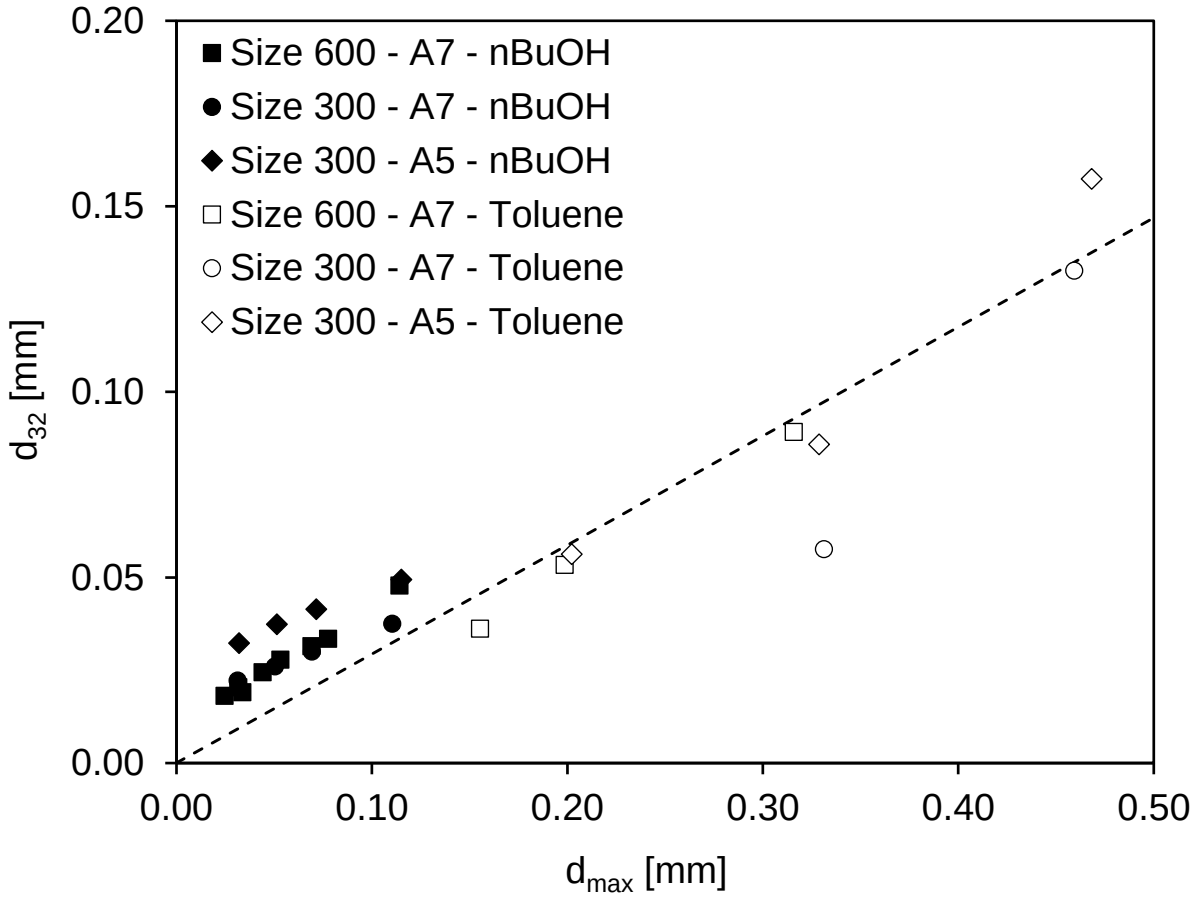

Figure 5.7 Surface-volume average drop diameter against the maximum stable diameter.

The results of Lobry et al. [48] demonstrated that the ratio of the surface-volume average diameter of drops by the maximum stable diameter in turbulent Sulzer SMV and SMX static mixers is usually between 0.33 and 0.38. The value obtained from Model 1 is similar. For Model 2, an exponent of -0.6 is expected for the Weber's number. This is outside of the confidence interval, but this is could be due to the limited interfacial tensions investigated. The Reynolds number exponent was found to be statistically non-significant (≈ 0). In general, its exponent depends on the flow regime and relates how the energy is primarily dissipated in the system (via turbulent eddies or viscous shear). Micro-reactors have shown to yield a gradual transition from laminar to turbulent flow and their friction factor can be usually modeled as a packed-bed reactor with relative contributions from both flow regimes. The near-zero value of the Reynolds' exponent

indicates that the break-up of droplets in micro-reactors follow a mechanism similar to that of turbulent flow.

Model 2 is shown on **Figure 5.8**. From visual observation, drop flow occurs only for $We \gtrsim 20$. At smaller Weber number, the generated droplets and the channel become of similar size. The dispersed phase is then constricted by the walls and takes the form of a slug. In gas-solid fluidized beds, the transition from bubbling to slugging fluidization is defined when the ratio between the maximum stable bubble diameter and column diameter is greater than 0.66 [142]. In the case of the micro-mixer presented in this work, the transition between slug and drop flow seem to occur when the model predicts a value of $d_{32}/d_h = 0.26$ or $d_{max}/d_h = 0.90$.

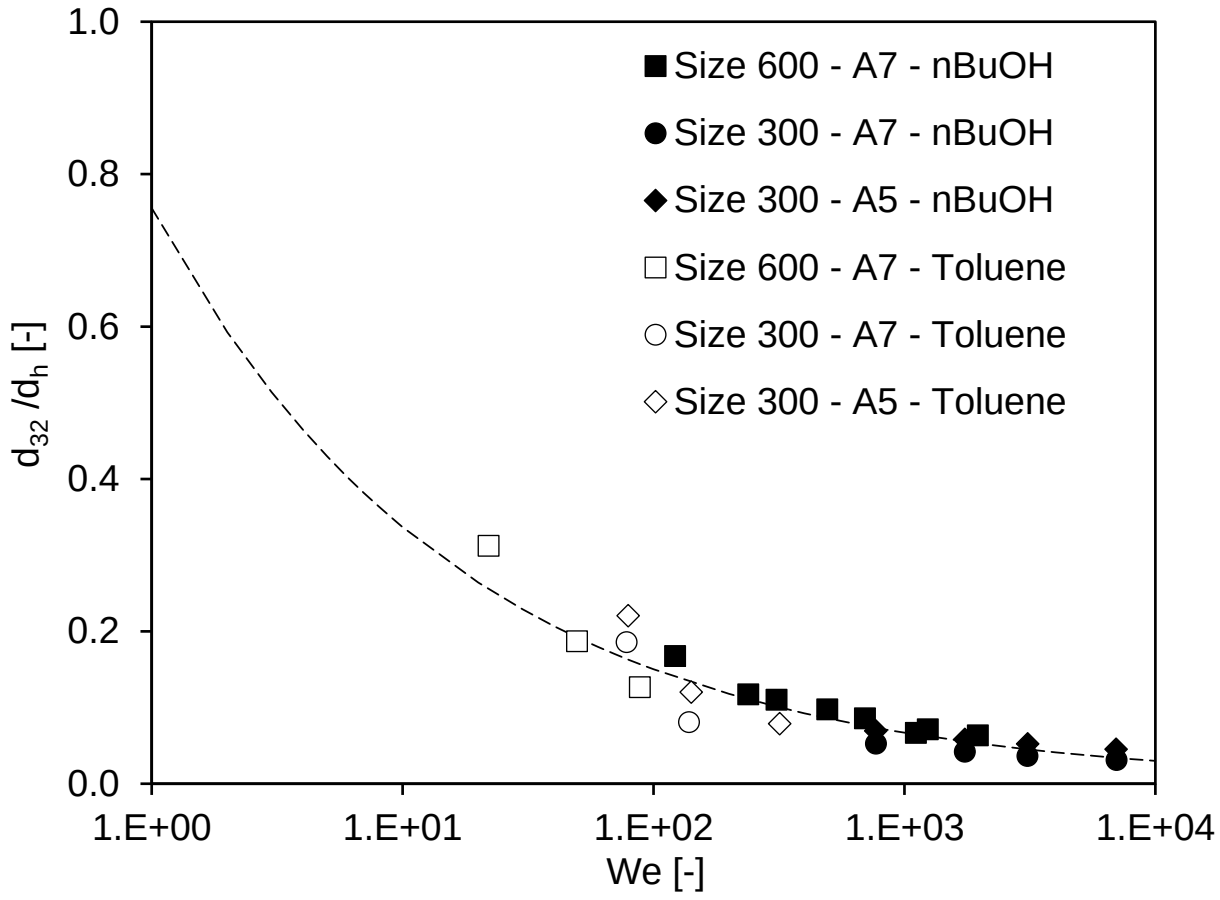

Figure 5.8 Dimensionless drop diameter against the Weber number.

5.4 Larger scale alternatives

The sizing up approach should not be strictly pursued for scale-up when the hydraulic diameter exceeds ~1 mm because the sized-up reactors no longer benefit from the advantages of miniaturization, especially in terms of heat transfer. At these scales, using a progressive channel size adapted to the reaction rate evolution may be necessary to ensure satisfactory heat transfer rates.

5.4.1 Heat transfer limitations

Micro-reactors have a high area-to-volume ratio for wall-to-fluid heat transfer due to their reduced dimensions. The enhanced heat transfer rates enable reactions that generate or consume large amounts of heat and the use of more concentrated reactants while greatly reducing the potential of a runaway. The thermal control performance of a reactor can be expressed using the fourth Damköhler number Da_{IV} (Equation (5.10)) representing the ratio of heat generation, calculated from the reaction rate r, the reaction enthalpy ΔH and the reactor volume V_R, to heat transfer in the reactor, calculated from the overall heat transfer coefficient U, the total area for heat transfer A_{HE} and the temperature driving force (T - T_{TF}) between the reactive media and thermal fluid used to control the temperature. To be satisfactory, this ratio is ideally smaller than one.

$$Da_{IV} = \frac{q_{rxn}}{q_{HE}} = \frac{|r\Delta H| \cdot V_R}{UA_{HE}(T - T_{TF})} \ll 1 \tag{5.10}$$

For a given reaction, this can be achieved independently of the reactor scale by lowering the reaction rate using diluted solutions and/or colder temperatures, but these options go against the philosophy of process intensification and a particular temperature or concentration may be required for yield optimization. Alternatively, the temperature of the thermal fluid can be adjusted, but this cannot realistically impact Da_{IV} by much more than one order of magnitude.

The remaining parametric options, U, A_{HE} and V_R, all vary with scale. The overall heat transfer coefficient is a function of the different resistances to heat transfer in the system (reactor side convective resistance, metallic wall conductive and contact resistances, and thermal fluid side convective resistance). The reactor side convection coefficient, h_i, will not vary greatly with the scale-up as shown in Equations (5.11) to (5.13), nor will the

overall U once the other resistances are considered [74]. Note that the ratio Q_2/Q_1 of Equation (5.13) is changed into a hydraulic diameter ratio using Equation (5.2).

$$h_i = Nu_i \frac{k}{d_{h,i}} = C \cdot Re_i^m \cdot Pr^n \cdot \frac{k}{d_{h,i}} \quad (5.11)$$

$$m \approx 0.8 \text{ [143]} \quad (5.12)$$

$$\frac{h_{i2}}{h_{i1}} \propto \left(\frac{Re_{i2}}{Re_{i1}}\right)^m \left(\frac{d_{h1}}{d_{h2}}\right) = \left(\frac{Q_2}{Q_1} \cdot \frac{d_{h1}}{d_{h2}}\right)^m \left(\frac{d_{h1}}{d_{h2}}\right) = \left(\frac{d_{h2}}{d_{h1}}\right)^{\frac{7m}{3}} \left(\frac{d_{h1}}{d_{h2}}\right)^{m+1} \approx 1 \quad (5.13)$$

The ratio between the heat transfer area and the reactor volume is dependent on the scale and on the aspect ratio, α, of the channels as shown on Equation (5.14) (assuming heat transfer through the top and bottom of the channel only). The contraction of the micro-mixers used in this work has a maximum aspect ratio of 2.5 (depth/width) due to their manufacturing method. To minimize the negative impact of scale-up on heat transfer, it may be considered to progressively adapt the channel aspect ratio towards a wide and shallow rectangular shape while maintaining a constant hydraulic diameter. However, extreme aspect ratios may suppress the formation of secondary flow patterns and reduce the local convection coefficient.

$$\frac{A_{HE}}{V_R} = \frac{2}{\delta} \quad (5.14)$$

$$d_h = \frac{2\delta w}{\delta + w} = \frac{2}{1+\alpha}\delta \quad (5.15)$$

If a fixed aspect ratio $\alpha = 2.5$, an overall heat transfer coefficient $U = 1000$ W/m^2K [74] and a temperature driving force $T - T_{tf} = 20$ K are assumed, then it is possible to plot the Da_{IV} as a function of the hydraulic diameter for various volumetric heat generation rate $r\Delta H$. The Da_{IV} of four case studies were evaluated and are discussed below. These are displayed on **Figure 5.9** along with standard sizes used in this article.

The first case study is the Grignard type homogenous synthesis of methyl 2-oxobutanoate from dimethyl-oxalate and ethylmagnesium chloride. The reaction enthalpy change is approximately 225 kJ/mol and, under the described conditions in

Plouffe et al. [67] at -15°C, it is reasonable to assume that the reaction is completed within the first 100 milliseconds in the reactor. This corresponded to an average reaction rate of ~5000 mol/m^3/s and to a heat generation rate $r\Delta H$ of 1125 MW/m^3. The necessary hydraulic diameter to avoid a temperature spike would need to be below 20 µm, i.e., below the smallest dimension presented in this work. An alternate solution is to distribute the Grignard reactant along the reactor volume using multiple inlet ports (multi-injection approach). The limiting reactant lowers the average heat generation throughout the reactor.

The second case study is the homogenous nitration of salicylic acid using a solution of acetic and nitric acid. The experimental details are described again in Plouffe et al. [67]; the reaction needed to be operated at 60°C or above to avoid delays associated with the auto-catalytic behaviour of the reaction. At this temperature, the initial reaction rate was estimated to be ~230 mol/m^3/s, and the reaction enthalpy is 146 kJ/mol [60], which yielded a heat generation rate of 33 MW/m^3. This is sufficiently low to be operated in some micro-reactors, but not in structures with internal diameters greater than 700 µm. Upon scale-up, it would then be best to use an adaptive channel design starting at a small size where the reactants meet and where the heat generation is high, and progressing into larger channels as the reaction rate decreases, i.e., maintaining the value $\frac{rV_R}{A_{HE}}$ constant (multi-scale approach). Typically, a plate with a channel depth starting in the micrometer domain will be selected and increased in size until it meets with conventional heat exchanger technology in the millimeter domain when needed.

The third and fourth case studies are the liquid-liquid hydrolysis reaction depicted in this work. While the hydrolysis step itself is not very exothermic, it is followed by two neutralization steps that results in an overall enthalpy change of about 112 kJ/mol. The cases considered the use of a 0.5 mol/L solution of the acetate (instead of 0.05 mol/L) in drop flow operated at an energy dissipation rate of ~100 m^2/s^3. Under homogenous conditions, the initial reaction rate would be 3500 mol/m^3/s and the total heat release rate at around 390 MW/m^3. However, these liquid-liquid cases have the particularity of being mass transfer limited, which reduces the observed reaction rate r_A. The rate

constant is instead equal to the dispersed side overall volumetric mass transfer coefficient.

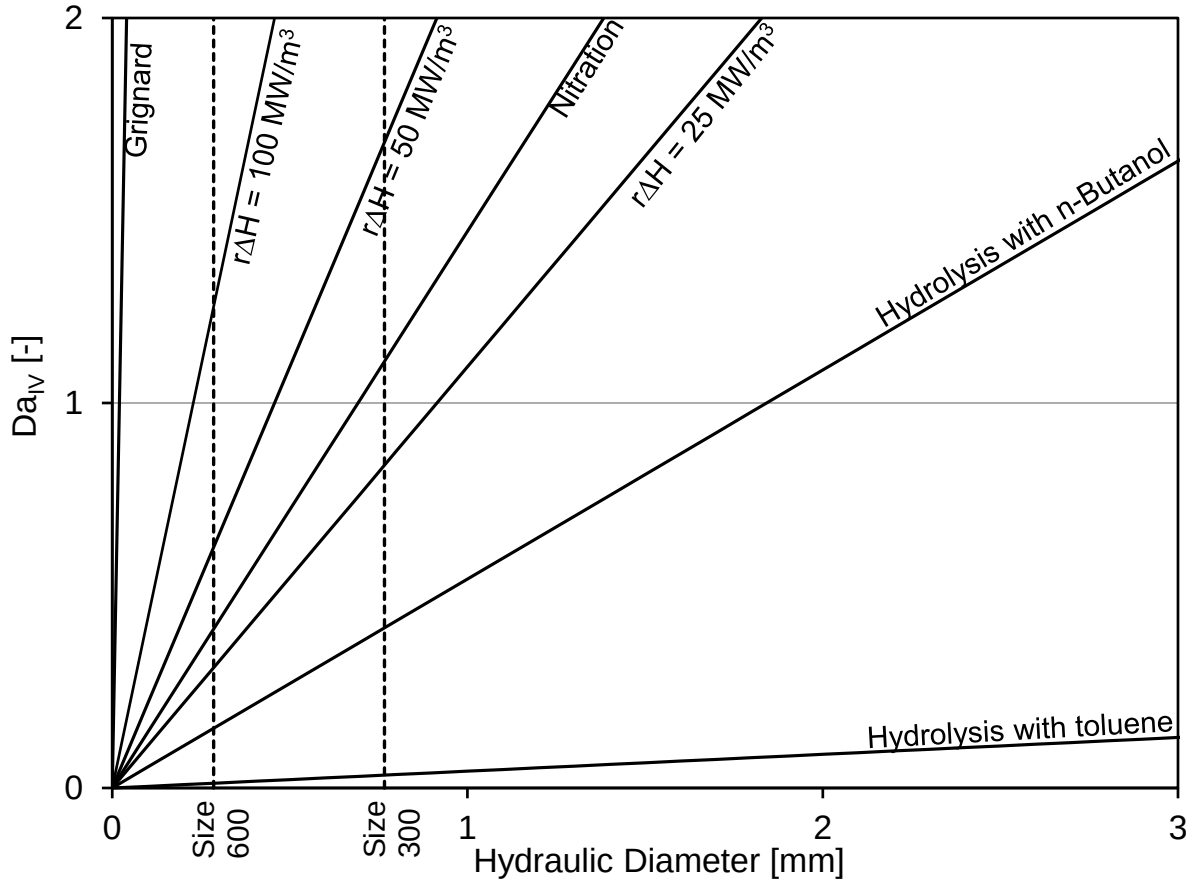

Figure 5.9 Fourth Damköhler number at different heat generation rates as a function of the sized-up hydraulic diameter and with $\alpha = 2.5$, $U = 1000$ W/m^{2}K and $T\text{-}T_{tf} = 20$ K.

The third case analyzes the use of n-butanol as the organic solvent. At these conditions, the coefficient $K_d a$ was $2.22 \cdot 10^{-1}$ s^{-1}, which would result in an initial reaction rate of ~110 mol/m^3/s. and a heat generation rate $r\Delta H$ of 12.5 MW/m^3. Clearly, the results indicate that a micro-structure is no more needed to control reaction heat.

The fourth case considers the use of toluene instead of butanol as the organic solvent. In such case, the coefficient $K_d a$ is reduced to $1.66 \cdot 10^{-2}$ s^{-1} and the heat generation rate $r\Delta H$ to 0.9 MW/m^3.

Low heat generation rates such as in the fourth case can be safely operated in a reactor with internal diameters below 2.5 cm. However under the flow rates studied in this work, the energy dissipation rate in such a large reactor would be very low and the system even more mass transfer limited. The use of a micro-reactor for fast liquid-liquid reactions was necessary to obtain interphase mass transfer rates that are greater than what would be achieved in larger reactor.

Even at high energy dissipation rates using toluene, the acetate hardly transferred to the aqueous phase due to its affinity with the organic solvent (demonstrated by its high partition coefficient H_A). Consequently, large residence times are still needed and cannot realistically be achieved in micro-reactors within reasonable pressure drops. For example, at energy dissipations rates of 100 m^2/s^3, the overall volumetric mass transfer coefficient $K_d a$ with toluene was such that to obtain a conversion of 90%, a residence time of about 60 seconds would be needed and would result in a pressure drop of 60 bars ($\Delta P = \rho_c \varepsilon \tau$).

In such cases and when heat transfer is not limiting, reactors combining larger channels with an active mixing technique might present the best solution. Active mixing techniques use an external source of energy to agitate the fluids such as mechanical actuators. The energy dissipation rates that can be achieved are generally independent from the overall flow rate and thus high values can be obtained at the same time as large residence times and low pressure drops. A promising technology is the use of pulsating flow in baffled reactors [144].

5.4.2 Alternative technologies

Micro-reactors are a niche technology that fulfills the requirements of small scale continuous production. Conventional static mixers do not generate sufficient energy dissipation at flow rates in the order of mL/min to provide effective mixing, mass transfer and heat transfer; hence the need for miniaturisation and novel mixing geometries. Upon scale-up, there exists operating conditions at which point the performances of the sized-up micro-reactor and conventional static mixers overlap.

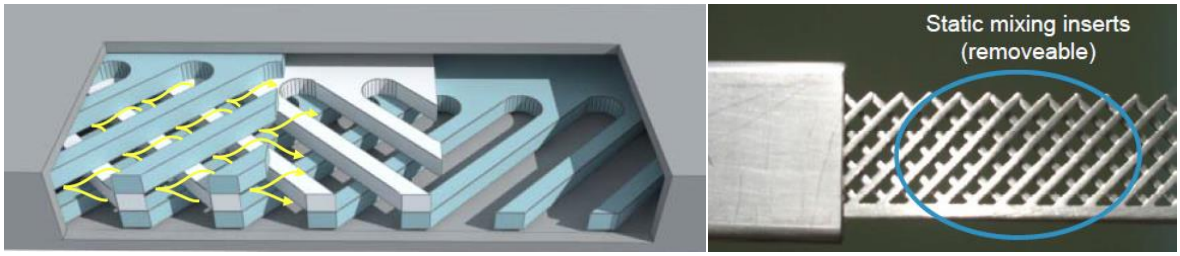

Figure 5.10 Miprowa reactor channel side-view (used with permission from Ehrfeld Mikrotechnik).

This is demonstrated by the experimental results of a Miprowa reactor by Ehrfeld Mikrotechnik BTS shown on **Figure 5.10**. The reactor uses three comb-like static mixers stacked onto each other and inserted in a rectangular channel to agitate the fluids and create secondary flow patterns. The channel is 12 mm wide by 1.5 mm deep and 2633 mm long. With the inserts (type NK 2241), the solid volumetric fraction (α) in the channel was equal to 0.41 and the characteristic pore diameter 0.96 mm. The reactor was mounted on the experimental setup displayed on **Figure 5.2**.

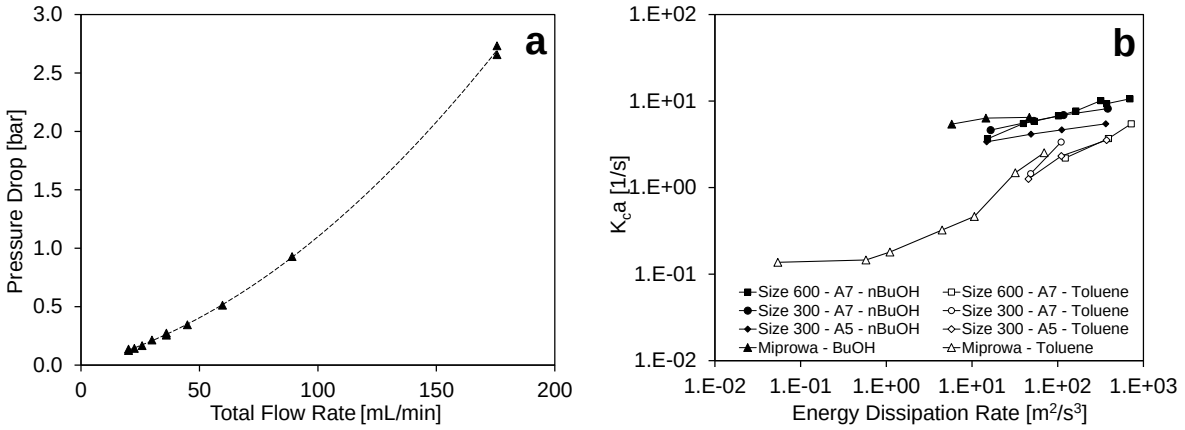

Figure 5.11 Single phase pressure drop curve (A) and overall mass transfer coefficient (B) in the Miprowa reactor using water at 23°C.

Single phase pressure drop measurements and the two-phase hydrolysis of 4-NPA using toluene and n-butanol were performed. The experimental results, displayed on **Figure 5.11**, demonstrate that the overall mass transfer coefficient $K_c a$ in the Miprowa reactor is similar to that of the other micro-reactors at the same energy dissipation when a drop flow regime is obtained. The micro-mixer presented in this work and other static mixers

of different scales can then be compared using the average energy dissipation as a function of flow rate [75].

The energy dissipation rate of "conventional" static mixers (Sulzer SMV [48], Sulzer SMX [114], Chemineer Kenics A [145]) was estimated as a function of flow rate and is plotted on **Figure 5.12** along with the measured energy dissipation rates of the Size 600 and Size 300 micro-reactors, and the Miprowa reactor. Calculation details are found in the appendix.

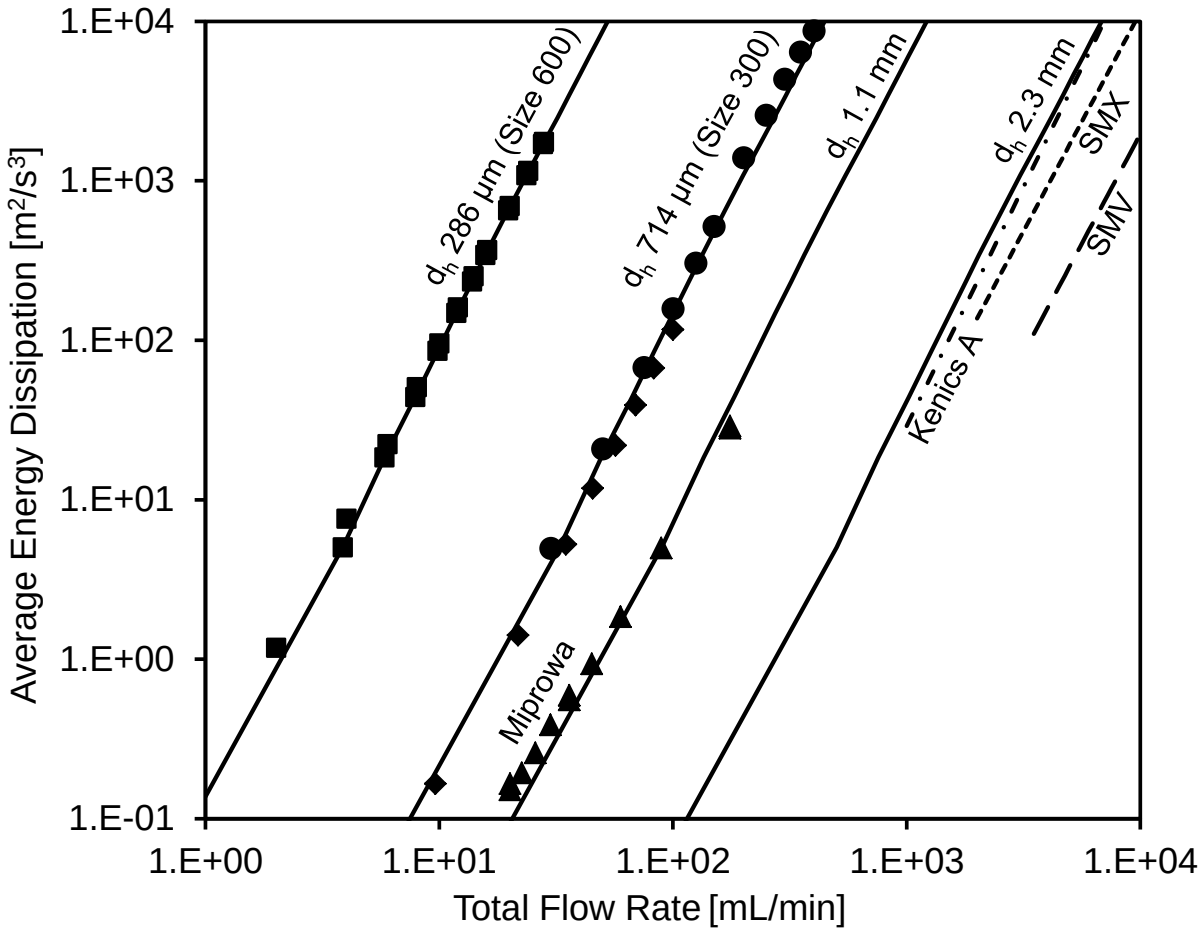

Figure 5.12 Experimental and predicted single phase energy dissipation rate at different flow rates for different reactor sizes and alternative static mixers using properties of water at 23°C.

Figure 5.12 demonstrates that the Miprowa reactor offers level of energy dissipation similar to a micro-reactor with a hydraulic diameter of ~1.1 mm. Other conventional static mixers and the sized-up micro-reactors become similar only beyond ~10^3 mL/min

($d_h \geq 2.3$ mm). These static mixers have the advantage of being usually simpler to manufacture than micro-reactors that are machined into a metallic plate. However, they may not guarantee a drop flow regime, since their larger diameters may result in different force ratios leading to the potentially undesired parallel flow pattern [75]. Moreover, they will have a lower specific heat transfer area than the micro-reactor, resulting in larger Fourth Damköhler numbers and potentially temperature control issues.

5.5 Conclusion

A power to the $3/7^{th}$ sizing-up rule was presented for the scale-up of micro-reactors used in pharmaceutical and fine chemical process development and intensification. The approach was tested using two differently sized micro-reactors. Single phase pressure drop measurements showed that the size 300 ($d_h = 714$ μm) reactor produced the expected amount of energy dissipation at increased design flow rates based on the size 600 ($d_h = 286$ μm) results. Using the liquid-liquid alkaline hydrolysis of 4-nitrophenyl acetate, it was demonstrated that the overall mass transfer coefficients in the size 300 reactor were similar to those of the size 600 for the same energy dissipation rate and that the $3/7^{th}$ sizing rule remained adequate in the drop flow regime. The data in the drop flow regime was further analyzed in order to calculate the average surface-volume drop diameter, d_{32}. The results were correlated for the different operating conditions and reactors as a fraction of the maximum stable diameter or as a function of dimensionless numbers.

The scale-up approach is further analyzed for larger scales. Calculation shows that the sizing-up approach might become heat transfer limited for the more reactive systems. For a Grignard reaction ($r\Delta H = 1125$ MW/m^3), very small micro-reactors would be needed to control the temperature; alternatively a multi-injection configuration can be used to dampen the heat release over a larger volume. For a nitration reaction, an adaptive mixer size can be used, where Size 600 are used initially followed by larger sizes once the heat release decreases. The sized-up reactors were compared with conventional/commercial static mixers and it could be demonstrated that they offer

better energy dissipation rates at lower flow rates for mixer sizes up to ~2.3 mm in diameter.

5.6 Acknowledgement

The authors would like to thank the Natural Sciences and Engineering Research Council of Canada and Lonza AG for their financial contribution. Also Ehrfeld Mikrotechnik BTS is acknowledged for the reactor manufacturing. Finally, the authors would like to thank Eric Mielke and Sébastien Mongeon for their help and time.

5.7 Appendix

5.7.1 Appendix A: Energy dissipation curve for the SMV and SMX

The SMV Mixer by Sulzer is made of corrugated sheets of metal inserted in a circular tube. The energy dissipation curve was calculated based on the experimental results of Lobry et al. [48] as shown in Equations (5.16) to (5.19). They used a 3.5 mm hydraulic diameter SMV in a 10 mm tube with a solid volumetric fraction of 0.17.

$$\Delta P = 2f\frac{L}{d_h}\frac{\rho u^2}{(1-\alpha)^2} \tag{5.16}$$

$$Re_h = \frac{\rho d_h u}{\mu(1-\alpha)} \tag{5.17}$$

$$\frac{f}{2} = \frac{1}{Re_h^{0.25}} \tag{5.18}$$

$$\varepsilon = \frac{\Delta P Q}{V_R \rho_c} = 2f\frac{1}{d_h}\frac{u^3}{(1-\alpha)^3} \tag{5.19}$$

The SMX Mixer is very similar, but the insert differs slightly. The energy dissipation curve was calculated based on the experimental results of Theron et al. [114]. The procedure is similar to the SMV, except that the characteristic length of the system is the tube diameter (see Equations (5.20) and (5.21)). They used a tube of 10 mm in diameter and a mixer with a solid volumetric fraction of 0.33.

$$\frac{f}{2} = \frac{24}{Re_h^{0.25}} \tag{5.20}$$

$$\varepsilon = \frac{\Delta P Q}{V_R \rho_c} = 2f \frac{1}{d_h} \frac{u^3}{(1-\alpha)^3} \tag{5.21}$$

5.7.2 Appendix B: Energy dissipation curve for the Kenics A

The Kenics static mixer by Chemineer uses a twisted ribbon-like insert to divide the flow and create rotational secondary flow patterns. Song et al. [145] did CFD simulations for multiple dimensions and compared them with literature results; this work uses the smallest Kenics dimensions (Type A, diameter of 4.93 mm, unit aspect ratio 1.74). The energy dissipation curve is calculated according to Equations (5.22) to (5.25). The parameters "K" and "n" for the coefficient of friction are empirical and depend on the ratio between the Reynolds number and the aspect ratio.

$$\Delta P = f \frac{L}{d_h} \frac{\rho_c u^2}{2} \tag{5.22}$$

$$Re = \frac{\rho_c d_h u}{\mu_c} \tag{5.23}$$

$$f = \frac{K}{AR^{2.04}} \left(\frac{Re}{AR^{2.15}} \right)^n \tag{5.24}$$

$$\varepsilon = \frac{\Delta P Q}{V_R \rho_c} = \frac{f u^3}{2 d_h} \tag{5.25}$$

5.8 Nomenclature

General

Symbol	Description	Units
A	Area	m^2
a	Specific interfacial area	m^2/m^3
C_{ij}	Concentration of molecule "i" in phase "j"	mol/m^3
d_{32}	Surface-volume average droplet diameter	m
d_h	Hydraulic diameter at the contraction	m
d_{max}	Maximum stable droplet diameter	m
D_{ij}	Molecular diffusion coefficient of molecule "i" in the phase "j"	m^2/s
f	Friction factor	-
h	Local convective heat transfer coefficient	$W/m^2/K$

H	Organic/aqueous concentration distribution coefficient or height	-
ΔH	Reaction enthalpy change	J/mol
k_{rxn}	Second order reaction rate constant	$m^3/mol/s$
k	Local convective mass transfer coefficient	m/s
K	Overall mass transfer coefficient	m/s
Nu	Nusselt number	-
ΔP	Pressure drop across the reactor	Pa
Q	Volumetric flow rate	m^3/s
q	Heat generation/transfer rate	W
r	Volumetric reaction/reactive extraction rate	$mol/m^3/s$
R^2	Coefficient of determination	-
Re	Reynolds number	-
s_{res}^2	Mean squared residual	- or m^2
Sh	Sherwood number	-
u	Superficial velocity at the contraction	m/s
U	Overall heat transfer coefficient	$W/m^2/s$
V_R	Reactor volume	m^3
We	Weber number	-
w	Channel width	-
α	Channel aspect ratio or solid hold-up	-
β	Fitting parameter	*
δ	Channel depth	m
ε	Average rate of energy dissipation	m^2/s^3
η	Conversion of 4-NPA	%
μ	Dynamic viscosity	Pa·s
ρ	Density	kg/m^3
σ	Interfacial tension between the organic and aqueous phase	J/m^2
τ	Average residence time	s
φ	Volumetric phase fraction	-

Indices

A	Of the 4-nitrophenyl acetate
B	Of the sodium hydroxide base
c	Of the continuous phase
CSTR	Of the stirred tank reactor
d	Of the dispersed phase
HE	Of heat transfer
rxn	Of the reaction
TF	Of the thermal fluid
tot	Total of the continuous and dispersed phase

5.9 References

See thesis references.

6 Conclusion

Continuous processes using micro-reactors present multiple advantages compared to batch chemistry, mainly with respect to transport rates. The possibility of better controlling the temperature allows the use of more concentrated reactants and of elevated temperatures and pressures without compromising safety. This is of particular interest for the production drugs during clinical trials where an improvement of the yield would reduce the quantity of material used and the operating costs, and for enabling novel synthesis pathways. Nevertheless, the use of continuous processes in production campaigns still remains low due to the delays and complexity required for their setup.

6.1 Development of a toolbox approach

A modular toolbox approach was developed to facilitate the selection of a reactor. It considered the intrinsic kinetics of the reaction, the phases of the reactants and the reaction network in order to determine the type of reactor that should be used. The approach divided reactions between those requiring seconds or less (Type A) to achieve full conversion, those requiring seconds to minutes (Type B), and those requiring more than 10 minutes (Type C).

For single phase applications, it determined what combination of plate and coil reactors were needed. In multiphase applications however (ex.: liquid-liquid), the agitation of the reactants must be sustained in order to maintain a dispersion throughout the reactor volume, especially for Type A reactions which are more likely to be mass transfer limited. For these systems, micro-reactors with continuous mixing elements were presented. In the case of gas-liquid reactions, the use of higher pressures was suggested as it will increase the driving force for mass transfer or potentially fully solubilize the gas stream into the liquid stream. For reactions involving solids, the risk of plugging limits the use of some mixers, but the use of pulsation might prove to be a solution in the future. Alternatively, reactions with solids may be operated continuously with the use of a stirred tank reactor.

Depending on the reaction network, the use of a mixed flow reactor like stirred tanks can significantly affect the yield of the process. Networks with competitive parallel reactions of higher order will have their yield favoured by the low concentration environment resulting from a mixed flow reactor. An example was shown with the ring closing metathesis where the undesired isomerization of the substrate is favoured in plug flow reactors. For a network of consecutive reactions, the nitration of salicylic acid with an autocatalysis like behaviour was given as an example. In such cases, the use of a tandem mixed flow-plug flow reactor reduces the required reactor volume. In that particular case however, the use of a single plug flow reactor at higher temperatures was preferred for safety reasons.

It was also demonstrated that the injection of a reactant using multiple inlets and a micro-reactor improved the yield of a Grignard reaction and enabled it to operate at temperatures greater than usual, further reducing costs.

6.2 Micro-reactors for liquid-liquid systems

The alkaline hydrolysis of 4-nitrophenyl acetate was used to evaluate the mass transfer rates of liquid-liquid systems. The effect of the physical properties of the reactants was investigated in a micro-reactor with a serpentine mixer by using four different organic solvents, i.e., n-butanol, n-hexanol, MTBE and toluene. These solvents were chosen because they covered a large range of densities, viscosities, and especially interfacial tension with the aqueous phase.

Slug flow, parallel flow, and drop flow regimes were observed through a sight glass in the reactor. Only the more viscous organic phases (n-butanol and n-hexanol) formed a stable parallel flow within a certain flow rate; this was not observed using toluene. Drop flow was observed only at the higher flow rates and occurred latest for systems with greater interfacial tension values.

The overall volumetric mass transfer coefficients, $K_c a$, were greatest in the drop flow regime and smallest in the parallel flow regime. A mass transfer model for the drop flow regime was proposed to calculate the size of the droplets, which was then correlated as

a function of the average rate of energy dissipation in the reactor, and as a function of the Weber and Reynolds numbers.

The mass transfer rates were highest when a solvent with a low interfacial tension was used, because it resulted in smaller droplets, which increases both the convective mass transfer coefficient and interfacial area. Also, systems with a low partition coefficient favoured the penetration of the organic molecule into the aqueous phase. Overall however, the conversions observed within the serpentine mixer were not very high either because of low mass transfer rates at low flow rates due to slug or parallel flow regimes, or of low residence time at high flow rates once drop flow was achieved.

Hence, a better understanding of the effect of geometry was required to generate drop flow at lower flow rates. The serpentine mixer was compared with four other structures. A distinction was made between micro-reactors with curvature based mixers (SZ, TG, Spade) and those with obstacle based mixers (Venturi, Sickle). The reactive liquid-liquid extraction was performed in these reactors using n-butanol and toluene as organic solvents, which represented the limiting systems of the previous study.

It was demonstrated that a stable parallel flow was generated in the curvature based mixers due to stabilizing centrifugal forces. The denser fluid was pushed to the outside of the curve and droplets coalesced. Additionally in straight channels, instabilities could more easily form at the interface and break the parallel flow. In curved channels, the interface is forced to rotate, which increases its curvature and dampens short wavelength instabilities.

Obstacle based mixers were thus found to be better suited to the generation of drop flow in liquid-liquid systems. Once this flow regime was achieved however, the results demonstrated that at comparable energy dissipation rates, the mixers generated similar overall volumetric mass transfer coefficients. The geometry of the mixer generates macro scale secondary flow patterns that change the velocity profile in magnitude and direction. It is postulated that they transmit their kinetic energy downward to smaller secondary flow patterns, similarly to eddies in turbulent flow. Secondary flow patterns with sufficient energy and of a size equal to or smaller than the droplets would be able

to break them and dissipate their energy in interface creation rather than heat. This was supported by the fact that the friction factor in these mixers transitioned smoothly from laminar to turbulent flow rather than abruptly like in straight channels, and indicated that secondary flow patterns grow in strength and frequency as the average energy dissipation increases.

Using modified first and second Damköhler dimensionless numbers, the micro-reactors were compared to determine the best mixer for generating drops. The obstacle-based Sickle mixer had the highest Da'_{II} and would be most useful for competitive reaction networks requiring fast mass transfer rates.

The Sickle mixer used a curved triangular obstacle to desynchronize droplets and prevent the coalescence observed in the Venturi mixer. However, it was shown that curves are undesired for liquid-liquid systems and a novel mixer was designed. A small ($dh = 286$ μm) and a large ($dh = 714$ μm) version of the mixer was manufactured to test the effect of scale-up. A relation between energy dissipation, flow rate and hydraulic diameter was derived and demonstrated that the hydraulic diameter should be scaled according to flow rate with an exponent of $3/7^{th}$ in turbulent flow such that the energy dissipation of the small and large scale mixers be the same.

Single phase pressure drop measurements demonstrated that the energy dissipation rates in the scaled mixer were as expected. Secondary flow patterns were generated by the mixer and produced chaotic eddies that grew in strength and in instability with flow rate akin to turbulence. Using the liquid-liquid test reaction, it was demonstrated that the overall volumetric mass transfer coefficients of both sizes were similar at equal energy dissipation rates in the drop flow regime. The size of the droplets was correlated with respect to the maximum stable drop diameter and the results were comparable to past observations. It was shown that for Weber's number below 20, the drops are too large to form in the mixer and interact with the side walls, resulting in slug flow instead.

A sizing up approach was preferred over a numbering up approach due to its greater practicality. As the internal dimensions increase however, the reactor loses the advantages of miniaturisation. Possible heat transfer limitations were discussed using

the fourth Damköhler number and four case scenarios. For a Grignard reaction, the heat generation rate was large (1125 MW/m^3) and require a multi-injection approach to dampen the heat release. For a nitration reaction, the heat generation rate was sufficiently small (65 MW/m^3) to be dissipated by mixers with a hydraulic diameter $d_h < 350$ µm. During scale-up, an adaptive channel size could be used to obtain high heat transfer rates at the contacting point of the reactants followed by larger channels when the heat release has decreased. For some mass transfer limited reactions, a larger channel with an active mixing technique such as pulsated flow might provide sufficient heat transfer rates in addition to large residence time and a low pressure drop.

The novel mixing structure was compared with commercially available static mixers. With the exception of the Miprowa reactor, the static mixers could not generate comparable energy dissipation rates at flow rates below 1000 mL/min. Such production rates correspond to the commercial campaigns druing drug development.

In sum, the studies that were performed allowed the development of a micro-reactor for fast liquid-liquid reactions. The reactor utilises a repetitive obstacle-based mixer to generate drop flow at low flow rates and sustain the droplets throughout the entire volume. Correlations that take into account the size of the reactor, the flow rate, and the physical properties of the phases were developed to predict the drop size and mass transfer rates.

For any liquid-liquid reaction to be performed under a plug flow pattern in the proposed mixer, the size and volume of the reactor can be determined accordingly:

1. Obtain the expression for the reaction rate and determine the physical properties of the system;

$$-r_A = k_{rxn} C_A^n \tag{6.1}$$

2. Calculate the overall volumetric mass transfer coefficient $K_c a$ needed to obtain a satisfactory Da'_{II};

$$K_d a = Da'_{II} \cdot (k_{rxn} C_A^{n-1}), \quad Da'_{II} \gg 1 \tag{6.2}$$

$$K_c a = \frac{K_d a}{H_A} \tag{6.3}$$

3. Calculate the required droplet size d_{32} to obtain that mass transfer;

$$d_{32} = \frac{Sh_d H_A D_{Ad}}{2\sqrt{D_{Ac} k_{rxn} C_{Bc}}} \left(\sqrt{1 + \frac{24\varphi_d}{K_c a} \frac{D_{Ac} k_{rxn}}{Sh_d H_A D_{Ad}}} - 1 \right) \tag{6.4}$$

4. Calculate the energy dissipation rate ε required to obtain this droplet size based on the physical properties of the phases;

$$d_{32} = \beta_0 \left(\frac{\sigma}{\rho_c} \right)^{\beta_1} \varepsilon^{\beta_2} \tag{6.5}$$

5. Calculate the required reactor size d_h that will result in the desired energy dissipation at the design production rate Q;

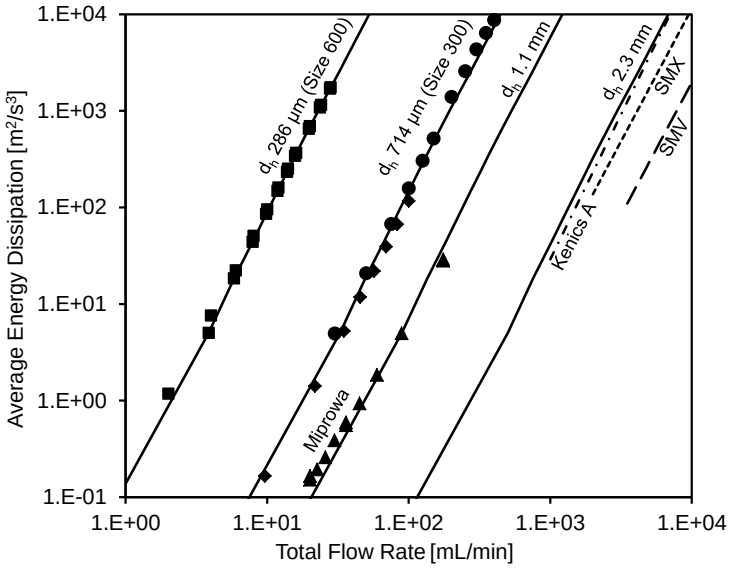

Figure 5.12

6. Determine the reactor volume V_R necessary for satisfactory conversion (i.e., Da_I');

$$V_R = \frac{Q \cdot Da_I'}{K_d a}, \quad Da_I' > 1 \tag{6.6}$$

7. Calculate the expected Da_{IV}. If it is too high, consider using a smaller reactor, multi-injection, or a progressive reactor size to minimize temperature spikes;

$$Da_{IV} = \frac{|r\Delta H| \cdot V_R}{UA_{HE}(T - T_{TF})} \ll 1 \tag{6.7}$$

8. Calculate the expected pressure drop ΔP and decide if it is within acceptable limits. If it is too high, consider using different solvents or surfactants to generate smaller droplets at lower flow rates, a larger reactor, active mixing techniques or operate at higher temperatures to decrease viscosity and required residence time for example.

$$\Delta P = \frac{\varepsilon \rho_c V_R}{Q} \tag{6.8}$$

6.3 Recommendations for future research

To further expand the application of continuous flow and micro-reactors for the production of active pharmaceutical ingredients, process development and fine chemistry, additional research avenues are proposed below:

- Continue the incremental geometric optimization of the novel mixing structure and minimize undesired features (ex.: dead zones) using test reactions, photographs or CFD;
- Test additional organic solvents to improve the accuracy of the drop size correlations in the novel mixing structure;
- Attempt other multiphase flow in the novel mixing structure. Determine if it can be used to disperse a gas in a liquid, or what is the maximum particle size that can flow through without plugging in a system with solids (e.g., precipitation reactions);

- Measure the heat transfer coefficient in the micro-mixers and in residence time channels for single- and multi-phase environments in order to calculate the Da_{IV} with better accuracy;
- Characterize the residence time distribution in the reactors in terms of plug-flow or mixed-flow patterns and develop a structure or a micro-reactor configuration (ex.: using recycle streams) that can produce each.

Additionally, it is recommended to perform experiments to further improve the understanding of multi-phase flow in micro-reactors:

- Accurately measure the length of slugs using high speed photography and model the effect of physical properties in liquid-liquid systems;
- Investigate the formation and stability of parallel flow in straight or coiled channels. For unstable parallel flows, compare the location of the breakpoint with respect to physical properties and curvature radius;
- Determine the velocity profile using a μPIV technique and characterize the evolution and stability of secondary flow patterns as a function of Reynolds (see Hoffmann et al. [146] and Kockmann et al. [147]);

7 Appendix

The next sections contain supplementary materials complementing or further supporting this thesis. In Section 7.1, information about the patent application for the novel mixing structure is presented. A paper that was presented at the 10th International Conference on Nanochannels, Microchannels and Minichannels is joined in Section 7.2. It presents early results on how the friction factor, heat transfer and mass transfer vary in micro-reactors, techniques for measuring them and potential sources of error.

7.1 Patent Application

A provisional patent application has been submitted for the mixing structure used in the micro-reactors of Section 5.

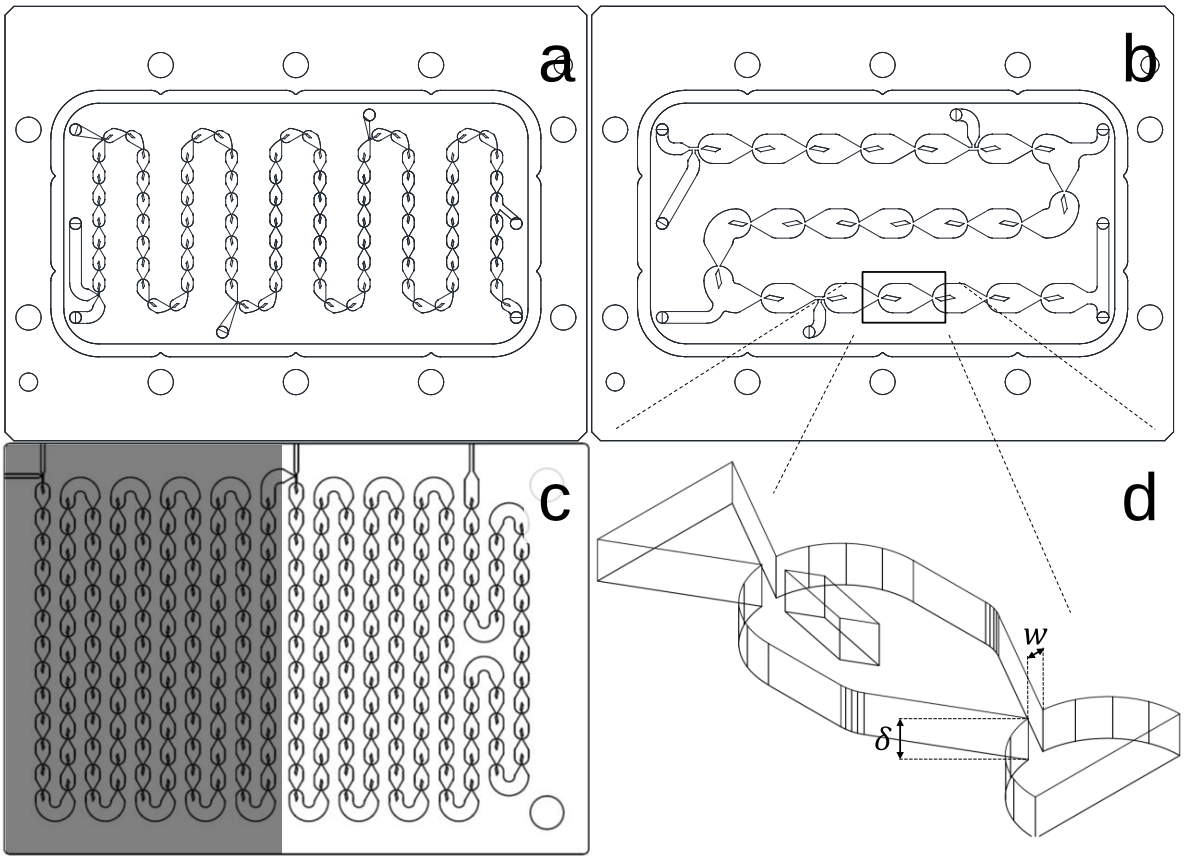

Figure 5.1 Micro-Reactor Plates A7 Size 600 (a) and Size 300 (b), A5 Size 300 (c), and Micro-Mixer (d).

The patent was submitted in December 2014th, and is titled "**FlowPlate Structures for Liquid-Liquid reactions (FlowPlate LL) – Microreactor XIII**". The patent has been submitted by Lonza AG and is a collaboration between Dr. Roberge, Dr. Macchi and me.

7.2 Transport phenomena in two-phase liquid-liquid micro-reactors

*PATRICK PLOUFFE, ROSS ANTHONY, ARTURO MACCHI**

Centre for catalysis Research and Innovation, Department of Chemical and Biological Engineering, University of Ottawa, K1N6N5, Ottawa, Canada

ADAM DONALDSON

Department of Process Engineering & Applied Science, Dalhousie University

*DOMINIQUE M. ROBERGE**

Chemical Development, Lonza AG, CH-3930, Visp, Switzerland

NORBERT KOCKMANN

Dept. of Biochemical and Chemical Engineering, Equipment Design, TU Dortmund University, Germany

This manuscript has been published in Proceedings of the ASME 2012 10th International Conference on Nanochannels, Microchannels,&Minichannels (ICNMM2012), July 8-12, 2012, Rio Grande, Puerto Rico, ICNMM2012-73040

Abstract

Micro-reactors offer distinct advantages over batch reactors currently used within the pharmaceutical and fine chemical industries. Their high surface area-to-volume ratios allow for increased heat and mass transfer, important for controlling reaction selectivity. In addition, micro-reactors are compatible with continuous processing technology, circumventing the time delays inherent to batch systems. Rapid mixing of reactants within micro-reactors is, however, limited by the inherent difficulty of generating turbulence at reduced geometry scales. Several different passive mixing strategies have been proposed in order to produce eddy-based secondary flows and chaotic mixing. This study examines the effectiveness of these strategies by comparing the energy-density normalized heat and mass transfer coefficients for a selection of industrial micro-reactors. First single, then two-phase liquid-liquid experiments were conducted.

Pressure drop measurements were obtained to calculate friction factors and to verify the presence of eddy-based secondary flows. A hot heat exchange fluid and temperature measurements were used to estimate the internal convective heat transfer coefficients within each structure. Volumetric mass transfer coefficients were also determined for the mutual extraction of partially miscible n-butanol and water. Semi-empirical correlations for the reactors' friction factor and Nusselt number as well as a description of the overall mass transfer coefficient based on energy dissipation are presented.

Keywords

Liquid-liquid, micro-reactor, friction factor, heat transfer, interphase mass transfer, energy dissipation.

7.2.1 Introduction

The field of micro-reactors has gained increasing attention in recent years, going from 66 related articles published in 1999 to 413 published in 2009 [148]. Due to its small size, micro-reactor technology is ideal for low flow rate processes requiring tightly controlled conditions. Indeed, its high surface area-to-volume ratio allows efficient heat transfer. A good example of a field that could benefit from such a technology is the development of pharmaceutical drugs, where industry frequently relies on batch and semi-batch production campaigns to develop new components for clinical tests.

An analysis performed by Roberge et al. [3] showed that at Lonza Ltd., ca. 20% of the reactions performed in these campaigns could benefit from continuous processing, increasing to 50% if reactions involving solids can be accommodated. It was also observed that a general isolated yield of 77% was achieved, a value that could be increased using micro-reactors and continuous processing when applied properly to selected reaction.

While micro-reactors and continuous processes bring advantages to the industry, they also bring challenges related to capital and operating costs and flexibility that must be overcome to be competitive and replace existing batch processes [3,4].

Additionally for micro-reactors, the low flow rate and dimensions responsible for heat transfer and safety advantages often result in laminar flow conditions. Under such situations, mixing of the reacting streams can be problematic. Thus, it is necessary to develop active or passive structures that will improve mixing between streams and enhance heat and mass transfer [149]. While this can be achieved with certain ease in homogenous systems, it is more challenging for heterogeneous systems where mechanisms for increasing interfacial area are balanced against separation and extraction of the product. Moreover, at such small channel sizes, surface tension becomes a significant force that counteracts efforts to break-up immiscible phases in order to increase mass transfer.

This research investigates hydrodynamic trends in micro-reactors in order to illustrate relations between flow rate and transport parameters such as the friction factor, heat transfer coefficient and mass transfer coefficient, which are essential to reactor performance. Four generic reactors are tested with a single phase liquid, water, for pressure drop and heat transfer tests and with partially-miscible liquids for mass transfer. The mutual extraction of water and n-butanol was chosen to represent a two-phase system with low interfacial tension.

7.2.2 Experimental setup

Four micro-reactors with different size and geometry were used (**Table 7.1**). The hydraulic diameters of the structures are taken at the smallest contraction where all the flow passes. The first and second structure are similar to the Advanced Flow™ reactor designed by Corning Inc. [38], with the 411S being half the size of 411L. The third reactor, 412S, is made of a series of hexagon of the same size. The fourth reactor, 413, is a series of increasing size octagons. During operation, reactor plates are sandwiched between a thick glass plate and either a cooling or heating block for thermal fluid contacting, allowing the user to visualize the flow.

Table 7.1 Geometric details of micro-reactor structures used.

Reactor	Photo	Contraction (d_h)
411L		1.0 x 1.0 (1.00 mm)
411S		0.5 x 1.0 (0.67 mm)
412S		0.5 x 0.6 (0.54 mm)
413		0.5 x 1.5 (0.75 mm)

The equipment used to carry out the experiments were pre-calibrated pulseless gear pumps (IsmatecMicroshoe with 0.017 mL/rev head from Cole Parmer), a wet/wet differential pressure transducer (0-5 psi from Omega) and four plug-in-pipe RTD (100Ω Class A from Omega). A pair of rotameters (Omega), one with a glass bead for low flow rates and the other with a stainless steel bead for high flow rates, was mounted on each (organic/aqueous) side. Hot water for the heat transfer tests was supplied from a thermal bath (Polyscience), and injected on the thermal fluid side. For mass transfer tests, a high precision alcohol densitometer (Anton Paar) was used to determine the composition of both phases. For heat transfer tests, distilled water was boiled and cooled without agitation prior to being used to remove dissolved gas and avoid bubble formation within the reactors during heating. For pressure drop and mass transfer tests, deionoized water and n-butanol (Fisher Scientific) were used. **Figure 7.1** depicts the experimental setup.

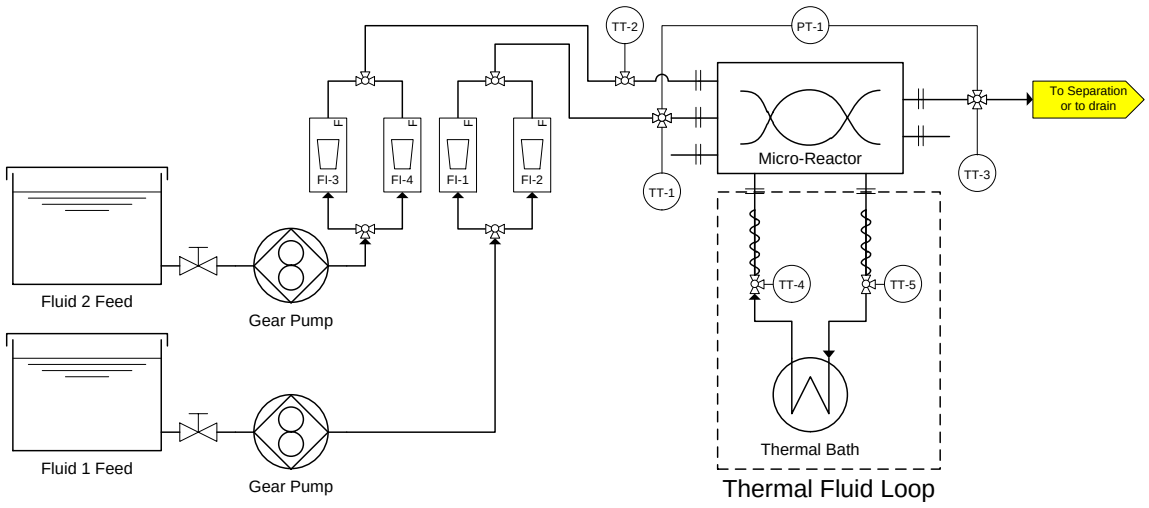

Figure 7.1 Experimental apparatus.

7.2.3 Single phase pressure drop

The pressure drops through the micro-reactors (corrected to remove fittings' losses) are shown in **Figure 7.2**. The figure is composed of the results for isothermal (squares) and non-isothermal experiments (circles), obtained during heat transfer tests. Each of the geometries underwent a transition from laminar to turbulent flow over the range of Reynolds numbers tested (20 to 1600), characterized by the shift from linear to quadratic behaviour at low to high flow rates, respectively.

This transitional flow behaviour was modeled via a dual-contribution friction factor equation with both laminar, f_L, and chaotic, f_C, terms.

$$f = \frac{\Delta P}{N}\frac{2}{\rho u^2} = \frac{f_L}{Re} + f_c \qquad (7.1)$$

For a reactor comprised of repeating microstructures, the traditional L/d_h term in Eq. (1) is replaced by N, the number of structures in series. Thus, N is equal to 12 for reactor 411S, 6 for 411L, 13 for 412S and 11 for 413. While octagons are increasing in size for 413, the location where most of the pressure drop and friction will occur is at the contractions between two octagons, which are identical throughout the reactor. Curved geometries and mixers are known to yield a smooth transition from laminar to turbulent conditions due to the formation of complex secondary flows [26,69,150]. This is analogous to the flow field in a packed bed, where laminar flow is gradually replaced by

localized regions of turbulence. Modeling the pressure drop thus requires contributions from both a laminar friction factor and a chaotic secondary flow friction factor as a means of interpolation within the transitional regime

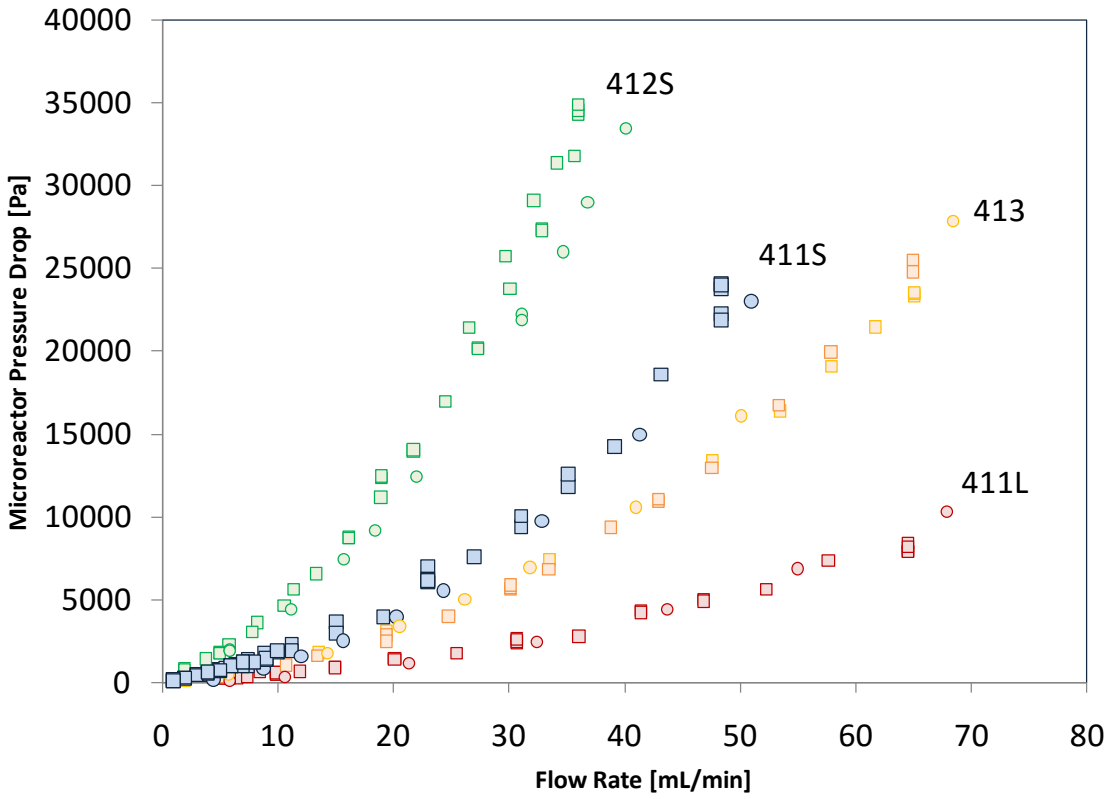

Figure 7.2 Experimental pressure drops of the micro-reactors. Isothermal (□) and non-isothermal (○) data.

As seen on **Figure 7.3** and **Table 7.2**, the linear fits of the reactors' friction factor against 1/Re are satisfactory, with R^2 ranging from 0.87 to 0.96. The variation, higher at low Reynolds, is likely due to the relative error of the pressure sensor. It is worth noting that while being geometrically similar, 411S and 411L do not have the same coefficients. This is due to the fact that while the 2D pattern is very similar, the depth of the structure is different. At their contraction, 411S has an aspect ratio of 2 deep:1 high while 411L has a ratio of 1:1. Thus, wall effects are stronger in 411L because it is shallower than 411S and results into increased friction, especially the laminar one.

Table 7.2 Comparison of the friction factors' parameters and fit.

Reactor	Re Tested	f_L	f_C	R^2
411S	23-1385	396	1.05	0.87
411L	88-1378	830	1.58	0.94
412S	62-1587	633	0.625	0.96
413	34-1505	432	1.64	0.94

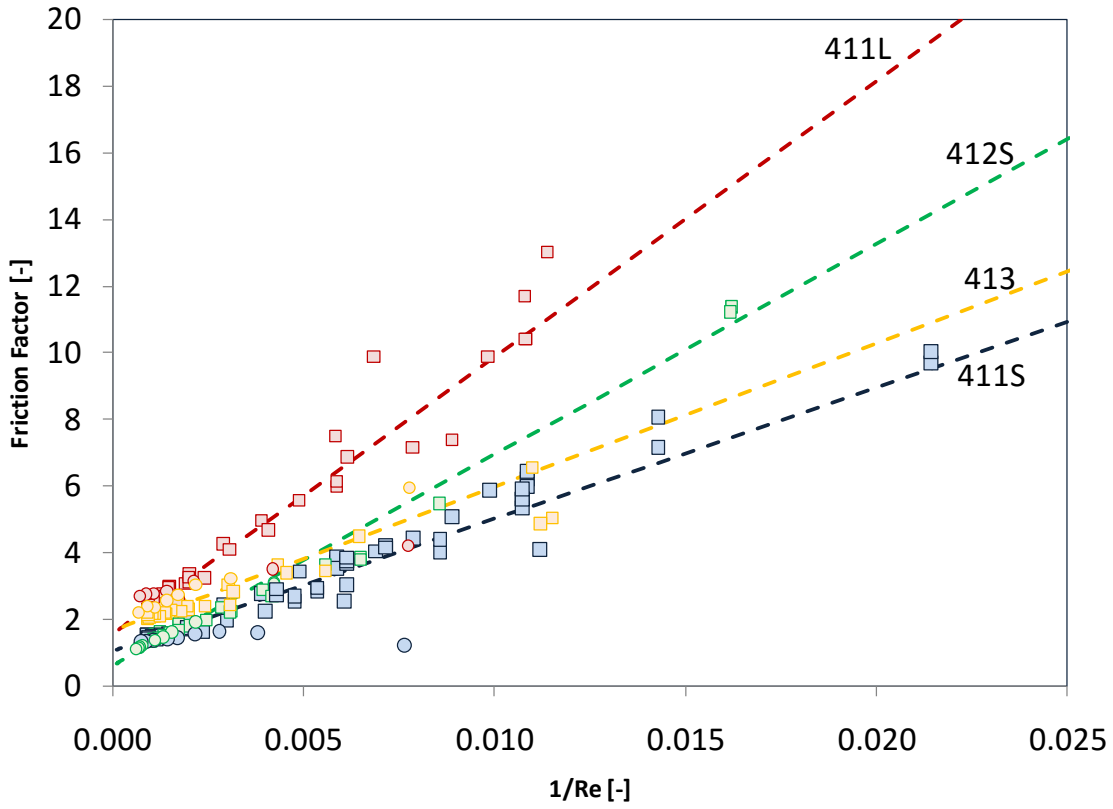

Figure 7.3 Comparison of the micro-reactors' friction factors. Isothermal (□) and non-isothermal (○) data and fitted models (---).

7.2.4 Single phase heat transfer

Heat transfer rates were calculated by measuring the inlet and outlet temperatures of both the reactor and thermal fluid streams. The thermal fluid flowed counter-current to the reactor at 200 mL/min and 2000 mL/min to produce two different thermal

resistances external to the reactor. The overall heat transfer coefficient was calculated as shown in Equation (7.2).

$$U = \frac{q}{A\Delta T_{LM}} = \frac{Q_{MR}\rho c_P\left(T_{MR}^{out} - T_{MR}^{in}\right)}{A\Delta T_{LM}} \quad (7.2)$$

Assuming one-dimensional heat transfer between the hot thermal fluid and reactor, the heat transfer area used was based on the milled foot-print of each reactor, neglecting area contributions from side walls of the structures. Heat flux through the adjacent glass plate was assumed negligible.

The overall heat transfer coefficient increases with reactor flow rate, gradually reaching a maximum once the thermal resistances of the dividing metal plate and flowing thermal fluid become dominant. By plotting the inverse of the heat transfer coefficient (1/U) against the inverse of the Reynolds number (1/Re), it is possible to extrapolate each reactor's intercept, which represents $1/U_{max}$ obtained at infinite reactor side flow rate. This is done for both thermal fluid side flow rate. The resulting plateau values are shown in **Table 7.3**.

Table 7.3 Comparison of the micro-reactors' heat transfer coefficient plateau values for different thermal side flow rate and metal plate thickness.

Reactor	U_{max} (W/m²/K)		Metal Plate Thickness (mm)
	200 mL/min	2000 mL/min	
411S	3051	7759	5
411L	2035	5142	5
412S	842	2451	3.5
413	328	1468	3.5

As expected, the maximum overall heat transfer coefficient increases when the thermal fluid side flow rate is greater. Plates 411S and 411L exhibited a higher plateau value than 412S and 413, despite an anticipated increase in thermal resistance in the 411S and 411L reactors due to a greater metallic plate thickness separating the reactor and thermal fluid side. This difference is likely due to a dead zone in the centre of the hexagons and octagons that is not contributing as much to heat exchange and increases the surface area

in an inefficient way. The phenomenon is displayed in **Figure 7.4**, which depicts the dead zones while purging prior to mass transfer tests. Also, because they occupy a large fraction of their plate, the structures in 412S and 413 may not benefit as much from side diffusion of heat than 411L and 411S.

Figure 7.4 Purging prior to mass transfer test in reactor 412S showing dead zones (total flow rate approx. 35 mL/min) in the centre.

Assuming resistances in series, it is possible to isolate the reactor side heat transfer coefficient and to correlate the resulting Nusselt number against Reynolds and Prandtl numbers as shown on **Figure 7.5**.

$$Nu_{MR} = \frac{U_{MR} d_h}{\lambda} = C Re^m Pr^n \quad (7.3)$$

Since there was minimal variation in the Prandtl number, its exponent was assumed equivalent to that of the Dittus-Boelter correlation for heating by internal convection [143]. The resulting correlations are shown below for each of the reactor plates.

$$Nu_{411S} = (1.101 \cdot 10^{-4}) Re^{1.874} Pr^{0.4} \quad (7.4a)$$

$$Nu_{411L} = (1.667 \cdot 10^{-3}) Re^{1.362} Pr^{0.4} \quad (7.4b)$$

$$Nu_{412} = (7.845 \cdot 10^{-5}) Re^{1.458} Pr^{0.4} \quad (7.4c)$$

$$Nu_{413} = (6.116 \cdot 10^{-5}) Re^{1.568} Pr^{0.4} \quad (7.4d)$$

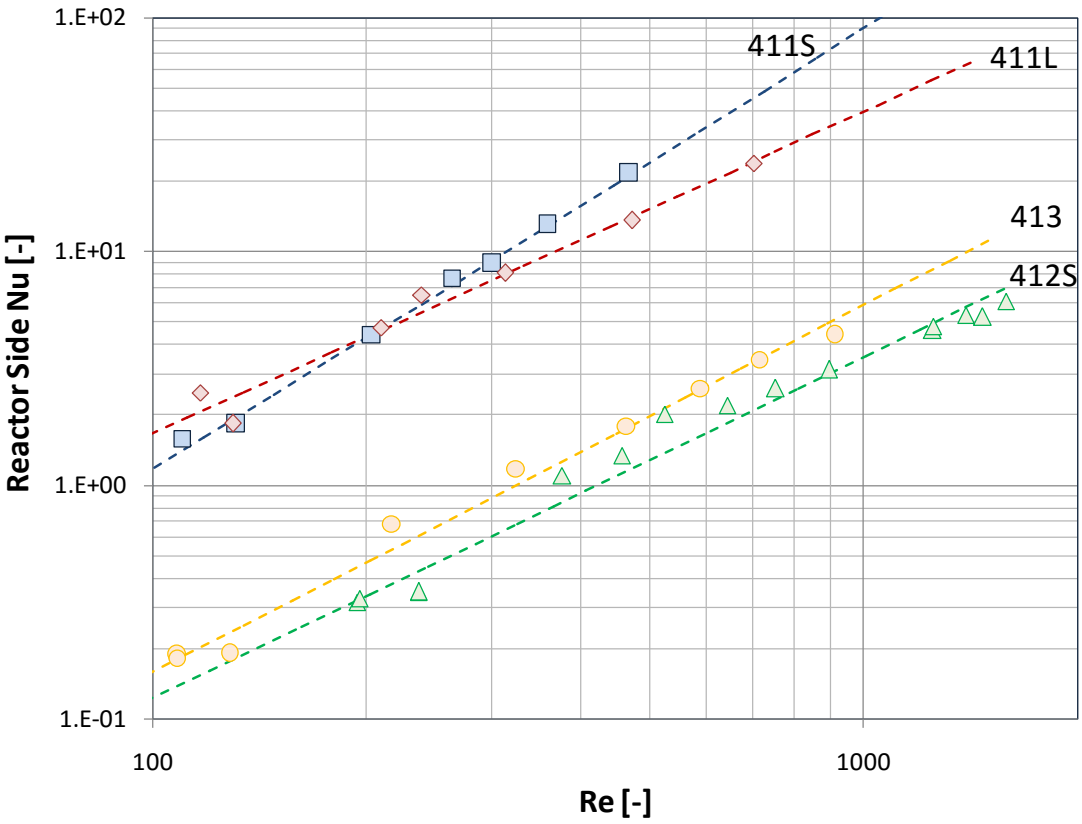

Figure 7.5 Reactor side only Nusselt number as a function of reactor side Reynolds number. Combined 200 and 2000 mL/min thermal fluid side flow rate data and fitted model (---).

The exponents of the Reynolds number for these correlations are relatively high compared to literature values of ~0.8. Even packed beds, with which micro-reactors showed similarity for pressure drop behaviour, show a rather constant Nu at low Re and a linear trend afterwards [151–153]. Heat conducted via the temperature sensing element is significant relative to the energy content of the local volume of fluid, which is a common problem as micro-reactors have a large area-to-volume ratio. This results, especially at the lower Re numbers, in a lower temperature reading that reduces the log mean temperature difference, increases the calculated overall heat transfer coefficients and creates unrealistic curvature.

7.2.5 Two phase mass Transfer

To determine the interphase mass transfer rates, pure water and pure n-butanol were fed into the micro-reactors at equal flow rates. The two liquids are partially miscible. The outlet stream phases were separated with care to minimize further inter-phase mass

transfer and a sample of each phase was analyzed using a densitometer to obtain the composition. The outlet water concentration in the n-butanol phase is shown in **Figure 7.6**. The dashed line corresponds to complete saturation. A similar trend was obtained for the n-butanol concentration in the water phase.

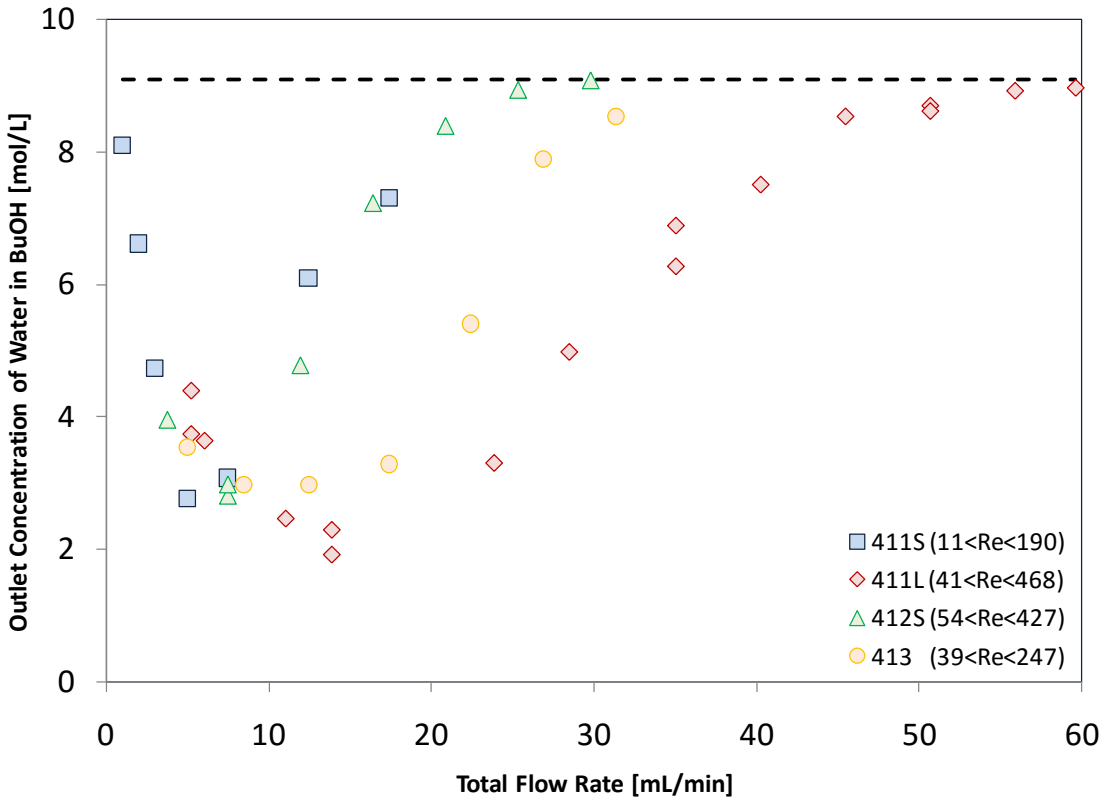

Figure 7.6 Concentration of water in the organic phase at the outlet of each micro-reactors. Saturation line (---) is at 9.09 mol/L.

Initially, the outlet concentration drops as total flow rate is increased because the increase in overall mass transfer coefficient, $K_w a$, is not sufficient to compensate for the reduction in residence time. The outlet concentration decreases to a minimum after which the relationship between $K_w a$ and flow rate changes. The dominant mechanism of mass transfer and interfacial area change such that the increased $K_w a$ has a greater impact than the reduction in residence time. The moment at which the minimum is reached depends on the reactor.

The model used to calculate the overall mass transfer coefficient is the same as the one used to calculate the overall heat exchange coefficient, but normalized by reactor volume

rather than by the exchange area. The partition coefficient of water in n-butanol, E, necessary to calculate the mass transfer coefficient, was determined experimentally to be 0.1793 mol/L in n-BuOH/mol/L in water.

$$K_w a = \frac{n_w}{V_R \Delta[W]_{LM}} = \frac{Q_{out}^{org}[w]_{out}^{org}}{V_R[w]_{LM}} \quad (7.5)$$

$$\Delta[w]_{LM} = \frac{([w]_{out}^{org} - E[w]_{out}^{aq}) - ([w]_{in}^{org} - E[w]_{in}^{aq})}{\ln\left(\frac{[w]_{out}^{org} - E[w]_{out}^{aq}}{[w]_{in}^{org} - E[w]_{in}^{aq}}\right)} \quad (7.6)$$

The mass transfer coefficient in mixing elements are frequently correlated to the volume normalized rate of energy consumption due to the dependence of the diffusive boundary layer thickness and the phase size on agitation [154]. At increasing flow rates, convective mass transfer and interfacial area are primarily governed by the energy dissipated due to chaotic secondary flow rather than laminar shear stress at the channel walls. The energy dissipation was thus split into these two categories using the packed bed analogy to calculate the contribution to the friction factor made by the chaotic coefficient, f_C. In order to use single phase correlations in two-phase situations, two-phase pressure drop tests were also carried out. The two phase system was analyzed using an average density and viscosity and compared with single phase values.

$$\bar{\rho} = \frac{Q_{aq}\rho_{aq} + Q_{org}\rho_{org}}{Q_{aq} + Q_{org}} \quad (7.7)$$

$$\bar{\mu} = \frac{Q_{aq} + Q_{org}}{\frac{Q_{aq}}{\mu_{aq}} + \frac{Q_{org}}{\mu_{org}}} \quad (7.8)$$

For these reactors and fluids, there was no significant difference between single and two-phase friction factors. This may be different for a system where interfacial tension is higher and the Laplace pressure contributions are significant. The overall mass transfer coefficient was subsequently compared to the chaotic eddy-based energy dissipation, ε_C, (**Figure 7.7**).

$$\varepsilon = \frac{\Delta PQ}{V_R} \quad (7.9)$$

$$\varepsilon_C = \frac{\Delta PQ}{V_R}\left(\frac{f_C}{f}\right) \tag{7.10}$$

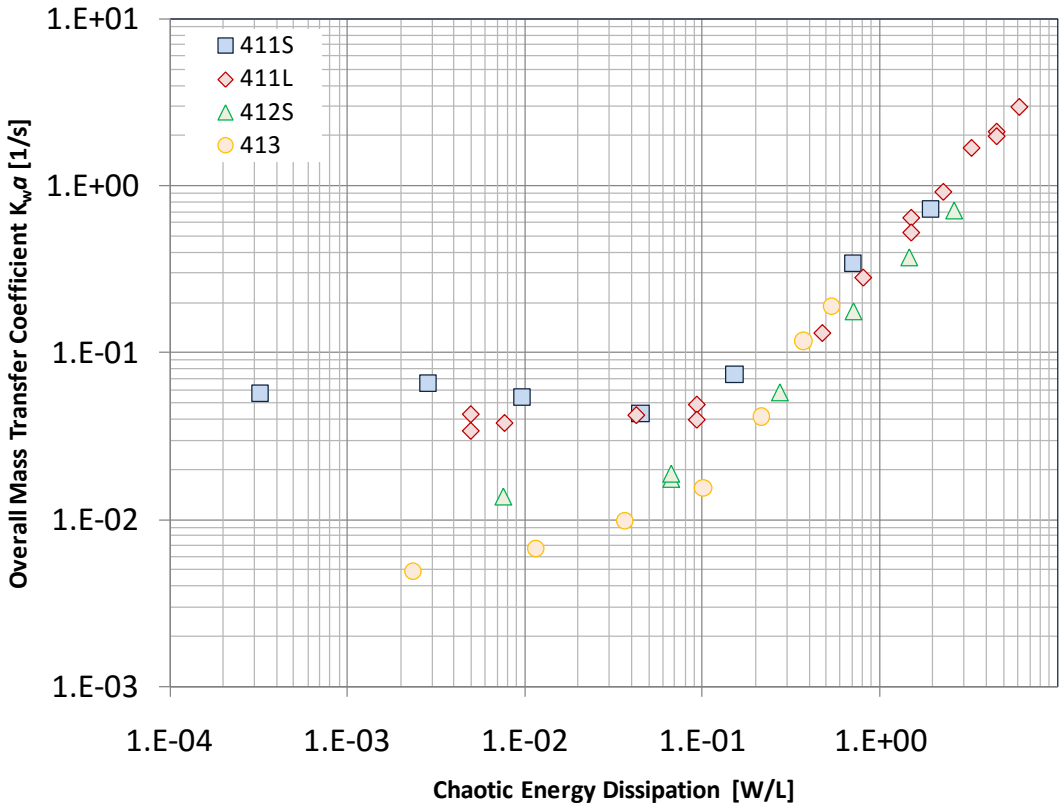

Figure 7.7 Comparison of the overall mass transfer coefficient of water in n-butanol, $K_w a$, against chaotic eddy-based energy dissipation.

Below a chaotic energy dissipation of 0.1 W/L, reactors 411S and 411L exhibit constant overall mass transfer coefficients. Insufficient data was obtained for 412S to make similar conclusions regarding the pivot point, while reactor 413 does not exhibit the same constant region.

411S and 411L have the same geometry where the flow is focused in a small contraction before being split, curved and recombined. The contraction is believed to initially control the dispersion's size. In such flow regime, the structure imposes a maximum possible droplet size on the dispersed phase and this maximum is smaller than what would be generated by the turbulent energy dissipation rate, resulting in a higher than expected *a*. Thus if *a* is relatively constant, then K_w must also be relatively constant suggesting that the mechanism of mass transfer is primarily by diffusion rather than convection. As the

flow rate is increased, energy dissipation is still not sufficient to further break the droplets or create significant eddies and $K_w a$ remains essentially constant. Once the chaotic energy dissipation is such that it can produce droplets the same size as that imposed by the contraction, $K_w a$ will increase with flow rate due to an increasing a and/or K_w. For the laminar regime, the 411 series reactors are better designed.

In contrast, reactor 413 forces the flow into a narrow channel and exits in a large recirculation zone where formed droplets can recombine with others before moving to the next structure element. From visual observation, this resulted in larger droplets than in 411S or 411L for similar chaotic energy dissipation which decreases a. This conclusion could be different for liquid-liquid systems with reduced rate of coalescence, using for example a surfactant. In such systems, droplets formed may be stable enough so that the contraction would control the dispersion. Just as with U, values of $K_w a$ will be lower if the volume of reactor is occupied by a dead zone not equally contributing to mass transfer, which is the case for plates 412 and 413.

In all reactors, the outlet concentration starts increasing after 0.1 W/L of chaotic energy dissipation. This seems to be the key number to achieve for the water-n-butanol system. It would likely be different for a system with different physical properties. Moreover, after this point, all reactors have similar values of $K_w a$ for a given chaotic energy dissipation. However, the geometry of the structure determines the amount of laminar energy dissipation generated to obtain the desired chaotic energy dissipation, which then translates into the convective mass transfer coefficient. The more efficient structure will have a lower percentage of energy dissipate via laminar shear stress.

7.2.6 Conclusion

From the single phase pressured drop data, it can be seen that secondary flow patterns are generated gradually in micro-reactors and provide a smooth transition from laminar to turbulent flow. This allows for the friction factor to be correlated in a similar fashion as packed beds, using a laminar and a chaotic flow coefficient.

The heat transfer coefficients gradually increases with reactor side flow rate before reaching a maximum. This maximum is due to two external resistances to heat transfer: the metallic plate between the reactor and the thermal fluid side and the convective heat transfer on the thermal fluid side. Because they occupy less area on their plate, 411L and 411S seems to benefit from side diffusion of heat, which increases the amount of heat dissipated through the metal segment in a 2D rather than a 1D pattern. Moreover, dead zones inefficiently contributing to heat and mass transfer were observed in the center of the structures of plates 412 and 413.

During mass transfer tests, it was observed that the outlet concentration of the transferred molecule drops to a minimum before returning to equilibrium as the flow rate is increased. Investigation of the mass transfer coefficient revealed that transfer in reactors 411S and 411L were controlled by the contraction and were initially in a regime where droplet size remained roughly constant. This differed from reactor 413, where recirculation and droplet coalescence had a significant effect. The packed-bed analogy allows the partitioning of the pressure drop and energy dissipation due to laminar and chaotic flow patterns. At chaotic energy dissipation rates above 0.1 W/L, the mass transfer coefficient in each of the four reactors exhibited similar behaviour. The geometry primarily affected the onset conditions for chaotic energy dissipation.

Future work will focus on the effect of physical properties such as interfacial tension on transport phenomena in different structures.

7.2.7 Acknowledgement

The authors would like to thank Paul Beaulieu for his contribution in the laboratory. Additionally, they would also like to thank the micro-reactor research team and financial support at Lonza Ltd. and the support and academic staff at the University of Ottawa for their help and guidance.

7.2.8 Nomenclature

a	Specific surface area [m^2/m^3]
A	Area of heat transfer [m^2]
c_P	Heat capacity [J/kg/K]
d_h	Hydraulic diameter of the contraction [m]
E	Partition coefficient [mol lean/mol rich]
f	Friction factor [-]
K	Convective mass transfer coefficient [m/s]
n	Molar rate of transfer [mol/s]
N	Number of structure elements [-]
Nu	Nusselt Number [-]
ΔP	Systems Pressure Drop [Pa]
Pr	Prandtl Number [-]
q	Amount of heat exchanged [W]
Q	Flow rate [mL/min or m^3/s]
Re	Reynolds Number [-]
T	Temperature [K]
u	Velocity at the contraction [m/s]
U	Overall heat transfer coefficient [$W/m^2/K$]
V_R	Reactor's volume [m^3]
[w]	Concentration of water [mol/m^3]

Greek letters

ε	Energy dissipation [W/L]
η	Extraction efficiency [-]
λ	Thermal conductivity of the fluid [W/m/K]

ρ Density [kg/m^3]

τ_{res} Average residence time [s]

Indices and Exponents

aq Aqueous phase side

C Chaotic contribution

L Laminar contribution

LM Log Mean difference

MR Reactor-Side

org Organic phase side

* Equilibrium point

7.2.9 References

See thesis references.

8 References

[1] L. Malet-Sanz, F. Susanne, Continuous flow synthesis. A pharma perspective., J. Med. Chem. 55 (2012) 4062–98. doi:10.1021/jm2006029.

[2] D.M. Roberge, An integrated approach combining reaction engineering and design of experiments for optimizing reactions, Org. Process Res. Dev. 8 (2004) 1049–1053. doi:10.1021/op0400160.

[3] D.M. Roberge, L. Ducry, N. Bieler, P. Cretton, B. Zimmermann, Microreactor Technology: A Revolution for the Fine Chemical and Pharmaceutical Industries?, Chem. Eng. Technol. 28 (2005) 318–323. doi:10.1002/ceat.200407128.

[4] N. Kockmann, D.M. Roberge, Harsh Reaction Conditions in Continuous-Flow Microreactors for Pharmaceutical Production, Chem. Eng. Technol. 32 (2009) 1682–1694. doi:10.1002/ceat.200900355.

[5] J.J. Brandner, W. Benzinger, U. Schygulla, S. Zimmermann, K. Schubert, Metallic micro heat exchangers: properties, applications and long term stability, in: H. Müller-Steinhagen, M.R. Malayeri, A.P. Watkinson (Eds.), Heat Exch. Fouling Clean. VII, Tomar, Portugal, 2007: pp. 383–393. http://dc.engconfintl.org/heatexchanger2007/49/.

[6] J.R. Burns, C. Ramshaw, A Microreactor for the Nitration of Benzene and Toluene, Chem. Eng. Commun. 189 (2002) 1611–1628. doi:10.1080/00986440214585.

[7] S.G. Newman, K.F. Jensen, The role of flow in green chemistry and engineering, Green Chem. 15 (2013) 1456. doi:10.1039/c3gc40374b.

[8] S. Borukhova, V. Hessel, Process Intensification for Green Chemistry, John Wiley & Sons, Ltd, Chichester, UK, 2013. doi:10.1002/9781118498521.

[9] Velocys Technologies Ltd, Microchannel reactors, Our Prod. (2015). http://www.velocys.com/our_products_core_technologies_reactors.php.

[10] G. Markowz, S. Schirrmeister, J. Albrecht, F. Becker, R. Schütte, K.J. Caspary, et al., Microstructured Reactors for Heterogeneously Catalyzed Gas-Phase Reactions on an Industrial Scale, Chem. Eng. Technol. 28 (2005) 459–464. doi:10.1002/ceat.200407146.

[11] C.P. Holvey, D.M. Roberge, M. Gottsponer, N. Kockmann, A. Macchi, Pressure drop and mixing in single phase microreactors: Simplified designs of micromixers, Chem. Eng. Process. Process Intensif. 50 (2011) 1069–1075. doi:10.1016/j.cep.2011.05.016.

[12] D.M. Roberge, B. Zimmermann, F. Rainone, M. Gottsponer, M. Eyholzer, N. Kockmann, Microreactor technology and continuous processes in the fine chemical and pharmaceutical industry: Is the revolution underway?, Org. Process Res. Dev. 12 (2008) 905–910. doi:10.1021/op8001273.

[13] D.M. Roberge, M. Gottsponer, M. Eyholzer, N. Kockmann, Industrial design, scale-up, and use of microreactors, Chem. Today. 27 (2009) 8–11. http://www.scopus.com/inward/record.url?eid=2-s2.0-70349441037&partnerID=tZOtx3y1 (accessed March 1, 2012).

[14] N. Kockmann, M. Gottsponer, B. Zimmermann, D.M. Roberge, Enabling continuous-flow chemistry in microstructured devices for pharmaceutical and fine-chemical production., Chemistry. 14 (2008) 7470–7. doi:10.1002/chem.200800707.

[15] B.P. Mason, K.E. Price, J.L. Steinbacher, A.R. Bogdan, D.T. McQuade, Greener approaches to organic synthesis using microreactor technology., Chem. Rev. 107 (2007) 2300–18. doi:10.1021/cr050944c.

[16] N. Kockmann, Pressure Loss and Transfer Rates in Microstructured Devices with Chemical Reactions, Chem. Eng. Technol. 31 (2008) 1188–1195. doi:10.1002/ceat.200800065.

[17] G. Dummann, U. Quittmann, L. Gröschel, D.W. Agar, O. Wörz, K. Morgenschweis, The capillary-microreactor: a new reactor concept for the intensification of heat and mass transfer in liquid–liquid reactions, Catal. Today. 79-80 (2003) 433–439. doi:10.1016/S0920-5861(03)00056-7.

[18] L. Ducry, D.M. Roberge, Controlled autocatalytic nitration of phenol in a microreactor., Angew. Chem. Int. Ed. Engl. 44 (2005) 7972–5. doi:10.1002/anie.200502387.

[19] A. Ghaini, M.N. Kashid, D.W. Agar, Effective interfacial area for mass transfer in the liquid–liquid slug flow capillary microreactors, Chem. Eng. Process. Process Intensif. 49 (2010) 358–366. doi:10.1016/j.cep.2010.03.009.

[20] M.N. Kashid, L. Kiwi-Minsker, Microstructured Reactors for Multiphase Reactions: State of the Art, Ind. Eng. Chem. Res. 48 (2009) 6465–6485. doi:10.1021/ie8017912.

[21] V. Hessel, D. Kralisch, N. Kockmann, T. Noël, Q. Wang, Novel process windows for enabling, accelerating, and uplifting flow chemistry., ChemSusChem. 6 (2013) 746–89. doi:10.1002/cssc.201200766.

[22] M.E. Steinke, S.G. Kandlikar, Review of single-phase heat transfer enhancement techniques for application in microchannels, minichannels and microdevices, Int.

J. Heat Technol. 22 (2004) 3–11. http://www.rit.edu/kgcoe/mechanical/taleme/Papers/Journal Papers/J037.pdf.

[23] V. Hessel, S. Hardt, H. Löwe, F. Schönfeld, Laminar mixing in different interdigital micromixers: I. Experimental characterization, AIChE J. 49 (2003) 566–577. doi:10.1002/aic.690490304.

[24] V. Hessel, T. Dietrich, A. Freitag, S. Hardt, C. Hofmann, H. Löwe, et al., Fast Mixing in Interdigital Micromixers achieved by Means of Extreme Focusing, in: Proc. IMRET 6, New Orleans, USA, 2002: p. 297.

[25] S.A. Berger, L. Talbot, L.S. Yao, Flow in Curved Pipes, Annu. Rev. Fluid Mech. 15 (1983) 461–512. doi:10.1146/annurev.fl.15.010183.002333.

[26] N.R. Rosaguti, D.F. Fletcher, B.S. Haynes, Laminar Flow and Heat Transfer in a Periodic Serpentine Channel, Chem. Eng. Technol. 28 (2005) 353–361. doi:10.1002/ceat.200407148.

[27] D.M. Fries, P.R. von Rohr, Liquid mixing in gas–liquid two-phase flow by meandering microchannels, Chem. Eng. Sci. 64 (2009) 1326–1335. doi:10.1016/j.ces.2008.11.019.

[28] S. Dreher, N. Kockmann, P. Woias, Characterization of Laminar Transient Flow Regimes and Mixing in T-shaped Micromixers, Heat Transf. Eng. 30 (2009) 91–100. doi:10.1080/01457630802293480.

[29] F. Jiang, K.S. Drese, S. Hardt, M. Küpper, F. Schönfeld, Helical flows and chaotic mixing in curved micro channels, AIChE J. 50 (2004) 2297–2305. doi:10.1002/aic.10188.

[30] V. Hessel, H. Löwe, F. Schönfeld, Micromixers—a review on passive and active mixing principles, Chem. Eng. Sci. 60 (2005) 2479–2501. doi:10.1016/j.ces.2004.11.033.

[31] S. Castellano, L. Tamborini, M. Viviano, A. Pinto, G. Sbardella, P. Conti, Synthesis of 3-aryl/benzyl-4,5,6,6a-tetrahydro-3aH-pyrrolo[3,4-d]isoxazole derivatives: a comparison between conventional, microwave-assisted and flow-based methodologies., J. Org. Chem. 75 (2010) 7439–42. doi:10.1021/jo1014323.

[32] A.A.-M. Wilhelm, F. Laugier, R. Kidak, B. Ratsimba, H. Delmas, Ultrasound to Enhance a Liquid–Liquid Reaction, J. Chem. Eng. JAPAN. 43 (2010) 751–756. doi:10.1252/jcej.08We187.

[33] N. Kockmann, M. Gottsponer, D.M. Roberge, Scale-up concept of single-channel microreactors from process development to industrial production, Chem. Eng. J. 167 (2011) 718–726. doi:10.1016/j.cej.2010.08.089.

[34] N. Kockmann, D.M. Roberge, Scale-up concept for modular microstructured reactors based on mixing, heat transfer, and reactor safety, Chem. Eng. Process. Process Intensif. 50 (2011) 1017–1026. doi:10.1016/j.cep.2011.05.021.

[35] L. Ducry, D.M. Roberge, Dibal-H Reduction of Methyl Butyrate into Butyraldehyde using Microreactors, Org. Process Res. Dev. 12 (2008) 163–167. doi:10.1021/op7002002.

[36] E. Georget, J.L. Sauvageat, A. Burbidge, A. Mathys, Residence time distributions in a modular micro reaction system, J. Food Eng. 116 (2013) 910–919. doi:10.1016/j.jfoodeng.2013.01.041.

[37] M. Saber, J.M. Commenge, L. Falk, Microreactor numbering-up in multi-scale networks for industrial-scale applications: impact of flow maldistribution on the reactor performances, Chem. Eng. Sci. 65 (2010) 372–379. http://www.sciencedirect.com/science/article/pii/S0009250909003923.

[38] E.D. Lavric, P. Woehl, Advanced-Flow glass reactors for seamless scale-up, Chim. Oggi. 27 (2009) 45–48.

[39] M.J. Nieves-Remacha, A.A. Kulkarni, K.F. Jensen, Hydrodynamics of Liquid–Liquid Dispersion in an Advanced-Flow Reactor, Ind. Eng. Chem. Res. 51 (2012) 16251–16262. doi:10.1021/ie301821k.

[40] P. Barthe, C. Guermeur, O. Lobet, M. Moreno, P. Woehl, D.M. Roberge, et al., Continuous Multi-Injection Reactor for Multipurpose Production - Part I, Chem. Eng. Technol. 31 (2008) 1146–1154. doi:10.1002/ceat.200800132.

[41] Y. Su, Y. Zhao, G. Chen, Q. Yuan, Liquid–liquid two-phase flow and mass transfer characteristics in packed microchannels, Chem. Eng. Sci. 65 (2010) 3947–3956. doi:10.1016/j.ces.2010.03.034.

[42] S.W. Lee, D.S. Kim, S.S. Lee, T.H. Kwon, A split and recombination micromixer fabricated in a PDMS three-dimensional structure, J. Micromechanics Microengineering. 16 (2006) 1067–1072. doi:10.1088/0960-1317/16/5/027.

[43] J. Gunnarsson, I. Sinclair, F.J. Alanis, Compact Heat Exchangers: Improving Heat Recovery, Chem. Eng. (2009) 44–47.

[44] A. Palmieri, S. V. Ley, K. Hammond, A. Polyzos, I.R. Baxendale, A microfluidic flow chemistry platform for organic synthesis: the Hofmann rearrangement, Tetrahedron Lett. 50 (2009) 3287–3289. doi:10.1016/j.tetlet.2009.02.059.

[45] A. Renken, V. Hessel, P. Löb, R. Miszczuk, M. Uerdingen, L. Kiwi-Minsker, Ionic liquid synthesis in a microstructured reactor for process intensification, Chem.

Eng. Process. Process Intensif. 46 (2007) 840–845. doi:10.1016/j.cep.2007.05.020.

[46] M. Damm, T.N. Glasnov, C.O. Kappe, Translating High-Temperature Microwave Chemistry to Scalable Continuous Flow Processes, Org. Process Res. Dev. 14 (2010) 215–224. doi:10.1021/op900297e.

[47] M. Kashid, A. Renken, L. Kiwi-Minsker, Mixing efficiency and energy consumption for five generic microchannel designs, Chem. Eng. J. 167 (2011) 436–443. doi:10.1016/j.cej.2010.09.078.

[48] E. Lobry, F. Theron, C. Gourdon, N. Le Sauze, C. Xuereb, T. Lasuye, Turbulent liquid–liquid dispersion in SMV static mixer at high dispersed phase concentration, Chem. Eng. Sci. 66 (2011) 5762–5774. doi:10.1016/j.ces.2011.06.073.

[49] S. Lawton, G. Steele, P. Shering, L. Zhao, I. Laird, X.-W. Ni, Continuous Crystallization of Pharmaceuticals Using a Continuous Oscillatory Baffled Crystallizer, Org. Process Res. Dev. 13 (2009) 1357–1363. doi:10.1021/op900237x.

[50] X.-W. Ni, Flow chemistry technologies handling solids including crystallisation, in: ACHEMA, Frankfurt, Germany, 2012.

[51] D.L. Browne, B.J. Deadman, R. Ashe, I.R. Baxendale, S. V Ley, Continuous Flow Processing of Slurries: Evaluation of an Agitated Cell Reactor, Org. Process Res. Dev. 15 (2011) 693–697. doi:10.1021/op2000223.

[52] L. Fan, G. Yang, D. Lee, K. Tsuchiya, X. Luo, Some aspects of high-pressure phenomena of bubbles in liquids and liquid–solid suspensions, Chem. Eng. …. 54 (1999) 4681–4709. http://www.sciencedirect.com/science/article/pii/S0009250999003486.

[53] LonzaGroup, FlowPlateTM MicroReactor Gas Liquid Reaction, Youtube. (2012). https://www.youtube.com/watch?v=TcyQLciyg3Q.

[54] D.M. Roberge, C. Noti, E. Irle, M. Eyholzer, B. Rittiner, G. Penn, et al., Control of Hazardous Processes in Flow: Synthesis of 2-Nitroethanol, J. Flow Chem. 1 (2013) 1–1. doi:10.1556/JFC-D-13-00016.

[55] O. Levenspiel, Chemical reaction engineering, 3rd ed., New York, 1999. doi:10.1016/0009-2509(64)85017-X.

[56] H.S. Fogler, Elements of chemical reaction engineering, 1999. doi:10.1016/0009-2509(87)80130-6.

[57] D.M. Roberge, N. Bieler, M. Mathier, M. Eyholzer, B. Zimmermann, P. Barthe, et al., Development of an Industrial Multi-Injection Microreactor for Fast and

Exothermic Reactions - Part II, Chem. Eng. Technol. 31 (2008) 1155–1161. doi:10.1002/ceat.200800131.

[58] R. Andreozzi, V. Caprio, I. Di Somma, R. Sanchirico, Kinetic and safety assessment for salicylic acid nitration by nitric acid/acetic acid system., J. Hazard. Mater. 134 (2006) 1–7. doi:10.1016/j.jhazmat.2005.10.037.

[59] R. Andreozzi, M. Canterino, V. Caprio, I. Di Somma, R. Sanchirico, Salicylic Acid Nitration by Means of Nitric Acid/Acetic Acid System: Chemical and Kinetic Characterization, Org. Process Res. Dev. 10 (2006) 1199–1204. doi:10.1021/op060148o.

[60] R. Andreozzi, M. Canterino, V. Caprio, I. Di Somma, R. Sanchirico, Batch salicylic acid nitration by nitric acid/acetic acid mixture under isothermal, isoperibolic and adiabatic conditions., J. Hazard. Mater. 138 (2006) 452–8. doi:10.1016/j.jhazmat.2006.05.104.

[61] J.G. Hoggett, Nitration and aromatic reactivity, Cambridge University Press, 1971.

[62] S. Monfette, M. Eyholzer, D.M. Roberge, D.E. Fogg, Getting ring-closing metathesis off the bench: reaction-reactor matching transforms metathesis efficiency in the assembly of large rings., Chem. Eur. J. 16 (2010) 11720–5. doi:10.1002/chem.201001210.

[63] S. Monfette, D.E. Fogg, Equilibrium ring-closing metathesis., Chem. Rev. 109 (2009) 3783–816. doi:10.1021/cr800541y.

[64] J.C. Pastre, D.L. Browne, S. V Ley, Flow chemistry syntheses of natural products., Chem. Soc. Rev. 42 (2013) 8849–69. doi:10.1039/c3cs60246j.

[65] R.L. Hartman, J.P. McMullen, K.F. Jensen, Deciding whether to go with the flow: evaluating the merits of flow reactors for synthesis., Angew. Chem. Int. Ed. Engl. 50 (2011) 7502–19. doi:10.1002/anie.201004637.

[66] C. Wiles, P. Watts, Continuous process technology: a tool for sustainable production, Green Chem. 16 (2014) 55. doi:10.1039/c3gc41797b.

[67] P. Plouffe, A. Macchi, D.M. Roberge, From Batch to Continuous Chemical Synthesis—A Toolbox Approach, Org. Process Res. Dev. 18 (2014) 1286–1294. doi:10.1021/op5001918.

[68] A. Günther, S.A. Khan, M. Thalmann, F. Trachsel, K.F. Jensen, Transport and reaction in microscale segmented gas-liquid flow., Lab Chip. 4 (2004) 278–86. doi:10.1039/b403982c.

[69] N. Kockmann, T. Kiefer, M. Engler, P. Woias, Convective mixing and chemical reactions in microchannels with high flow rates, Sensors Actuators B Chem. 117 (2006) 495–508. doi:10.1016/j.snb.2006.01.004.

[70] M.N. Kashid, D.W. Agar, Hydrodynamics of liquid–liquid slug flow capillary microreactor: Flow regimes, slug size and pressure drop, Chem. Eng. J. 131 (2007) 1–13. doi:10.1016/j.cej.2006.11.020.

[71] M.N. Kashid, A. Gupta, A. Renken, L. Kiwi-Minsker, Numbering-up and mass transfer studies of liquid–liquid two-phase microstructured reactors, Chem. Eng. J. 158 (2010) 233–240. doi:10.1016/j.cej.2010.01.020.

[72] M. N. Kashid, A. Renken, L. Kiwi-Minsker, Influence of Flow Regime on Mass Transfer in Different Types of Microchannels, Ind. Eng. Chem. Res. 50 (2011) 6906–6914. doi:10.1021/ie102200j.

[73] M.N. Kashid, A. Renken, L. Kiwi-Minsker, Gas-liquid and liquid-liquid mass transfer in microstructured reactors, Chem. Eng. Sci. 66 (2011) 3876–3897. doi:10.1016/j.ces.2011.05.015.

[74] P. Plouffe, R. Anthony, A. Donaldson, D.M. Roberge, N. Kockmann, A. Macchi, Transport Phenomena in Two-Phase Liquid-Liquid Micro-Reactors, in: ASME 2012 10th Int. Conf. Nanochannels, Microchannels, Minichannels, ASME, 2012: p. 611. doi:10.1115/ICNMM2012-73040.

[75] P. Plouffe, D.M. Roberge, A. Macchi, Liquid-liquid flow regimes and mass transfer in various micro-reactors, Chem. Eng. J. (2014). doi:10.1016/j.cej.2014.10.072.

[76] F. Guo, B. Chen, Numerical Study on Taylor Bubble Formation in a Micro-channel T-Junction Using VOF Method, Microgravity Sci. Technol. 21 (2009) 51–58. doi:10.1007/s12217-009-9146-4.

[77] Y. Su, G. Chen, Q. Yuan, Effect of Viscosity on the Hydrodynamics of Liquid Processes in Microchannels, Chem. Eng. Technol. 37 (2014) 427–434. doi:10.1002/ceat.201300468.

[78] N. Kockmann, S. Karlen, C. Girard, D.M. Roberge, Liquid–Liquid Test Reactions to Characterize Two-Phase Mixing in Microchannels, Heat Transf. Eng. 34 (2013) 169–177. doi:10.1080/01457632.2013.703508.

[79] E.L. Paul, V.A. Atiemo-Obeng, S.M. Kresta, Handbook of Industrial Mixing: Science and Practice, John Wiley & Sons, 2004.

[80] Ehrfeld Mikrotechnik BTS, Products Catalogue, Ehrfeld.com/en/products.html. (2015). http://www.ehrfeld.com/en/products.html.

[81] Chemtrix DV, Labtrix® Start Systems, http://www.chemtrix.com/products/Labtrix-Start-1. (2015). http://www.chemtrix.com/products/Labtrix-Start-1.

[82] A.K. Nanda, M.M. Sharma, Effective interfacial area in liquid—liquid extraction, Chem. Eng. Sci. 21 (1966) 707–713. doi:10.1016/0009-2509(66)80022-2.

[83] B. Ahmed, D. Barrow, T. Wirth, Enhancement of Reaction Rates by Segmented Fluid Flow in Capillary Scale Reactors, Adv. Synth. Catal. 348 (2006) 1043–1048. doi:10.1002/adsc.200505480.

[84] B. Ahmed, D. Barrow, T. Wirth, Effect of segmented fluid flow, sonication and phase transfer catalysis on biphasic reactions in capillary microreactors, Chem. Eng. J. 135 (2008) S280–S283. doi:10.1016/j.cej.2007.07.017.

[85] V.D. Parker, Instantaneous rate constants in physical organic chemistry: application to acyl transfer reactions ofp-nitrophenyl acetate to hydroxide ion, J. Phys. Org. Chem. 19 (2006) 714–724. doi:10.1002/poc.1064.

[86] H.M. Backes, M. Jing Jun, B. E., M. G., Interfacial tensions in binary and ternary liquid—liquid systems, Chem. Eng. Sci. 45 (1990) 275–286. doi:10.1016/0009-2509(90)87099-E.

[87] A. Berthod, N. Schmitt, Water—organic solvent systems in countercurrent chromatography: Liquid stationary phase retention and solvent polarity, Talanta. 40 (1993) 1489–1498. doi:10.1016/0039-9140(93)80358-X.

[88] D.J. Donahue, F.E. Bartell, U. Michigan, A. Arbor, The boundary tension at water-organic liquid interfaces, J. Phys. Chem. 56 (1952) 480–484. doi:10.1021/j150496a016.

[89] S. Matsuo, T. Makita, Volumetric properties of 1-alkanols at temperatures in the range 298–348 K and pressures up to 40 MPa, Int. J. Thermophys. 10 (1989) 885–897. http://link.springer.com/article/10.1007/BF00514479.

[90] S. Viswanathan, M. Anand Rao, D.H.L. Prasad, Densities and Viscosities of Binary Liquid Mixtures of Anisole or Methyl tert -Butyl Ether with Benzene, Chlorobenzene, Benzonitrile, and Nitrobenzene, J. Chem. Eng. Data. 45 (2000) 764–770. doi:10.1021/je990288b.

[91] A. Hickel, C.J. Radke, H.W. Blanch, Role of Organic Solvents on Pa-Hydroxynitrile Lyase Interfacial Activity and Stability, Biotechnol. Bioeng. 74 (2001).

[92] R. Stephenson, Mutual solubilities: water-ketones, water-ethers, and water-gasoline-alcohols, J. Chem. Eng. Data. 37 (1992) 80–95. http://pubs.acs.org/doi/pdf/10.1021/je00005a024.

[93] A. Alexandrov, The Equations for Thermophysical Properties of Aqueous Solutions of Sodium Hydroxide, in: M. Nakahara, N. Matubayasi, M. Ueno, Y. Yasuoka, K. Watanabe (Eds.), Water, Steam Aqueous Solut. Electr. Power Adv. Sci. Technol. Proc. 14th Int. Conf. Prop. Water Steam, Maruzen Co Ltd., Kyoto, 2005: pp. 86–90. http://www.iapws.jp/Proceedings/Symposium02/086Alexandrov.pdf.

[94] C.R. Wilke, P. Chang, Correlation of diffusion coefficients in dilute solutions, AIChE J. 1 (1955) 264–270. doi:10.1002/aic.690010222.

[95] P. Guillot, A. Colin, Stability of parallel flows in a microchannel after a T junction, Phys. Rev. E. 72 (2005) 066301. doi:10.1103/PhysRevE.72.066301.

[96] D.M. Fries, S. Waelchli, P.R. von Rohr, Gas–liquid two-phase flow in meandering microchannels, Chem. Eng. J. 135 (2008) S37–S45. doi:10.1016/j.cej.2007.07.052.

[97] F.P. Bretherton, The motion of long bubbles in tubes, J. Fluid Mech. 10 (2006) 166. doi:10.1017/S0022112061000160.

[98] P. Garstecki, M.J. Fuerstman, H.A. Stone, G.M. Whitesides, Formation of droplets and bubbles in a microfluidic T-junction-scaling and mechanism of break-up., Lab Chip. 6 (2006) 437–46. doi:10.1039/b510841a.

[99] A. Leclerc, R. Philippe, V. Houzelot, D. Schweich, C. de Bellefon, Gas-liquid Taylor flow in square micro-channels: New inlet geometries and interfacial area tuning, Chem. Eng. J. 165 (2010) 290–300. doi:10.1016/j.cej.2010.08.021.

[100] J.D. Tice, A.D. Lyon, R.F. Ismagilov, Effects of viscosity on droplet formation and mixing in microfluidic channels, Anal. Chim. Acta. 507 (2004) 73–77. doi:10.1016/j.aca.2003.11.024.

[101] J. Jovanović, W. Zhou, E. V. Rebrov, T. a. Nijhuis, V. Hessel, J.C. Schouten, Liquid–liquid slug flow: Hydrodynamics and pressure drop, Chem. Eng. Sci. 66 (2011) 42–54. doi:10.1016/j.ces.2010.09.040.

[102] M. Al-Rawashdeh, F. Yu, T.A. Nijhuis, E.V. Rebrov, V. Hessel, J.C. Schouten, Numbered-up gas–liquid micro/milli channels reactor with modular flow distributor, Chem. Eng. J. 207-208 (2012) 645–655. doi:10.1016/j.cej.2012.07.028.

[103] M. Roudet, K. Loubiere, C. Gourdon, M. Cabassud, Hydrodynamic and mass transfer in inertial gas-liquid flow regimes through straight and meandering millimetric square channels, Chem. Eng. Sci. 66 (2011) 2974–2990. doi:10.1016/j.ces.2011.03.045.

[104] A.H.P. Skelland, R.M. Wellek, Resistance to mass transfer inside droplets, AIChE J. 10 (1964) 491–496. doi:10.1002/aic.690100416.

[105] N. Di Miceli Raimondi, L. Prat, C. Gourdon, J. Tasselli, Experiments of mass transfer with liquid-liquid slug flow in square microchannels, Chem. Eng. Sci. 105 (2014) 169–178. doi:10.1016/j.ces.2013.11.009.

[106] P. Sobieszuk, R. Pohorecki, P. Cygański, J. Grzelka, Determination of the interfacial area and mass transfer coefficients in the Taylor gas–liquid flow in a microchannel, Chem. Eng. Sci. 66 (2011) 6048–6056. doi:10.1016/j.ces.2011.08.029.

[107] P. Sobieszuk, F. Ilnicki, R. Pohorecki, Contribution of Liquid- and Gas-Side Mass Transfer Coefficients to Overall Mass Transfer Coefficient in Taylor Flow in a Microreactor, Chem. Process Eng. 35 (2014) 35–45. doi:10.2478/cpe-2014-0003.

[108] P. Sobieszuk, J. Aubin, R. Pohorecki, Hydrodynamics and Mass Transfer in Gas-Liquid Flows in Microreactors, Chem. Eng. Technol. 35 (2012) 1346–1358. doi:10.1002/ceat.201100643.

[109] W.R. Dean, XVI. Note on the motion of fluid in a curved pipe, London, Edinburgh, Dublin Philos. Mag. J. Sci. 4 (1927) 208–223. doi:10.1080/14786440708564324.

[110] T. Lemenand, D. Della Valle, Y. Zellouf, H. Peerhossaini, Droplets formation in turbulent mixing of two immiscible fluids in a new type of static mixer, Int. J. Multiph. Flow. 29 (2003) 813–840. doi:10.1016/S0301-9322(03)00032-6.

[111] T. Lemenand, P. Dupont, D. Della Valle, H. Peerhossaini, Comparative efficiency of shear, elongation and turbulent droplet breakup mechanisms: Review and application, Chem. Eng. Res. Des. 91 (2013) 2587–2600. doi:10.1016/j.cherd.2013.03.017.

[112] G. Zhou, S.M. Kresta, Correlation of mean drop size and minimum drop size with the turbulence energy dissipation and the flow in an agitated tank, Chem. Eng. Sci. 53 (1998) 2063–2079. doi:10.1016/S0009-2509(97)00438-7.

[113] T. Wang, J. Wang, Y. Jin, A novel theoretical breakup kernel function for bubbles/droplets in a turbulent flow, Chem. Eng. Sci. 58 (2003) 4629–4637. doi:10.1016/j.ces.2003.07.009.

[114] F. Theron, N. Le Sauze, A. Ricard, Turbulent Liquid—Liquid Dispersion in Sulzer SMX Mixer, Ind. Eng. Chem. Res. 49 (2010) 623–632. doi:10.1021/ie900090d.

[115] T. Illg, V. Hessel, P. Löb, J.C. Schouten, Novel Process Window for the safe and continuous synthesis of tert.-butyl peroxy pivalate in a micro-reactor, Chem. Eng. J. 167 (2011) 504–509. doi:10.1016/j.cej.2010.08.081.

[116] A. Alam, K.-Y. Kim, Analysis of mixing in a curved microchannel with rectangular grooves, Chem. Eng. J. 181-182 (2012) 708–716. doi:10.1016/j.cej.2011.12.076.

[117] A. Afzal, K.-Y. Kim, Passive split and recombination micromixer with convergent–divergent walls, Chem. Eng. J. 203 (2012) 182–192. doi:10.1016/j.cej.2012.06.111.

[118] L. Falk, J.-M. Commenge, Performance comparison of micromixers, Chem. Eng. Sci. 65 (2010) 405–411. doi:10.1016/j.ces.2009.05.045.

[119] C. Galletti, M. Roudgar, E. Brunazzi, R. Mauri, Effect of inlet conditions on the engulfment pattern in a T-shaped micro-mixer, Chem. Eng. J. 185-186 (2012) 300–313. doi:10.1016/j.cej.2012.01.046.

[120] A.-L. Dessimoz, L. Cavin, A. Renken, L. Kiwi-Minsker, Liquid–liquid two-phase flow patterns and mass transfer characteristics in rectangular glass microreactors, Chem. Eng. Sci. 63 (2008) 4035–4044. doi:10.1016/j.ces.2008.05.005.

[121] E. Šinkovec, A. Pohar, M. Krajnc, Phase transfer catalyzed esterification: modeling and experimental studies in a microreactor under parallel flow conditions, Microfluid. Nanofluidics. 14 (2012) 489–498. doi:10.1007/s10404-012-1067-7.

[122] P. Plouffe, A. Macchi, A. a. Donaldson, Enhancement of Interphase Transport in Mini-/Microscale Applications Using Passive Mixing, Heat Transf. Eng. 34 (2013) 159–168. doi:10.1080/01457632.2013.703476.

[123] T. Illg, V. Hessel, P. Löb, J.C. Schouten, Continuous synthesis of tert-butyl peroxypivalate using a single-channel microreactor equipped with orifices as emulsification units., ChemSusChem. 4 (2011) 392–8. doi:10.1002/cssc.201000368.

[124] T. Illg, V. Hessel, P. Löb, J.C. Schouten, Orifice microreactor for the production of an organic peroxide – non-reactive and reactive characterization, Green Chem. 14 (2012) 1420. doi:10.1039/c2gc35043b.

[125] J.. Fang, D.. Lee, Micromixing efficiency in static mixer, Chem. Eng. Sci. 56 (2001) 3797–3802. doi:10.1016/S0009-2509(01)00098-7.

[126] Chemineer, Kenics Products, Chemineer.com/products/kenics.html. (2014).

[127] Y. Zhao, G. Chen, Q. Yuan, Liquid–liquid two-phase mass transfer in the T-junction microchannels, AIChE J. 53 (2007) 3042–3053. doi:10.1002/aic.11333.

[128] Y. Zhao, G. Chen, Q. Yuan, Liquid-liquid two-phase flow patterns in a rectangular microchannel, AIChE J. 52 (2006) 4052–4060. doi:10.1002/aic.11029.

[129] A. Gupta, S.M.S. Murshed, R. Kumar, Droplet formation and stability of flows in a microfluidic T-junction, Appl. Phys. Lett. 94 (2009) 164107. doi:10.1063/1.3116089.

[130] A. Salim, M. Fourar, J. Pironon, J. Sausse, Oil-water two-phase flow in microchannels: Flow patterns and pressure drop measurements, Can. J. Chem. Eng. 86 (2008) 978–988. doi:10.1002/cjce.20108.

[131] R. Raj, N. Mathur, V. V. Buwa, Numerical Simulations of Liquid−Liquid Flows in Microchannels, Ind. Eng. Chem. Res. 49 (2010) 10606–10614. doi:10.1021/ie100626a.

[132] T.W.F. Russell, M.E. Charles, The effect of the less viscous liquid in the laminar flow of two immiscible liquids, Can. J. Chem. Eng. 37 (1959) 18–24. doi:10.1002/cjce.5450370105.

[133] A. Pohar, M. Lakner, I. Plazl, Parallel flow of immiscible liquids in a microreactor: modeling and experimental study, Microfluid. Nanofluidics. 12 (2011) 307–316. doi:10.1007/s10404-011-0873-7.

[134] M.M. Sharma, A.K. Nanda, Extraction with second order reaction, Trans. Inst. Chem. Eng. 46 (1968) T44–T52.

[135] P.H. Calderbank, M.B. Moo-Young, The continuous phase heat and mass transfer properties of dispersions, Chem. Eng. Sci. 50 (1995) 3921–3934. doi:10.1016/0009-2509(96)81823-9.

[136] A. Woitalka, S. Kuhn, K.F. Jensen, Scalability of mass transfer in liquid–liquid flow, Chem. Eng. Sci. 116 (2014) 1–8. doi:10.1016/j.ces.2014.04.036.

[137] Norbert Kockmann, Transport Phenomena in Micro Process Engineering, 2008. doi:10.1007/978-3-540-74618-8.

[138] P. Morancais, K. Hirech, G. Carnelle, J. Legrand, Friction factor in static mixer and determination of geometric parameters of SMX Sulzer mixers, Chem. Eng. Commun. 171 (1999) 77–93. doi:10.1080/00986449908912750.

[139] A.N. Kolmogorov, The Local Structure of Turbulence in Incompressible Viscous Fluid for Very Large Reynolds Numbers, Proc. R. Soc. A Math. Phys. Eng. Sci. 434 (1991) 9–13. doi:10.1098/rspa.1991.0075.

[140] A.N. Kolmogorov, Dissipation of Energy in the Locally Isotropic Turbulence, Proc. R. Soc. A Math. Phys. Eng. Sci. 434 (1991) 15–17. doi:10.1098/rspa.1991.0076.

[141] J.O. Hinze, Fundamentals of the hydrodynamic mechanism of splitting in dispersion processes, AIChE J. 1 (1955) 289–295. doi:10.1002/aic.690010303.

[142] H.T. Bi, J.R. Grace, Flow regime diagrams for gas-solid fluidization and upward transport, Int. J. Multiph. Flow. 21 (1995) 1229–1236. doi:10.1016/0301-9322(95)00037-X.

[143] T.L. Bergman, A.S. Lavine, F.P. Incropera, D.P. DeWitt, Fundamentals of heat and mass transfer, 7th ed., 2011.

[144] J.R. McDonough, A.N. Phan, A.P. Harvey, Rapid process development using oscillatory baffled mesoreactors – A state-of-the-art review, Chem. Eng. J. 265 (2015) 110–121. doi:10.1016/j.cej.2014.10.113.

[145] H.-S. Song, S.P. Han, A general correlation for pressure drop in a Kenics static mixer, Chem. Eng. Sci. 60 (2005) 5696–5704. doi:10.1016/j.ces.2005.04.084.

[146] M. Hoffmann, M. Schlüter, N. Räbiger, Experimental investigation of liquid–liquid mixing in T-shaped micro-mixers using -LIF and -PIV, Chem. Eng. Sci. 61 (2006) 2968–2976. doi:10.1016/j.ces.2005.11.029.

[147] N. Kockmann, M. Engler, D. Haller, P. Woias, Fluid Dynamics and Transfer Processes in Bended Microchannels, Heat Transf. Eng. 26 (2005) 71–78. doi:10.1080/01457630590907310.

[148] V. Kumar, M. Paraschivoiu, K.D.P. Nigam, Single-phase fluid flow and mixing in microchannels, Chem. Eng. Sci. 66 (2011) 1329–1373. doi:10.1016/j.ces.2010.08.016.

[149] M.E. Steinke, S.G. Kandlikar, Single-Phase Heat Transfer Enhancement Techniques in Microchannel and Minichannel Flows, in: ASME 2nd Int. Conf. Microchannels Minichannels, ASME, 2004: pp. 141–148. doi:10.1115/ICMM2004-2328.

[150] N. Kockmann, D.M. Roberge, Transitional flow and related transport phenomena in curved microchannels, Heat Transf. Eng. 32 (2011) 595–608. doi:10.1080/01457632.2010.509753.

[151] A.D. Caldwell, Wall heat transfer coefficients with gas flow through packed beds, Chem. Eng. Sci. 23 (1968) 393–395. doi:10.1016/0009-2509(68)87011-3.

[152] A.O.O. Denloye, J.S.M. Botterill, Heat transfer in flowing packed beds, Chem. Eng. Sci. 32 (1977) 461–465. doi:10.1016/0009-2509(77)87001-2.

[153] A.G. Dixon, Thermal resistance models of packed bed effective heat transfer parameters.pdf, AIChE J. 31 (1985) 826–834. doi:10.1002/aic.690310519.

[154] B.D. Prasher, G.B. Wills, Mass Transfer in an Agitated Vessel, Ind. Eng. Chem. Process Des. Dev. 12 (1973) 351–354. doi:10.1021/i260047a023.

End of document